# Understanding Mg isotope systematics of variably saline water along the west coast of southern Africa

**By Alice Lea Petronio**

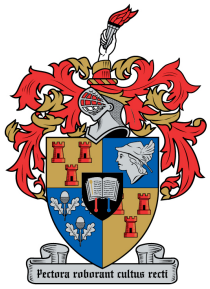


UNIVERSITEIT
iYUNIVESITHI
STELLENBOSCH
UNIVERSITY


*Dissertation presented for the Degree of Master of Science in Geology at Stellenbosch University*

**Supervisor: Dr Jodie Miller**

**Co-supervisor: Dr Petrus le Roux**

March 2018

# DECLARATION

By submitting this thesis electronically, I declare that the entirety of the work contained therein is my own, original work, that I am the sole author thereof (save to the extent explicitly otherwise stated), that reproduction and publication thereof by Stellenbosch University will not infringe any third-party rights and that I have not previously in its entirety or in part submitted it for obtaining any qualification.

December 2017

# ABSTRACT

Isotope techniques are a highly effective tool for fulfilling critical hydrologic information and are therefore crucial for supporting effective water management. The most frequently used isotopes in hydrology are isotopes of the elements of the water molecule, hydrogen and oxygen, and of the element carbon. These stable environmental isotopes have been used for over four decades in the study of hydrology. With the almost exponential increase in analytical capabilities in recent years, much focus has been on more novel isotope systems to provide further insights into hydrological processes. Magnesium isotopes are a potentially underutilised tool in the study of groundwater hydrology. The principle reasons for this are the technically challenging nature of magnesium isotope analysis and the relatively small fractionation range observed in nature. However, as magnesium is a major component in both water and rock, magnesium isotopes are a theoretically useful tracer. Sixty-six groundwater and surface water samples were collected from the catchments of nine major west-draining river systems along the west coast of southern Africa. Catchments were grouped into three regions based on their proximity to one another. The southern region catchments occur in the Western Cape province of South Africa. These catchments have NaCl-type waters, show intermediate

$\delta^{18}O$ and $\delta D$ values relative to the sample set, with characteristically low $\delta^{13}C$-DIC compositions consistent with soil $^{13}CO_2$ in $C_3$-vegetated regions. $\delta^{26}Mg$ values show enrichment in southern catchment waters, and Mg isotopes are fractionated by means of secondary clay formation in

catchment soils. The central region catchments occur in the Northern Cape province, and show similar characteristics to the southern region catchments, however with a strong $^{87}Sr/^{86}Sr$ component and

less negative $\delta^{13}C$-DIC values, which are influenced to a greater extent by atmospheric $^{13}CO_2$ in this region. The northern region catchments drain carbonate lithologies, and waters show a dominant $HCO_3^-$ anion chemistry, with mixed cations. $\delta^{13}C$-DIC compositions in the northern region are the least negative for the sample set, resulting from carbonate dissolution. $\delta^{18}O$ and $\delta D$ values are more depleted relative to the southern and central region catchments, ranging between -5‰ and -7‰ for $\delta^{18}O$ and -30‰ to -50‰ for $\delta D$. $\delta^{26}Mg$ values are also low, and reflect a dominant contribution from carbonate lithologies. The use of Mg isotopes in west coast aquifers has provided insight into the processes controlling fractionation of their isotope ratios, and, when used in conjunction with other isotopic and hydrochemical parameters, provide a better understanding of the hydrological systems, which is essential for the formulation of sustainable resource development and management strategies.

KEYWORDS: $\delta^{26}$Mg variation, groundwater and surface water chemistry, baseline, water management strategies.

# ACKNOWLEDGEMENTS

I would like to express my heartfelt gratitude to the following people for their contribution to this project. Firstly, to my supervisor, Jodie Miller, for her support throughout this project. To my co-supervisors, Torsten Vennemann and John Higgins, who not only assisted me academically, but also helped me to settle in and find my feet in foreign countries. I would like to extend my thanks to the Water Research Commission (WRC) of South Africa, AEON and Maarten De Wit from Nelson Mandela University for funding this project. To the sampling team - Anya Eilers, Jared van Rooyen and Shane Teek – thank you for your assistance in the field as well as with data compilation. Thank you to the farm owners, resort and municipal managers, without whom this project would not have been possible. Thank you to Torsten Vennemann at the University of Lausanne in Switzerland for the oxygen, hydrogen and carbon-13 isotope analyses, John Higgins at Princeton University for the magnesium and calcium isotope data, and Petrus Le Roux from the University of Cape Town for the strontium isotope analysis. Special thanks to my friend and fellow hydrologist Kelley Swana for her continuous assistance and support over the past two years, and to my fellow MSc peers who provided a studious but light-hearted atmosphere in the postgraduate lab. Finally, I would like to thank my family – Aunty Helen, Uncle Peter, Kate & Guy – I am so grateful for your support and for making my time in America extra special! Gwen & Nick, thank you for the good advice, encouragement and guidance in preparation for my trip to Switzerland. Last but not least, I am forever grateful to my mom for her unwavering support and reassurance throughout my entire university career.

# DEDICATION

I dedicate my dissertation work to my father, Manlio Petronio, who instilled a love of nature, camping and the outdoors and encouraged me to always keep an open and enquiring mind.

# TABLE OF CONTENTS

# LIST OF FIGURES

# 1. INTRODUCTION

## 1.1 General Introduction

As the global population continues to rapidly increase, significant pressure is being placed on natural resources to provide an adequate supply of water while maintaining the integrity of ecosystems (Pimental, et al., 1997). Increases in the globally-averaged mean annual air temperature and variations in regional precipitation are expected to continue and intensify in the future (Solomon, et al., 2007). Furthermore, the impact of predicted climate change on both the quality and quantity of groundwater resources is of global importance, as an estimated 1.5-3 billion people rely on groundwater as a drinking water source worldwide (Kundzewicz & Doll, 2009). In sub-Saharan Africa, this situation is further intensified by the large number of semi-arid and arid regions and the effect of changing climatic conditions on the hydrological cycle (Bates, et al., 2008). The dryland regions of southern Africa, which cover almost all of Botswana and Namibia, an estimated 50% of South Africa, and substantial parts of southern Angola, Mozambique, Tanzania, Zambia and western Zimbabwe, are particularly at risk as severe drought conditions and highly variable rainfall can drastically limit water supplies (Tarr & Tarr, 2009).

Finding sufficient quantities of potable water is a growing concern, particularly in developing southern African countries, where high population growth accompanied by continued increases in the demand for water has limited development (Ashton, 2002). The lack of water is preventing many household and community-based activities for a significant number of people living in these areas (Shiferaw, et al., 2014). Water shortages are further exacerbated when communal water points lie broken and local people have neither the capacity nor the incentive to repair these state-owned resources (Lovell, 2000).

The dryland regions of South Africa, which occur predominately in the Northern Cape province, are underlain by crystalline basement rocks accommodating a widespread extent of aquifers (Adams, et al., 2004). These aquifers are complex in occurrence, spatially highly variable and have a low storage capacity. Nonetheless, they represent the only available water supply in these regions (Lovell, 2000). Traditionally, hard-rock aquifers have been exploited by shallow hand-dug wells and deep boreholes, which produce relatively low yields and failed water points during droughts (Titus, et al., 2009) .

In the early 1980s, a research programme was implemented to assess the feasibility of developing hard-rock aquifers to support income-generating activities in the dryland regions of southern Africa and determine the potential of productive water points (Lovell, 2000). The proposed outcome of this study was to eventually establish sustainable community-based management of natural resources in

drought-prone areas (Lovell, 2000). Productive community-managed water points empower local communities providing users with both the motivation and funds (through economic production) needed for local upkeep, thereby relieving pressure on the state, which often struggles to maintain rural water supplies (Sally, et al., 2013).

One of the main constraints to adopting this strategy has been a lack of information on hydrological systems resulting from poor data coverage (Lovell, 2000). These gaps are particularly profound with respect to groundwater resources, which are generally poorly understood and managed (IAEA, 2011). A qualitative and quantitative characterisation of groundwater recharge is essential to ensure the sustainable development and management of these groundwater resources (Adams, et al., 2004). Aquifers which receive little recharge, such as those found in dryland regions, experience negligible fluctuations in groundwater levels; consequently, reliable estimates of recharge rates cannot be easily obtained based on classical approaches alone (Aggarwal, 2011). It is therefore essential that more advanced tracers be identified for use in hydrological investigations and assessments in support of effective water management strategies (WRC, 2014).

Isotope techniques are one such tool and are highly effective for fulfilling critical hydrologic information needs such as the origin of waters, recharge, residence times, and interconnections between aquifers amongst other elements and are therefore crucial for supporting effective water management (Aggarwal, et al., 2009). The most frequently used isotopes in hydrology are isotopes of the elements of the water molecule, hydrogen ($^{2}H$ - deuterium, and $^{3}H$ - tritium), and oxygen ($^{16}O$ and $^{18}O$), and of the element carbon ($^{12}C$, $^{13}C$ and $^{14}C$), which occur in water as constituents of dissolved inorganic and organic compounds (Aggarwal, 2011). $^{18}O/^{16}O$ ($\delta^{18}O$) and $^{2}H/^{1}H$ ($\delta D$) are used to identify and characterise different water bodies, while $^{3}H$ and $^{14}C$ are applied to the assessment of groundwater ages (Froehlich, et al., 1998). These stable and radioactive environmental isotopes have been used for over four decades in the study of hydrology. Furthermore, because of the typically conservative behaviour of most stable isotope systems, these isotopes serve as highly effective tracers of numerous hydrological processes on a large temporal and spacial scale through their natural distribution in hydrological systems (Deodhar, et al., 2014).

Although stable isotopes of oxygen, hydrogen and carbon have long been shown to be excellent tracers, with the almost exponential increase in analytical capabilities in recent years, much focus has been on more novel isotope systems to provide further insights into hydrological processes (Geyh, 2000). Geochemists have begun to analyse less conventional stable isotope systems such as Ca, Mg, Si, B, Li, Fe, Zn, Hg and Cu, which all have the potential to yield additional constraints about geological and environmental processes, thereby contributing significantly to the field of Earth Sciences (Tipper, 2006).

Magnesium isotopes are a potentially underutilised tool in the study of groundwater hydrology. The principle reasons for this are the technically challenging nature of magnesium isotope analysis and the relatively small fractionation range observed in nature (Young & Galy, 2004). However, as magnesium is a major component in both water and rock, magnesium isotopes are a theoretically useful tracer. Furthermore, the advent of multiple-collector inductively coupled plasma mass spectrometry (MC-ICP-MS) and novel sample digestion and purification techniques have enabled the analysis of magnesium isotope ratios to a sufficient precision to resolve differences in the magnesium isotope composition of terrestrial reservoirs of magnesium, and the processes which induce mass dependent fractionations of magnesium isotope ratios (An & Huang, 2014).

In natural waters, magnesium is derived primarily from the weathering of carbonate and silicate rocks, each of which possess a distinct magnesium isotopic range (Immenhauser, et al., 2010). These weathering rates are strongly influenced by environmental factors such as temperature, precipitation and run-off (Egli, et al., 2008; Maher, 2010). Silicate weathering is more prevelant in warm and dryer climates, whereas carbonate weathering is enhanced under more humid conditions (Buhl, et al., 2007). Therefore magnesium isotopes, which have been shown to be fractionated by weathering processes, can be used to constrain the effects of different weathering processes within catchments and ultimately provide insight into global climate variations (Tipper, et al., 2006).

Magnesium isotopes in hydrological systems are also thought to hold potential clues to the ecological interactions between primary producers and consumers, as water impacts directly on food chains (Bouillon, et al., 2011). To date there have been no hydrological magnesium isotope studies conducted in southern Africa, however the resurgence of interest in hominid evolution with the release of the Naledi fossil discovery (Greshko, 2017) has precipitated an upsurgence in interest in their potential applications. In living organisms, magnesium isotopes have been measured in the calcite skeletons of marine invertebrates and in marine biogenic carbonate sediment (Hippler, et al., 2009; Wombacher, et al., 2009). In plants, magnesium also plays an important role as it represents the metal centre of chlorophyll (Black, et al., 2006). These observations suggest a link between metabolic processes and magnesium isotope fractionation. Exploration of the isotope variability of this bio-essential element between and within vertebrate communities may therefore produce insights into biological processes, and ultimately reveal trophic level effects (Martin et al., 2014). Thus magnesium, like other new isotope systems, could provide evidence for reconstructing food webs among extinct animals, and an opportunity to understand ecological interactions in deep time. However, prior to the application of magnesium isotopes to various studies, the baseline magnesium isotope variation in water bodies needs to be determined.

## 1.2 Research aims and objectives

The aim of this study is to apply and adapt the method of analysing magnesium isotopes in water samples, developed by Wombacher et al, 2009, to identify trends and variations that may exist in various water sources from selected southern African west coast catchments where saline groundwater is an impediment to economic development. Magnesium isotopes will be used in conjunction with strontium isotopes and conventional water chemistry data to obtain a better understanding of groundwater flow systems and the geochemical processes governing their hydrochemistry. This information will assist in the establishment of a baseline magnesium isotope study in hydrological systems that can be applied to various studies.

**Key objective one:** To determine the hydrochemical and isotopic characteristics of groundwater and surface water along the West coast and how they evolve along regional flow paths.

1. What is the hydrochemical and O, H, C and Sr isotope composition of groundwater and surface water along the West coast and does it vary spatially with respect to catchments?
2. What do these parameters indicate about the composition of the host rock aquifer and does this evolve along flow paths?
3. Do these parameters indicate the role of other processes controlling the isotopic compositions of West coast waters?

**Key objective two:** To determine the natural range of Mg isotope variations in groundwater and surface water along the west coast of Southern Africa and determine the processes responsible for this variation.

1. Does a distinct variation exist in the Mg isotope values of various surface and groundwater sources?
2. Is this variation more distinguished among the surface or the groundwater samples? Or are trends confined to catchments?
3. What processes control Mg isotope fractionation in West coast catchments and how do these relate to those processes indicated in objective 1.3?

**Key objective three:** To assess the usefulness of Mg isotopes as a routine tool for isotope hydrology

1. Do Mg isotopes provide additional information on processes controlling the hydrochemical character of groundwaters and surface waters on the west coast of southern Africa.
2. Can Mg isotopes be used to differentiate groundwater and surface water catchments on their own or in conjunction with other isotopes or hydrochemical parameters?
3. Are Mg isotopes a viable hydrological tool in a southern African context?

## 1.3 Isotopes and water management

The use of stable isotopes is an effective tool for fulfilling critical hydrological needs to ensure that sustainable management strategies are formulated. This includes a comprehensive understanding of the following knowledge requirements: (i) Aquifer recharge rates and their spatial and temporal variations (ii) The ages and origins of the water sources being abstracted, and (iii) The distribution of deep, high quality palaeogroundwater bodies, which represent potential strategic reserves (Adelana & Olasehinde, 2005). In addition, isotopes provide information that cannot always be obtained by classical hydrological methods and related scientific disciplines (Darling, et al., 2003).

The most commonly used environmental isotopes are the stable isotopes deuterium ($^{2}H$), oxygen ($^{18}O$) and carbon-13 ($^{13}C$); as well as the radioisotope molecules tritium ($^{3}H$) and carbon-14 ($^{14}C$) (Aggarwal, 2011). These isotope techniques have contributed to studies in the field of hydrology in the last three to four decades, complementing both physical and chemical hydrogeology (Clark & Fritz, 1997). However, the increased application of isotope techniques for comprehensive water resource management, as well as the exponential increase in analytical capabilities in recent years, has shifted focus to the development of more novel isotope systems to provide additional insights into hydrological processes (Geyh, 2000).

## 1.4 Stable Isotopes

### 1.4.1 Stable isotopes of oxygen and hydrogen

Oxygen has three stable isotopes: $^{16}O$ (99.63%), $^{17}O$ (0.0375%) and $^{18}O$ (0.1995). Hydrogen has two stable isotopes, $^{1}H$ (protium) and $^{2}H$ (deuterium), with relative abundances of 99.98% and 0.012% respectively. Ratios of $^{18}O$ to $^{16}O$ and $^{2}H$ to $^{1}H$ in waters, rocks, and most solutes are reported in ‰ (permille) relative to Vienna Standard Mean Ocean Water (VSMOW) (Kendall & Doctor, 2003). Isotopes of hydrogen and oxygen are ideal tracers of water sources and movement as they are integral components of the water molecule (Gupta & Deshpande, 2005) Additionally, these isotopes behave conservatively in most low-temperature, near-surface environments. Therefore, chemical exchanges between water molecules and oxygen and hydrogen in organic and inorganic materials through which flow occurs will have a negligible effect on the overall isotope ratios of the water (Kendall & Doctor, 2003). This conservative behaviour of isotopes in the subsurface provides a reliable tracer to determine the origin of water bodies, to quantify the water balance of surface and subsurface reservoirs, and to trace the mechanisms of salinisation of water resources (Gat, 1996). Therefore, the use of oxygen and hydrogen isotope are important for the effective management of water resources.

#### *1.4.1.1 Evaporation, condensation and precipitation*

During evaporation, the light molecules of water ($H_2{}^{16}O$) are preferentially evaporated as they are more volatile than the heavier water molecules ($^1H^2H^{16}O$ or $H_2{}^{18}O$) (Pradeep, et al., 2009). Successive cooling and condensation of evaporated atmospheric water vapour during cloud formation and precipitation condenses the heavier water molecules leaving a residual vapour that is depleted in $^2H$ and $^{18}O$ (Kendall & Caldwell, 1998). Therefore, successive precipitations derived from the same initial vapour mass will be more and more depleted in the heavy isotopes (Gat, 1996).

The isotopic character of precipitation at any given location is controlled by two main factors: (i) the temperature of condensation and (ii) the degree of rainout of an air mass, that is the ratio of water vapour that has already condensed into precipitation to the initial amount of water vapour in the air mass (Buttle, 1998). In addition, $\delta^{18}O$ and $\delta^2H$ of precipitation are influenced by altitude, distance inland along different storm tracks, environmental conditions at the source of the vapour, latitude and humidity (Hughes & Crawford, 2013). The $\delta^{18}O$ and $\delta^2H$ composition of precipitation does not display significant seasonal or annual variations from year to year. This occurs because the annual range and sequence of climatic conditions, such as temperatures, vapour source and direction of air mass movement, normally vary within a predictable range (Kendall & Doctor, 2003). Differences in the mean seasonal air temperatures produce summer rains with relatively higher δ values than winter rains (Srivastava, et al., 2014). Superimposed on seasonal cycles are storm-to-storm and intrastorm variations in the isotopic composition of precipitation, which can be as large as seasonal variations (Rindsberger, et al., 1990). It is these differences between relatively uniform old water and variable new water that allow isotope hydrologists to determine the contributions of old and new water to surface water sources during periods of high runoff (Kendall & Doctor, 2003).

#### *1.4.1.2 Shallow Groundwaters*

The $\delta^{18}O$ and $\delta^2H$ composition of shallow groundwaters does not necessarily reflect that of the local average precipitation, as selective recharge and fractionation processes may alter the $\delta^{18}O$ and $\delta^2H$ values of the precipitation before it reaches the saturated zone (Gat & Tzur, 1967). These processes include: (1) the exchange of infiltrating water with atmospheric vapour; (2) evaporation of water during infiltration; (3) selective recharge (for example, only from major storms) and (4) post depositional processes, such as evaporation during infiltration (Kendall & Doctor, 2003). Once water has moved into the saturated zone, the $\delta^{18}O$ and $\delta^2H$ (water-rock interaction does not influence O and H isotopes) values of the subsurface water moving along a flow path change only by mixing with waters of different isotopic compositions (Macpherson & Townsend, 1998).

#### *1.4.1.3 Deep groundwaters and paleorecharge*

Groundwater moves very slowly, typically at rates of one to two meters per month (Booth, 1991). Deep confined groundwater can therefore be very old, often having been recharged thousands of years in the past (Aggarwal, 2011). Because of the conservative behaviour of $\delta^{18}O$ and $\delta^{2}H$ in waters in the subsurface environment, these values typically reflect past climatic conditions under which recharge took place. Therefore, the isotopic composition of groundwater can serve as a powerful dating tool for the identification of paleorecharge (Kendall & Doctor, 2003). Furthermore, because the $\delta^{18}O$ and $\delta^{2}H$ values of precipitation contributing to aquifer recharge are strongly dependent on the temperature and humidity of the environment, these tracers are particularly useful for the identification of groundwater recharged during the last glacial period of the Pleistocene epoch, when average Earth surface temperatures were dramatically lower than during the Holocene (Leibundgut, et al., 2009).

Precipitation that is formed under cooler temperatures and more humid conditions compared to the present-day environment will be reflected in old groundwater as having significantly lower $\delta^{18}O$, $\delta^{2}H$ and deuterium excess values (Alvaradoa, et al., 2011). Climate changes in arid regions are often easily identified in paleowaters. This is mainly attributed to the strong variability in humidity which causes large shifts in the deuterium excess, and a corresponding shift in the vertical position of the Local Meteoric Water Line (Clark & Fritz, 1997). When evaporation occurs during times of lower relative humidity, the deuterium excess in the water vapour increases. Since a positive correlation exists between a deficit in air moisture and temperature, deuterium excess should be positively correlated with temperature. Alternatively, a high deuterium excess in groundwater indicates recharge derived from water evaporated under conditions of low relative humidity (Kendall & Doctor, 2003).

#### *1.4.1.4 Surface waters*

The water in most streams and rivers is made up of two components: (i) recent precipitation, which recharges surface waters either by runoff, channel precipitation or rapid flow through shallow subsurface paths; and (ii) groundwater (Kendall & Doctor, 2003; Price, 2001). The relative contributions of these sources differ in each watershed or basin and are dependent on the physical setting of the drainage basin (topography, vegetation, soil type), climatic factors such as the temperature and amount of precipitation, and anthropogenic activities (Price, 2001). Therefore, the $\delta^{18}O$ and $\delta^{2}H$ compositions of surface water systems are good indicators of the changing contributions of precipitation and groundwater with time, as well as the temporal variation of the isotopic contents of the sources themselves (Fan, et al., 2016). In streams where the main source of flow is recent precipitation, seasonal variations will be larger, while groundwater-dominated flow will produce small seasonal variations (Milner, et al., 2009). This dual nature of surface water is crucial in studies of both regional hydrology and climatology (Kendall & Doctor, 2003).

### 1.4.2 $^{13}$C-DIC

Carbon has two naturally occurring stable isotopes, $^{12}$C and $^{13}$C, with relative abundances of 98.89% and 1.11% respectively. Ratios of these isotopes are reported in ‰ relative to the standard VPDB (Vienna Pee Dee Belemnite) (Kendall & Doctor, 2003). The stable isotope composition of dissolved inorganic carbon ($^{13}$C-DIC) is not a conservative tracer. However, $^{13}$C ($^{13}$C/$^{12}$C)-DIC can trace the carbon sources and reactions for numerous interacting organic and inorganic species (Qiming, et al., 2014) . $^{13}$C compositions also provide insight into the geochemical evolution of waters, rock types in flow-path surroundings and recharge area conditions (Kebede, et al., 2004). Therefore, the use of $^{13}$C in hydrology serves as an important tool for the quantification of water-rock interactions, the identification of the proportion of different $CO_2$ sources in water, and the determination of the initial geological settings of groundwater recharge (Trček & Zojer, 2009). The main sources of carbon dissolved in waters are soil $CO_2$, $CO_2$ of geogenic or magmatic origin, carbonate minerals, organic matter in soils and rocks, fluid inclusions and methane. Each of these sources produce a distinct carbon isotopic signature that can be used to distinguish the relative proportions of source contributions to hydrological systems (Adelana, 2005).

The $^{13}$C composition of the atmosphere is -7‰ (Kendall & Doctor, 2003). During photosynthesis, the carbon that becomes fixed in plant tissue is markedly depleted in $^{13}$C relative to the atmosphere (Cerling, 1991). There is a bimodal distribution in the $^{13}$C concentration of terrestrial plant organic matter because of differences in the photosynthetic pathways utilised by plants (Deines, 1980). For $C_3$ plants, which comprise approximately 85% of all vegetation types and are temperate, cool-season plants, $^{13}$C values average around -25‰. $C_4$ plants, which occur in hot and sunny climates, have $^{13}$C values ranging from -6 to -19‰ (Moore, et al., 2003; Deines, 1980). The $^{13}$C of soil organic matter, which is derived from plant material, is comparable to that of the source plant, and changes in $C_3$ and $C_4$ vegetation will result in corresponding changes in the $^{13}$C of the soil organic matter (Novara, et al., 2013). Because most of the carbon stored in soil organic matter is stable on time scales of centuries to millennia, recent changes in the relative proportion of $C_3$ and $C_4$ plants can be determined by comparing the carbon isotopic composition of the current plant community to that of the soil organic matter (Kendall & Doctor, 2003). In addition, the $^{13}$C of plants and organisms can provide useful information about sources of nutrients and food web relations, particularly when combined with the analyses of nitrogen and sulphur isotopes (Coat, et al., 2009).

Isotope fractionation that occurs in the $CO_2$- $HCO_3$-$CaCO_3$ system results in the formation of calcite that is enriched in $^{13}$C by approximately 10‰ relative to atmospheric $CO_2$ (Hoefs, 2009). Marine carbonate rocks typically have $^{13}$C values of 0 ± 5 ‰ (Mozley & Burns, 1993). Because lacustrine carbonates incorporate $CO_2$ derived from decaying plant material in soils, they have much lower $^{13}$C

compositions, in the range of -2‰ and -8‰ (Talbot, 1990). $CO_2$ originating from geothermal and volcanic systems produce $^{13}C$ values between -3 to -8‰, while $^{13}C$ compositions originating from geothermal methane average approximately -30‰ (Trček & Zojer, 2009). Carbonates which form from the oxidation of biogenic methane are much more depleted in $^{13}C$ ($^{13}C$ as light as −69‰) (Drake, et al., 2015); whereas carbonates formed in organic-rich systems display very positive values, often exceeding 20‰ (Reitsema, 1980).

DIC in catchment waters is produced by three primary reactions, namely: (i) the weathering of carbonate minerals by acid rain and other strong acids; (ii) the weathering of silicate minerals by carbonic acid, which is produced by the dissolution of biogenic soil $CO_2$ from infiltrating rain water;

(iii) the weathering of carbonate minerals by carbonic acid (Kendall & Doctor, 2003). The $^{13}C$ in DIC produced from the first and second reactions is identical to that of the composition of the reacting carbonate and carbonic acid respectively, and the third reaction produces a DIC with a $^{13}C$ value intermediate between the compositions of the carbonate mineral and carbonic acid (Kemp, 1971).

Several processes may complicate $^{13}C$-DIC interpretations, such as carbonate precipitation and dissolution, exchange with atmospheric $CO_2$, carbon uptake and release by aquatic organisms, methanogenesis and methane oxidation (Retallack, 2005). Variations in $^{13}C$ should therefore be correlated with major ion chemistry (particularly $HCO_3^-$), redox conditions and other isotope tracers such as $^{24}S$, $^{87}Sr/^{86}Sr$ and $^{14}C$ to determine the significance of these processes for a specific study (Clark & Fritz, 1997; Bullen & Kendall, 1998).

### 1.4.3 Mg isotopes

Magnesium is the second most abundant rock-forming element and plays an important role in both hydrological and biological systems (Young & Galy, 2004). Magnesium has three stable isotopes, $^{24}Mg$, $^{25}Mg$ and $^{26}Mg$, with natural abundances of 78.99%, 10.00% and 11.01% respectively. Its stable isotopes data are reported using the standard per mil (‰) notation of $\delta^{26}Mg$, the ratio of $^{26}Mg$ to $^{24}Mg$, and $\delta^{25}Mg$, the ratio of $^{25}Mg$ to $^{24}Mg$, for the deviation of the measured ratio in the sample relative to the reference standard DSM-3 (Karasinski, et al., 2017) The standard per mil (‰) notation is used to report magnesium stable isotope data (Young & Galy, 2004). The relative mass difference between $^{24}Mg$ and $^{26}Mg$ (~8%) is large enough to produce significant Mg isotopic fractionations in geochemical processes (An & Huang, 2014). Historically, reliable measurements of $^{25}Mg$ and $^{26}Mg$ in natural systems have been limited due to instrumental mass fractionation effects. However, the advent of multi-collector inductively coupled mass spectrometry (MC-ICP-MS) and novel sample digestion and purification techniques have enabled the analysis of Mg isotope ratios to a sufficient precision to resolve differences in the Mg isotope composition of terrestrial reservoirs of Mg, and the processes which induce mass dependent fractionations of Mg isotope ratios (An & Huang, 2014).

Magnesium is abundant in continental crust, and incorporated into several minerals, for example in most silicate and carbonate minerals, and therefore is an important element for rock formation (Okrush and Matthes 2005). It is generally only present in trace amounts in carbonate minerals but forms a major constituent of silicate minerals (Tipper, et al., 2006b). Furthermore, Mg is a commonly occurring element in seawater, dust, aerosols of rainwater, soil water, river water and drip waters in caves (Riechelmann, 2013).

Magnesium silicates are a significant long-term sink of atmospheric $CO_2$, and Mg isotope ratios have the potential to trace biogeochemical processes at the surface of the Earth. Understanding chemical cycles is central to the study of Earth Science (Tipper, 2006). Therefore, quantifying the sources of Mg in the dissolved phases of hydrological systems, along with the relative proportions of weathered silicate and carbonate, is fundamental to the understanding of atmospheric $CO_2$ consumption rates and the link between the carbon cycle, climate change and silicate weathering (Galy, et al., 1999; Tipper, 2006). The molar ratios of (Ca, Mg)/Na, (Ca, Mg)/Sr and Sr isotope compositions in water and sediment are commonly used to distinguish between water solute fluxes derived from silicate and carbonate weathering (Galy, et al., 1999). This approach assumes congruent dissolution of carbonates, and conservative behaviour of Mg, Ca and Sr during transport (Brenot, et al., 2008). However, several studies have documented an excess of dissolved Mg and Sr relative to Ca in rivers and groundwater compared to the chemical composition of limestone rocks present in the basin. This excess has typically been attributed calcite or gypsum recrystallization from saturated waters (Brenot, et al., 2008). Furthermore, in basins where incongruent weathering of rocks occurs, waters do not reflect the compositions of the rocks drained at a basin scale (Galy & France-Lanord, 1999). Therefore, in mixed lithology basins, it is difficult to identify signatures induced by carbonate or silicate weathering alone (Brenot, et al., 2008). Because of the abundance of Mg in silicate rocks, and the significant differences that exist between the Mg isotopic composition of silicates and carbonates, Mg isotopes are a highly effective lithological source tracer and an essential component in the study of geological and environmental processes (Galy, et al., 2002; Tipper, et al., 2006).

Magnesium is an essential element for both plants and animals as it plays an important role in metabolic processes (Coudray, et al., 2005). Investigating isotope variability of this bio-essential element may provide insight into various biological processes, thereby providing evidence for reconstructing food webs among extinct animals and providing some insight into ecological interactions deep in time (Martin, et al., 2014). In bone apatite, where magnesium is the second most abundant metal after calcium, it has been suggested that magnesium is more resistant to alteration. Therefore, Mg isotopes may be unaffected by post-mortem processes that occur in fossil bones, and data obtained from these isotopes could be used to reconstruct trophic levels for which diagenesis has inhibited further interpretation (Trueman & Tuross, 2002).

To date, only a limited number of studies have reported Mg isotope variations in terrestrial systems, and before the work of Tipper (2006), only six Mg isotope measurements in rivers had been published (de Villiers, et al., 2005). So far, the global range in $^{26}Mg$ in rocks is 5‰, the lightest material analysed being foraminifera (-5‰) and the heaviest clinopyroxene (0.05‰) (Young & Galy, 2004). The available data has indicated that there are three main reservoirs of Mg on Earth which control $^{26}Mg$ in hydrological systems, namely mantle silicate, continental silicate and carbonate (dolostone and limestone) (Tipper, 2006). Of these reservoirs, the most significant differences arise between carbonates and silicates, and assuming Mg isotope ratios behave congruently (that is, the composition remains relatively constant throughout) during dissolution, water systems from each of the lithotectonic units should reflect that of the rock reservoirs (Tipper, 2006).

Both biogenic and abiogenic carbonates display the largest Mg isotopic variation among all types of terrestrial rocks (Saenger & Z., 2015). For calcite-rich carbonates, $^{26}Mg$ values range from -5.57 to -1.04. For dolomitic carbonates, $^{26}Mg$ compositions are less negative, varying between -3.25 and -0.38 (Blättler, et al., 2015). When compared to seawater, carbonates tend to have light Mg isotopic compositions, while silicates have heavy compositions. Several factors control Mg isotope fractionation in carbonates, the most important of which are mineralogy, temperature, rate of precipitation and kinetic isotope fractionation (Teng, 2017). Mineralogical differences between dolomites and other carbonate rocks, whereby dolomites are more enriched in magnesium, are responsible for the significantly heavier Mg isotopic signatures observed in these rocks, indicating a strong mineralogical control on Mg isotope fractionation in carbonates (Blättler, et al., 2015). Figure 1 indicates the Mg isotopic distribution in major extra-terrestrial and terrestrial reservoirs:

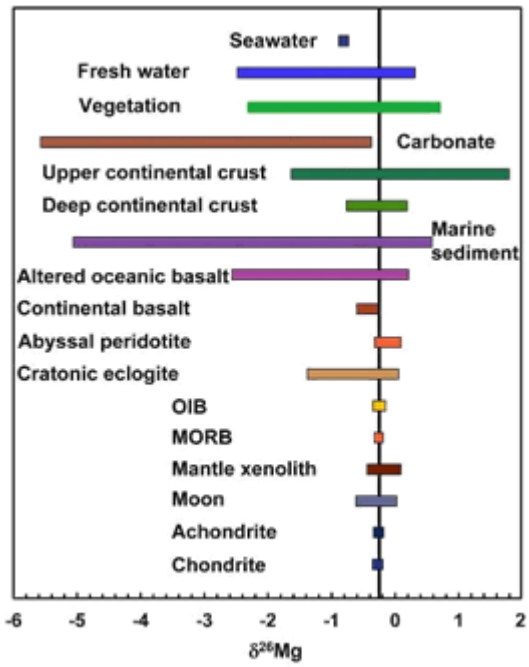


***Figure 1:*** Magnesium isotopic distribution in major extra-terrestrial and terrestrial reservoirs. The vertical bar represents the average Mg isotopic composition of the mantle (bulk earth) *(Teng, 2017)*.

### 1.4.3.1 Weathering of carbonate and silicate minerals

Minerals in soils and rocks undergo chemical weathering by water, which leads to the dissolution of the incorporated elements of these minerals (Sposito, 2008). Because Mg is soluble and mobile during weathering (Hoefs, 2009), the main source of Mg in soil waters, river waters and drip waters are the rocks and soils through which the waters percolate. The chemical weathering of silicates follows reaction pathway (1), producing only solute products (Riechelmann, 2013). The formation of secondary clay minerals represents a by-product of silicate dissolution and are not indicated in the reaction (Fairchild & Baker, 2012). The following reaction indicates the dissolution of silicate perovskite to form secondary clay minerals:

$$2CO_2 + 3H_2O + (Ca,Mg)SiO_3 \rightarrow (Ca, Mg)^{2+} + Si(OH)_4 + 2HCO_3^- \quad (1)$$

The process of carbonate-rock dissolution begins with rainwater dissolving $CO_2$ from the atmosphere via diffusion. After falling to the surface, rainwater infiltrates soil. Because $CO_2$-levels in the soil zone are increased by bioactivity, further dissolution of $CO_2$ occurs subsequent to the infiltration of rainwater (Haper, et al., 2005). The dissolution of $CO_2$ in water results in the formation of carbonic acid. Carbonic acid then dissolves carbonate rock via corrosion, along fissures and cracks in the host rock, provided it is undersaturated in carbonate (Fairchild & Baker, 2012).

$$H_2O + CO_2 \rightarrow H_2CO_3 \rightarrow H^+ + HCO_3^- \quad (\textit{formation of carbonic acid}) \quad (2)$$

$$(Ca, Mg)CO_3 + H^+ + HCO_3^- \rightarrow (Ca, Mg)_2+ + 2HCO_3^- \quad (\textit{weathering of carbonates}) \quad (3)$$

The weathering of silicates is prominent in warmer, dry climates compared to carbonate weathering, which is always dominant, but enhanced under colder and more humid conditions (White & Blum, 1995; Egli, et al., 2008; Maher, 2010). Because Mg is a major element in silicate minerals, silicate dissolution exerts a stronger influence on dissolved the Mg concentration compared to the dissolution of limestone (Tipper, et al., 2006b).

### 1.4.3.2 Rivers and streams

The Mg concentration in different rivers ranges from <1 to 50 ppm, with an average of 4 ppm. Although many terrains are lithologically complex, in the context of Mg isotope fractionation, carbonates and silicates are the primary sources of Mg in natural waters (Immenhauser, et al., 2010)

The Mg isotopic compositions of rivers are variable, with $^{26}Mg$ values typically ranging between -2.50 and 0.64‰ (Teng, 2017). On a catchment-scale, weathering reactions are the dominant factor controlling the fractionation of Mg isotope ratios (Tipper, et al., 2008). There are several mechanisms responsible for Mg-isotope fractionation during weathering process, most notably: (i) the incorporation of Mg into

biomass, which is typically observed in catchments with dense vegetation; (ii) formation of secondary carbonate, and (iii) precipitation of clay phases during incongruent weathering (de Villiers, et al., 2005; Tipper, et al., 2006; Pogge von Strandmann, et al., 2008). These mechanisms result in isotopic compositions which are fractionally shifted from those of the weathered parent rock. For example, Tipper, et al. (2008) observed that the formation of secondary clay phases.

Rivers draining limestone areas have low $^{26}$Mg values ranging from -1.1‰ to -2.1‰. For dolomitic regions, $^{26}$Mg signatures are slightly less negative (-1‰ to -2‰), while rivers draining acidic crystalline rocks and basalt and arc complexes have the heaviest $^{26}$Mg values typically between 0 and -1‰ and 0.8 to -1‰ respectively (Pogge von Strandmann, et al., 2008; Tipper, et al., 2006).

### *1.4.3.3 Groundwater*

Available data has revealed a variation in $^{26}$Mg from -1.70‰ to 0.23‰ (Teng, 2017). This variation is the result of source Mg-isotopic heterogeneity and isotope fractionation during mineral dissolution and secondary mineral formation (Pogge von Strandmann, et al., 2008). To date, the highest recorded isotopic value for groundwater ($^{26}$Mg = 0.23‰) was obtained from a monolithological basaltic catchment in Iceland and interpreted to be the result of secondary mineral formation (Pogge von Strandmann, et al., 2008). During this process, light Mg isotopes are preferentially removed from the groundwater system, leaving isotopically heavy water (Kendall & Caldwell, 1998). As for surface waters, groundwaters from carbonate-dominated environments have low $^{26}$Mg values, ranging between -1.70 and -1.18, reflecting the input of light Mg isotopes from carbonates.

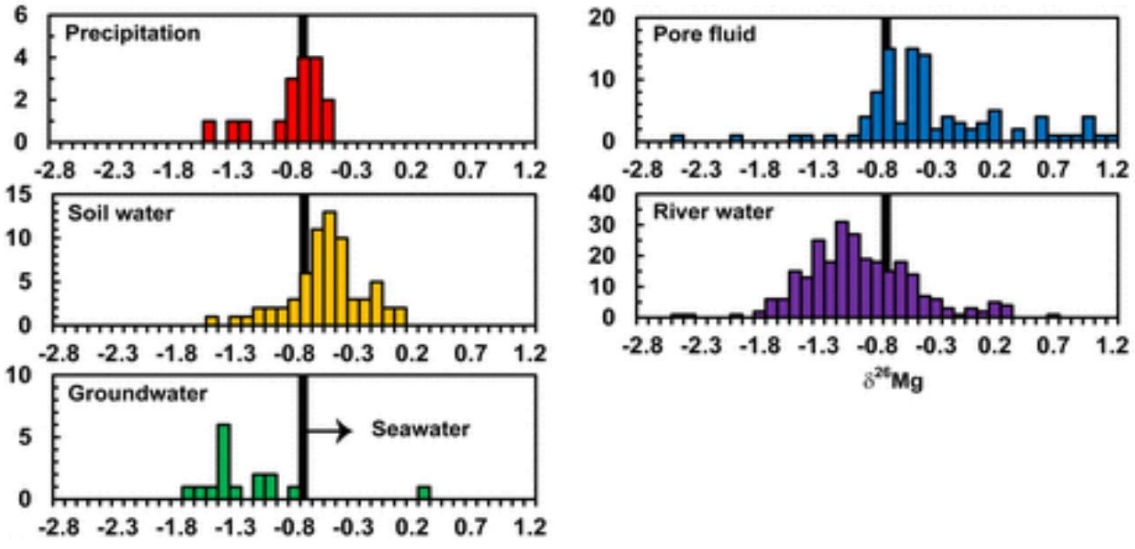


***Figure 2:*** Magnesium isotopic composition of the hydrosphere, where the vertical bar represents the average $^{26}$Mg of -0.83 for sea water (Teng, 2017).

#### *1.4.3.4 Anthropogenic and atmospheric contributions*

The isotopic compositions of river waters can be modified in agriculturally-dense regions, where the use of fertilisers is common (Vitòria, et al., 2004). A complication to determining the effect on $^{26}Mg$ is that chemical fertilisers have an average Mg isotopic composition very like that of carbonate rocks. However, if fertilisers alter riverine $^{26}Mg$, other isotope systems such as $^{87}Sr/^{86}Sr$ will also be affected (Böhlke & Horan, 2000). Because the $^{87}Sr/^{86}Sr$ composition of river water is much higher than that of chemical and organic fertilisers, the anthropogenic effects on riverine Mg can be considered negligible, with carbonate and silicate weathering remaining the most important controls on $^{26}Mg$ (Teng, 2017; Tipper, 2006).

#### *1.4.3.5 The effect of vegetation on $\delta^{26}Mg$*

The growth and decay of vegetation, which is typically enriched in magnesium and isotopically light, can significantly affect riverine Mg concentrations and isotope ratios (Pogge von Strandmann, et al., 2008). The formation of chlorophyll-based organic material depletes surface waters of Mg and drives the Mg isotopic composition of the surface waters towards heavier values. In contrast, decaying plant material enriches water in magnesium, which is easily leached from decaying organic matter, and drives isotopic compositions towards light values (Gosz, et al., 1973).

## 1.5 Radiogenic Isotopes - $^{87}Sr/^{86}Sr$ Ratios

The application of Sr isotope ratios in natural waters as a natural tracer for water-rock interactions and in assessing mixing relationships is well established as indicated by numerous journal publications and review articles (Graustein, 1989; Capo, et al., 1998; Stewart, et al., 1998; McNutt, 2000; Blum & Erel, 2005). Strontium isotopes ($^{87}Sr/^{86}Sr$) are therefore routinely used for de-convoluting the complex behaviour of solutes and water-rock interactions in natural environments, as well as constraining and testing geochemical and hydrological models (Shand, et al., 2009). Strontium is a divalent cation and shows a similar geochemical behaviour to calcium. It has four natural isotopes: $^{84}Sr$, $^{86}Sr$, $^{87}Sr$ and $^{88}Sr$, all of which are stable. $^{87}Sr$ is formed from the radioactive decay of $^{87}Rb$ and is expressed as a ratio against the stable $^{86}Sr$ isotope: $^{87}Sr/^{86}Sr$. Old, rubidium-rich materials, such as Palaeozoic granites, are characterised by high $^{87}Sr/^{86}Sr$ ratios, generally in the range of 0.710 and greater (Capo, et al., 1998). For geologically young rocks (<100 million year) with low rubidium concentrations, such as modern volcanic basalts, the $^{87}Sr/^{86}Sr$ ratio is low (i.e. 0.702 to 0.706) (Chesson, et al., 2012) . In groundwater, the strontium signature evolution along flow paths depends on the aquifer lithology, the rate of rock alteration and the intensity of water-rock interaction, which is conditioned by a time factor (Lasaga, et al., 1994). The $^{87}Sr/^{86}Sr$ ratio of stagnant water is generally higher than that of moving water due to a longer time of contact with the host rock (Santonia, et al., 2016) . The strontium concentration and isotopic

composition of surface water systems are largely defined by the mixing of strontium derived from two endmembers: (i) limestones and evaporites with high strontium concentrations and low $^{87}Sr/^{86}Sr$ ratios, and (ii) Silicate rocks, which contain lower strontium concentrations and radiogenic strontium (Palmer & Edmond, 1992).

Unlike stable isotopes of oxygen and hydrogen, the strontium isotope ratio is strictly controlled by rock-water interactions and is not affected by variations in atmospheric sources (McNutt, 2000). The extensive use of this element in both surface and groundwater studies is attributed to its significant occurrence in a wide variety of rocks and high solubility in aqueous solution (Bullen & Kendall, 1998; McNutt, 2000). Furthermore, the $^{87}Sr/^{86}Sr$ composition of natural waters is a useful tracer because the rock with which the water has been in contact introduces a unique isotopic signature to the water. This isotopic signature can be measured very precisely and hence followed along the flow path of the water (Lyons, et al., 1995).

# 2. METHODOLOGY

Potential sampling locations were selected in the west-draining river systems of nine major rivers along the west coast of southern Africa, namely the Berg, Verloren, Olifants, Groen, Buffels, Orange, Tsauchab, Tsondab and Kuiseb Rivers. Sample sites were identified by observation and personal communication with residents and local communities. Approximately six to eight locations were selected per catchment. For the Buffels, Tsauchab and Tsondab River catchments, more locations were selected based on prior knowledge of the locations of sampling sites. Sampling took place over a period of two weeks, from the 5th to the 20th of March 2016. A total of sixty-six samples were collected. Only three of these rivers (Berg, Olifants and Orange) were flowing, therefore groundwater samples were predominately collected.

## 2.1 Description of sampling catchments

Because of the extent of the field area, a separate description for each of the nine sampled west coast catchments is given, detailing the local geology, hydrology, climate and primary water uses in each region. The map below indicates the location of each of the sampling sites. Names are assigned according to the catchment in which the sample is situated, whether it is a surface or groundwater sample, and what number sample it represents in the catchment.

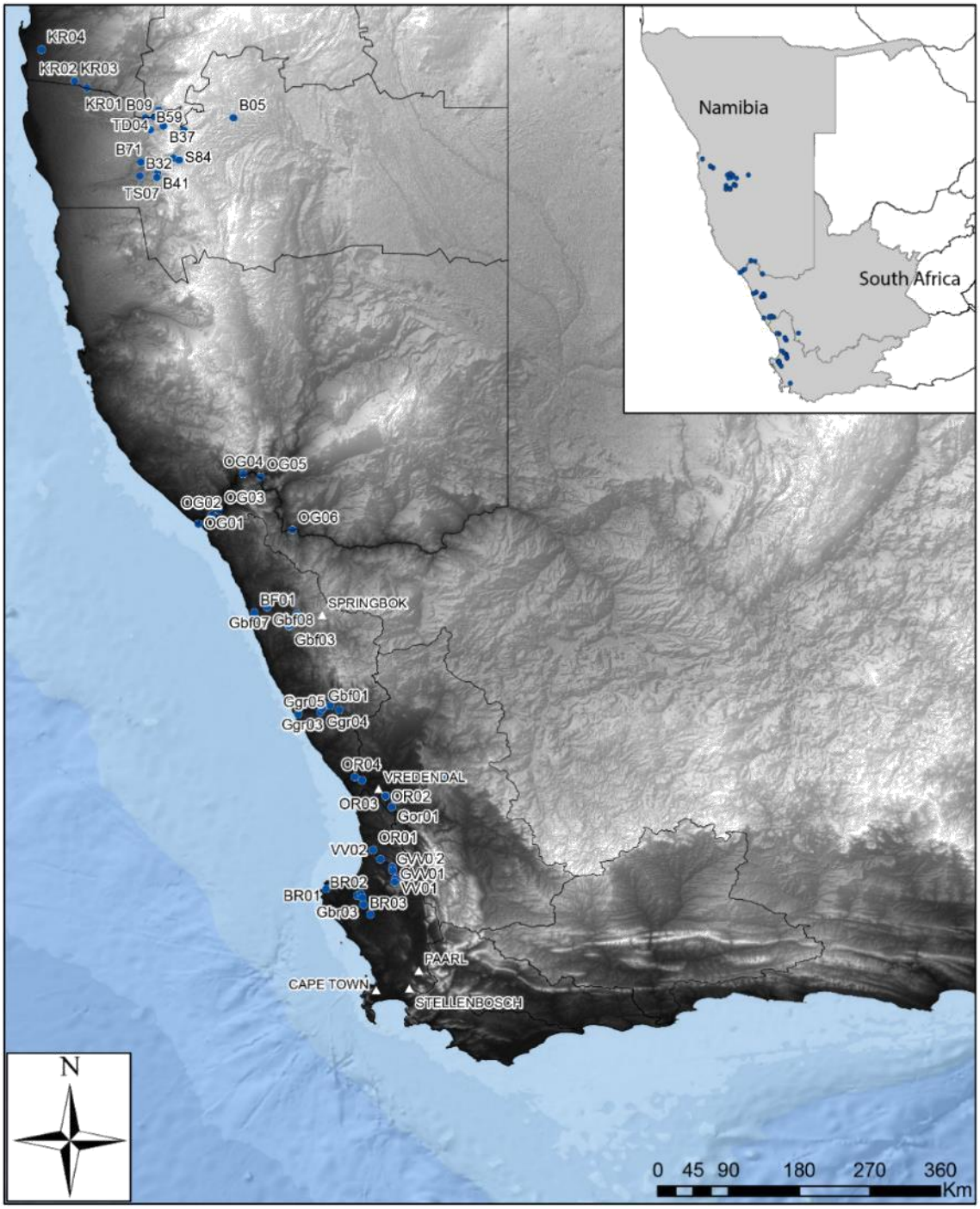


***Figure 3:*** *The location of the sampling sites within each of the catchments. Groundwater samples are denoted with a "G" at the start of the name. This is followed by the catchment in which the sample is situated as well as the sample number. For the Berg River, samples are labelled BR (surface water) or Gbr (groundwater); Verloren: VV/Gvv: Olifants: OR/Gor; Groen: Ggr (no surface water samples collected); Buffles: BF/Gbf; Orange: OG (no groundwater samples collected); Tsauchab: STS/TS; Tsondab: TD (no surface water samples collected); Kuiseb: KR (no surface water samples collected).*

### 2.1.1 Berg River

The Berg River is located just north of Cape Town in the Western Cape Province. The source of the Berg River is the Groot Drakenstein Mountains near Franschoek, approximately 80 kilometers East of Cape Town. The river, which is 300 kilometers long, enters the sea at the west coast town of Velddrif. The size of the Berg River catchment is about 9000 $km^2$ (de Villiers, 2007). The geology of the upper part of the catchment is dominated by sandstones and quartzites, Cape Granites in the middle and Tertiary to recent Aeolian deposits towards the coast (Cowling, et al., 1999). The primary use of Berg River water is for agriculture, particularly vineyards and fruit trees (De Villiers & Cadman, 2001). Samples were collected in the lower portion of the catchment, consisting predominately of coastal sands, along the 65-kilometer stretch from Piketberg to Velddrif. Six sampling sites were identified and sampled from this catchment.


***Figure 4:*** *Two samples from the Berg River catchment, (A) Gbr01 collected from Langrietvlei farm, near the town of Veldrif, and (B) BR02, sampled directly from the Berg River on Kersefontein farm, approximately five kilometres from Gbr01.*

### 2.1.2 Verloren River

The Verloren River is situated near Eland's Bay on the West coast of South Africa, approximately 180 kilometers north of Cape Town. The Verlorenvlei catchment is made up of a closed coastal estuarine-lake, a river with numerous tributaries and a reed-swamp system. The Verloren River and its tributaries are allogenic and non-perennial, recharging the swamp and lake system only during the Western Cape rainfall season (winter months). The source of the river is in the Piketberg and Olifantsrivier Mountains, from which it travels approximately 87 kilometers before reaching the coast at Eland's Bay. The catchment occupies an area of 1890 $km^2$ (Meadows, et al., 1996). The catchment falls within the Sandveld region of the West coast, which is characterised by shales of the Malmesbury Group, sandstone outcrops of the Table Mountain Group and Tertiary to recent unconsolidated sands (Baxter & Meadows, 1996). Shales of the Klipheuwel formation also occur within the catchment (Meadows, et al., 1996). The Verlorenvlei

wetlands provide a good source of natural veld grazing for sheep and cattle, and water is pumped from the vlei for the irrigation of crops. Samples were collected along a 30-kilometer stretch starting at Goudkop Guest farm, situated 47 kilometers North-West of Piketberg, to Eland's Bay, where the river enters the Atlantic Ocean. Four groundwater and two surface water samples were collected from this catchment.


***Figure 5:*** *Three of the samples collected from the Verloren River catchment: (A) Gvv03, sampled from a borehole on Namaquasfontein farm, (B) VV01, collected from a small mountain stream on Moutanshoek farm, and (c) Gvv04, from the farm Fonteinjie, situated near the West coast town of Elandsbaai.*

### 2.1.3 Olifants River

The Olifants River catchment is the second largest in South Africa and covers an area of just over 46 000 $km^2$ (Morant, 1984). The river rises in the Groot Winterhoek mountains of the Cedarberg mountain range, approximately 100 kilometers north-east of Cape Town. It runs north for 260 kilometers through mostly mountainous terrain to its Estuary at the small West coast village of Papendorp (Parkington, 1976). The main river and most of its tributaries drain Table Mountain Group sandstones and quartzites, and therefore carry a negligible silt load. The Doring River, which is the main tributary of the system, drains the more arid inland areas comprising soft tillites and shales, and thus contains a heavier silt load (Gore, et al., 1991). The mean annual precipitation over the Olifants River catchment is less than 300 mm, and occurs exclusively in winter (Pitman, et al., 1981). The catchment is almost entirely rural, and vegetation consists largely of indigenous fynbos on the mountain slopes and irrigated agricultural land in the valley of the mainstream (Soderberg & Compton, 2007). Irrigated agriculture is the predominant employer in this region, supporting a large citrus and wine-grape sector, supplemented by other produce such as tomatoes, deciduous fruits and vegetables (Gore, et al., 1991). The Clanwilliam and Bulshoek dams situated along the river's watercourse provide water for these commercial farmers and agricultural-related industry, as well as to the several small towns dotted along the Atlantic Ocean seaboard (King, et al., 1998).


***Figure 6:*** *Two sampling sites from the Olifants River catchment, collected from private farms within two kilometres of each other, (A) OR04, collected from a portion of the Olifants River running through Elrhyn farm, and (B) Gor04 from a borehole on the farm of Koekenaap. (C) OR06, a surface water sample collected from the Olifants River approx. 15 km outside Lutzville.*

### 2.1.4 Groen River

The Groen River is approximately 67 kilometers long and occurs in the Namaqualand region of the Northern Cape Province. The river originates in the Kamiesberge range, which is made up of large granite-gneiss intrusions and flows into the Atlantic Ocean in the Namaqua National Park, approximately 120 km NNW of Strandfontein. The size of the Groen river catchment is 4500 $km^2$. It is situated within the Namaqualand Metamorphic Complex and comprises predominately bedrock of quartzo-feldspathic gneisses of the Kookfontein subgroup, which typically outcrop on koppies and mountains as smooth rock faces or large rounded boulders (Albat, 1984). Soubattersfontein quartzite is also of geological significance in the catchment region and occurs as low-lying ridges or koppies. From about 30 kilometers inland from the mouth of the river, the geology of the catchment transitions to coastal plain sandy material of Aeolian origin (De Villiers & Cadman, 2001). The catchment falls within the winter rainfall region of the country and is associated with low but reliable rainfall patterns. The mean precipitation of the coastal duneveld area is below 100 mm per annum, and consequently the population density in the region is low and farming is limited to small livestock such as goats and sheep (Adams, et al., 2004). As the Groen River was not flowing at the time of our sampling trip (according to a local farmer, it flows once every five years) only groundwater samples were collected from this catchment.

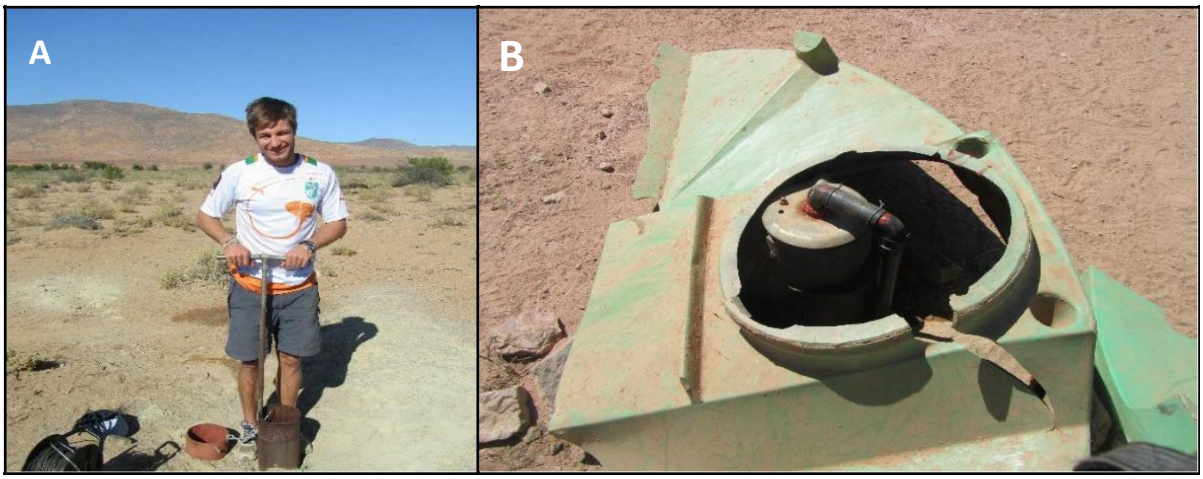


***Figure 7:*** *Only borehole samples were collected in this catchment. (A) Ggr02 sampled from Dikdoorn farm in the Groen River bed and (B) Ggr03, collected from a tank with flowing water a few meters from the borehole. Both samples were obtained from private farms on a district road off the N7 towards the Atlantic Ocean.*

### 2.1.5 Buffels River

The Buffels River, a 250-kilometer-long river situated in the Northern Cape Province, is the largest ephemeral river in Namaqualand. The area of the Buffels River catchment is approximately 9250 $km^2$ (Benito, et al., 2010). It flows from the Kamies Mountains (1200–1600 m in elevation) and discharges into the Atlantic Ocean at the small town of Kleinzee. The geology of the Buffels River catchment includes a bedrock of impermeable metasedimentary rocks, basic granites and ultrabasic intrusive rocks. These lithologies are cross-cut by basement faults (Marais, et al., 2001). Much of the planar landscape in Namaqualand (the area in which both the Buffels and Groen Rivers occur) is associated with extensive sheets of calcrete overlain by red wind-blown sands, which are late Pleistocene to Holocene in age (Pickford, et al., 1999).

Winter rainfall occurs in this area from May to September and is usually associated with frontal systems that provide drizzle and gentle rainfalls (Benito, et al., 2010). The water from the Buffels River catchment is used as a source of drinking water to the 2200 people living in five communal villages along the basin, as well as the livestock of goats, sheep and cattle. Knowledge of borehole locations and established contacts in the area due to prior sampling of this catchment allowed for more samples to be collected. In total, twenty groundwater samples and one spring water sample were collected from the Buffels River catchment.

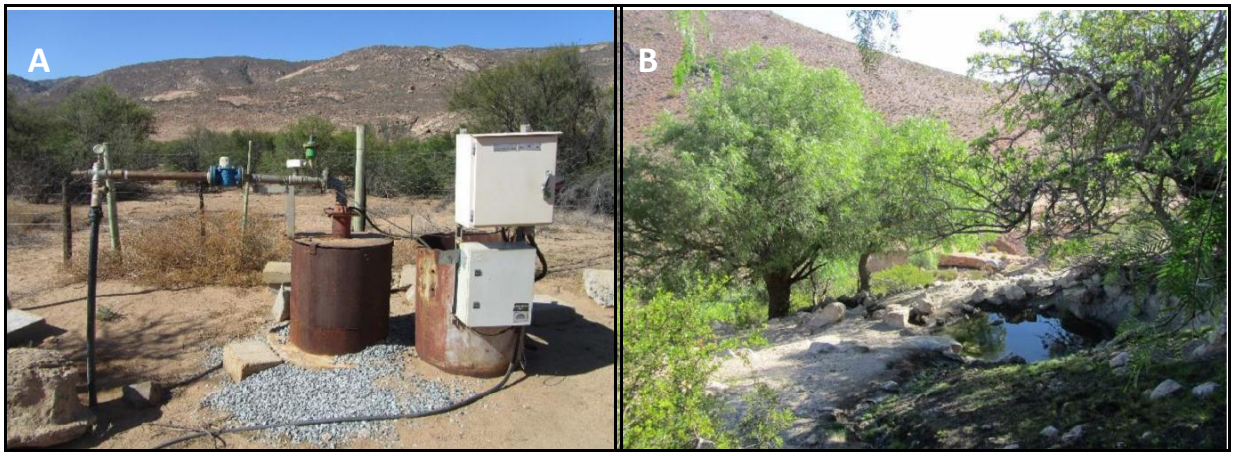


***Figure 8:*** *(A) Gbf08, collected from the De Beers borehole outside Buffels River and (B) BF01, the only surface water sample collected from this catchment, from "Ghost" spring outside Kommegas.*

### 2.1.6 Orange River

The Orange River, which is approximately 2350-kilometers long, is the largest westward-flowing river in southern Africa (Tooth & McCarthy, 2004). It rises in Lesotho, in the Drakensberg Mountains, and flows into the Atlantic Ocean at Alexander Bay, just south of the Namibian border. The area of the Orange River catchment is approximately 892 000 $km^2$. The region through which the River flows significantly influences the temperature of the water. The climate progressively changes from cool and wet in the east to arid and dry conditions moving westwards. The Orange River crosses several different geological lithologies and structures along its length. The geology around the portion of the river that was sampled (Alexander Bay to Vioolsdrif) consists of Proterozoic metamorphic and igneous rocks of the Kaapvaal Craton and Namaqualand mobile belt, overlain by a heterogenous succession of Karoo Supergroup strata (consisting of intervals of sandstone, siltstone and mudstone) (Tooth & McCarthy, 2004). In the lower reaches of this catchment, the River water is used predominately for irrigation. A total of six surface water samples (including one from the confluence of the Orange and Fish Rivers) were collected from this catchment.


***Figure 9:*** *(A) OG03, sampled from the Orange River on the farm Brandkoras, approximately fifteen kilometers from the Namibian border, and (B) OG06, collected from our campsite at Amanzi River trails, just after the border.*

### 2.1.7 Tsauchab River

The 100 kilometer-long ephemeral Tsauchab River is situated in the Southern Naukluft region, approximately 270 kilometers South-West of Windhoek. The Tsauchab River catchment has an area of 4000 $km^2$ and is bordered by the Naukluft Mountains to the North, the western escarpment' foothills to the East, and the Zaris Mountains to the South (Brook, et al., 2006). The River extends for 40-80 kilometers into the Western sand sea before terminating into a playa (Sossusvlei).

The climate in the area is hyper-arid to arid, with mean annual rainfall typically not exceeding 15 mm. The geology of the catchment is subdivided into two distinct regimes based on the depositional setting. These are (i) Non-depositional interdunes and (ii) Depositional interdunes. The geology of the latter includes, in addition to Aeolian sands, lacustrine carbonates, silts, evaporites and clays. Non-depositional interdune environments consists of a bedrock of Precambrian granites and schists and Late to Early Pleistocene fluvial deposits (Lancaster & Teller, 1988). The surface of Sossus Vlei is covered in a layer of light grey silt with deep dessication cracks towards the centre of the pan (Brook, et al., 2006). No surface samples were collected from the Tsauchab River, as it was not flowing, however eight borehole and three spring samples were collected from this catchment.


***Figure 10:*** *(A) STS01, sampled from a spring on the camping grounds of Hauchabfontein, with distinct conglomerate cliffs enclosing the water source, and (B) B41, collected from a borehole at Little Sossus Lodge guest farm.*

### 2.1.8 Tsondab River

The Tsondab River lies just south of Solitaire, a small town situated in the Khomas Region of central Namibia, near the Namib-Naukluft National Park. It is a 110-kilometer long ephemeral river originating in the Naukluft Mountains, and extends for 40-80 kilometers into the Namib Desert Sand Sea in well-defined valleys before terminating amongst the dunes in an extensive playa, Tsondabvlei (Lancaster & Teller, 1988). The catchment area of the Tsondab River is small, at only 3640 $km^2$ (Stengel, 1970). Rainfall in the catchment is unreliable and low (ranging from 100 mm to less than 50 mm per year), with exceptionally high evaporation rates (Lancaster, 1984).

The most prominent geological feature in this region is the Tsondab Sandstone Formation, which comprises thick horizontal cross-stratified beds of well-jointed red sandstone, and weathers to provide sand for the sand sheets and linear dunes of the Namib Desert (Marker, 1979). This formation is the principle bedrock geology in the lower parts of the catchment, while the upper parts comprise limestones, shales and dolomites of the Naukluft Nappe Complex. These sediments provide distinctive oblate and bladed-shaped clasts of a pale blue or black colour which dominate the lithology of fluvial deposits in the Tsondab Basin (Lancaster, 1984).

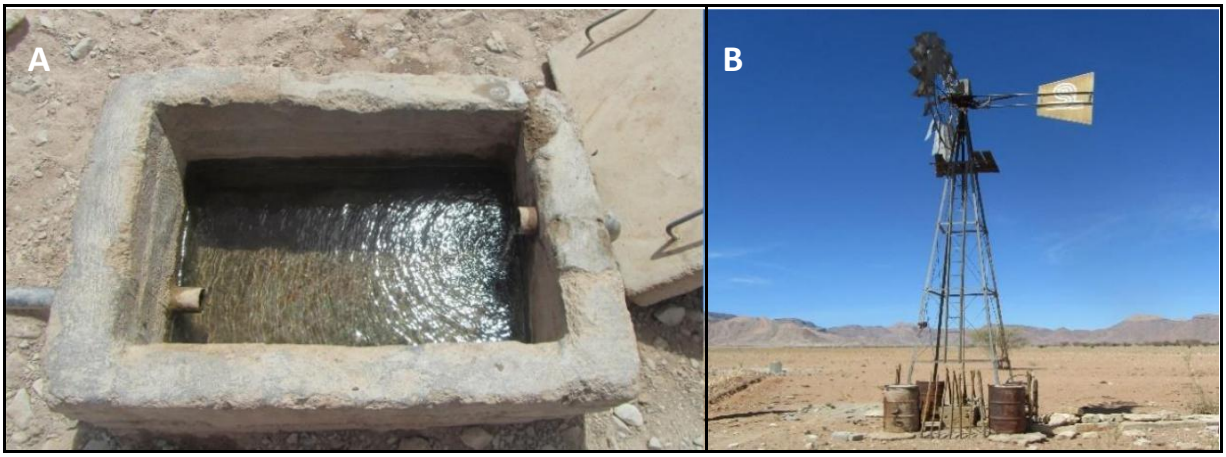


***Figure 11:*** *(A) B37, obtained from a borehole on Panorama farm, and (B) TD04, collected from Ababis guest lodge and farm, approximately five kilometres from Panorama.*

### 2.1.9 Kuiseb River

The Kuiseb River, which is approximately 560-kilometers long, is one of Namibia's longest ephemeral rivers, and drains the Great Escarpment of western Namibia with a catchment area of ~15 500 $km^2$ (Jacobson, 1995). It originates in a semiarid (250-350 mm/yr), high-elevation (~1700m) plateau, and crosses the hyperaird Namib Desert (10-50 mm/yr) before flowing into the Atlantic Ocean near Walvis Bay (Benito, et al., 2009). Most of the recharge to the Kuiseb River occurs in the 6600 $km^2$ area to the east of the Great Escarpment, where relatively wetter headwaters generate annual floods that overcome the transmission losses along its course (Morin, et al., 2009). In the middle-lower Kuiseb (lower 100 km), the river develops an extensive sandy, braided alluvial channel and floodplain (Benito, et al., 2009).

The geology in and around the Kuiseb Canyon comprises outcrops dominated by Precambrian rocks of Damara Orogen, typically exposed near Gobabeb. These outcrops include schist exposures of the Kuiseb Formation, gneissic feldspathic quartzites of the Khan Formation and dolomitic limestones of the Karibib formation (Eckardt, et al., 2013). To the south of the Kuiseb River is the Pliocene to Recent sand sea, underlain by Early to Middle age sediments of the Tsondab Sandstone Formation (TSF), which is exposed in small interdunal pockets on the south of the Kuiseb River catchment near Gobabeb. These exposed outcrops are overlain by deposits of the Karpfenkliff Conglomerate Formation, composed of calcified alluvial fan and braided channel deposits, which also outcrop on the Kuiseb canyon terraces (Ward, 1988). To the north of the Kuiseb River are extensive flat plains composed of schist and granite gravels.

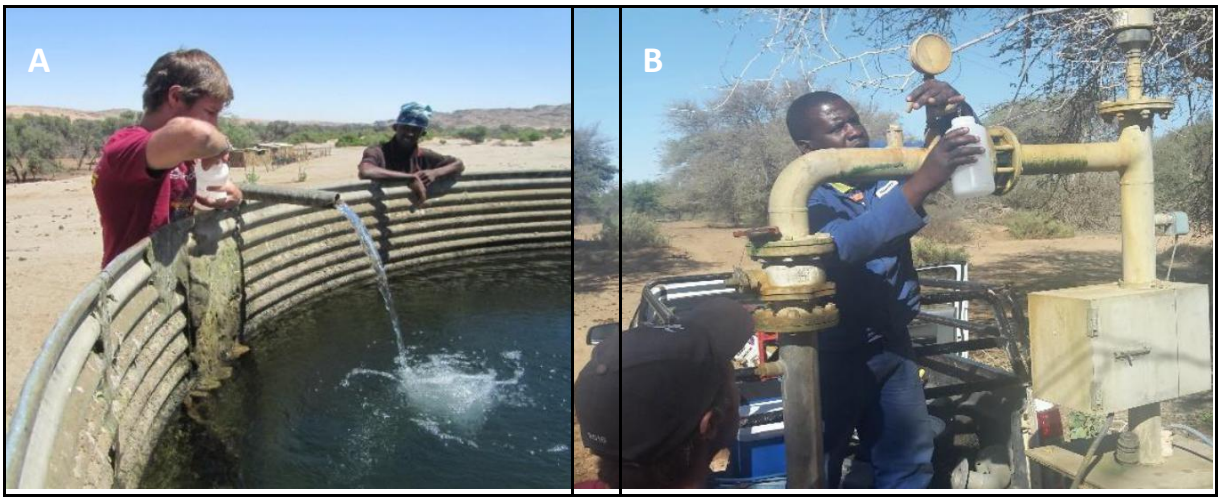


***Figure 12:*** *(A) Kr01 collected from a steel pipe running into a reservoir situated forty meters from the borehole, in the town of Homeb, and (B) KR04, sampled from a Nam Water municipal borehole in the Kuiseb River bed, near the town of Walvis Bay in Namibia.*

## 2.2 Sample Collection Techniques

River water samples were collected along their course, starting approximately 30 kilometers inland from the sea and ending just near the mouth of the river. Borehole samples were collected as close to the source as possible. For most of the borehole sites, samples were collected directly from the borehole. Where there was no take-off point at the borehole itself, samples were collected from nearby taps or pipes. Water from boreholes containing pumps was purged until a steady pH and EC state was achieved before samples were collected. Prior to bottling of the sample water, in situ EC (electrical conductivity), Eh (oxidation-reduction potential), pH and temperature were measured using an ExTech EC500, ORP instrument probe. The probe was calibrated daily with pH 4 and 7 solutions, and a 1413µS/cm EC solution. Where possible, the depth to water level in the boreholes was measured using a dip meter. Most of the borehole samples were collected from boreholes drilled for stock watering. They were equipped with wind mills and therefore water levels could not be measured continuously. All samples were collected in 1000ml Nalgene bottles and 50ml PP conical tubes at the sample sites. Prior to field work, the Nalgene bottles were filled with 1% $HNO_3$ and allowed to stand overnight. They were then rinsed with milli-Q water, filled with 1% $HNO_3$ and stood overnight again before rinsing twice with milli-Q. All collection vessels were rinsed with the water sample to be collected several times before collection. Samples for cations and anions were then filtered through 0.45µm cellulose acetate filters into the 50ml PP conical tubes. The cation samples were acidified to a pH less than 2 with concentrated ultrapure $HNO_3^-$. Samples for O, H and Sr isotope analysis were also filtered through 0.45µm cellulose acetate filters and transferred into acid washed 250ml (O and H) and 50 ml (Sr) polyethylene (PE) bottles. The Mg and Ca samples were filtered twice, firstly through a 0.45µm filter, followed by a 0.25µm filter, prior to being transferred into 50ml acid washed PE bottles. All collection vessels were filled completely and stored at 4°C until they were analysed.

## 2.3 Analytical Procedures

### 2.3.1 Major Ion Chemistry

The analysis of major cations and trace elements was performed on field-acidified samples by means of ICP-MS/AES in the Mass Spectrometry Laboratory in the Central Analytical Facility at Stellenbosch University, using an Agilent 7700 ICP-AES and 7700 ICP-MS respectively. Major anion concentrations were determined using a Waters IC-Pak 717 Autosample-conductivity detector-Agilent 1120 pump in the Department of Soil Science, also at Stellenbosch University. A charge balance was calculated using the following major anions and cations: $Cl^-$, $Br^-$, $NO_3^-$, $SO_4^{2-}$, $Ca^{2+}$, $K^+$, $Mg^{2+}$ and $Na^+$ as well as laboratory alkalinity (mg. $L^{-1}$ $HCO_3^-$). The samples produced good charge balances within a 10% difference.

### 2.3.2 Stable isotopes of oxygen and hydrogen

Stable oxygen and hydrogen isotopes were analysed at the Stable Isotopes Laboratory at the University of Lausanne in Switzerland, using a Picarro L1102i Wavelength-Scanned Cavity Ring-Down Spectroscopy (WS-CRDS) system. For the analysis, approximately 1.7ml of the filtered sample waters were transferred into small glass vials and sealed with septum screw caps. Three sequences were required to analyse all the samples. Each sequence was calibrated using two different internal standards: tap water from the city of Lausanne (INH) (with long term averages of -5‰ ($\delta^{18}O$) and - 18‰ (δD)), and and a light isotope standard (LIPE) from Tallinn, Estonia (with long term averages of - 3 ($\delta^{18}O$) and -12‰ (δD)). These standards are periodically calibrated against the international VSMOW (Vienna Standard Mean Ocean Water), and SLAP (Standard light Arctic precipitation) standards of the IAEA (International Atomic Energy Agency). The INH and LIPE standards were measured repeatedly within each sequence, producing values identical or very similar to the recorded long-term averages. Prior to analysis, distilled water was injected into the vaporisation chamber, followed by injections of the first sample to clean the chamber. Once the analyses were complete, an average of the last five measurement peaks was taken to calculate the raw value of the isotopic composition of each sample. Isotopic compositions are reported in the common delta notation (per mil deviation of the isotope ratio of the sample relative to that of the internal standard, VSMOW):

$$\delta\ (‰) = \left(\frac{\text{Rsample-Rstandard}}{\text{Rstandard}}\right) \times 1000 \qquad (4)$$

Where R represents the $^{18}O/^{16}O$ or D/H ratio isotope.

### 2.3.3. $\delta^{13}$C-Dissolved Inorganic Carbon (DIC)

The stable isotope compositions of $\delta^{13}$C-DIC were analysed in the Stable Isotopes Laboratory at the University of Lausanne using a Gasbench II coupled to a ThermoFinnigan Delta plus XL isotope ratio mass spectrometer (IRMS). Prior to sample analysis, glass vials were injected with concentrated phosphoric acid ($H_3PO_4$), sealed and flushed with helium. The vials were then injected with 1.5 ml of the sample and returned to the Gasbench for analysis. Each sequence was calibrated using an internal laboratory standard (Carrara Marble, $\delta^{13}C$ = 2.05 ‰ VPDB). Measurements of the carbonate standards were made per the method presented by Spoetl and Vennemann (2003). After completion of the analyses, an average of the last nine peaks was taken to calculate the raw value. Measured isotopic ratios are reported in the common delta notation (per mil deviation of the isotope ratio of the sample relative to that of the internal standard VPDB (Vienna Peedee Belemnite)).

### 2.3.4 $^{87}Sr/^{86}Sr$ Ratios

$^{87}Sr/^{86}Sr$ isotopic ratios were measured at the Department of Geological Sciences at the University of Cape Town. The analytical process consists of two stages: the preparation of samples (wet chemistry) and the running of the prepared samples through the mass spectrometer (Sr chemistry). Preparation involves decanting the filtered samples into 6 ml aliquots, which are subsequently dried down in a Teflon beaker. $HNO_3$ is then added to the remnant solution and again, the aliquots are dried down. After the samples are dried down for the second time, 1.5 ml of 2M $HNO_3$ is added. The resultant solutions are now ready for Sr chemistry, which involves introducing the sample into a standard cation exchange column, thereby extracting the Sr for analysis. The 200 ppb 0.2% $HNO_3$ solution is then ready to be analysed for $^{87}Sr/^{86}Sr$ ratios. These ratios are measured on a NuPlasma HR MC-ICP-MS, using the standard reference NIST987, with a value of 0.710255. The Sr isotopic data was corrected for Rubidium interference as well as instrumental mass fractionation using the exponential law and an $^{87}Sr/^{86}Sr$ value of 0.1194.

### 2.3.5 Magnesium stable isotopes

Mg isotopic analysis was carried out on a Thermo Neptune multi-collector inductively coupled plasma mass spectrometer (MC ICP-MS) at The Higgins Laboratory at Princeton University, United States. Prior to isotopic analysis, cations in the samples are separated using a coupled Dionex ICS5000 automated ion chromatography system with an AS-AP autosampler, capable of sample collection. A chromatograph for every sample shows a peak in conductivity when each cation system elutes from the resin-filled column. The autosampler is then programmed to collect the target cation, in this case $Mg^{2+}$, by elution time, excluding the peaks of other matrix ions.

Mg isotope analysis typically requires ~500ng of $Mg^{2+}$, diluted to 150–200 ppb in 2% $HNO_3^-$. Sample-standard-sample bracketing is used to correct for instrumental mass fractionation. Sample and standard solutions are carefully diluted to the same concentration to minimise concentration-dependent isotope effects. External precision is based on the long-term reproducibility of replicate standard analyses with a carbonate-like matrix, which are processed regularly with each batch of samples, and is 0.11% for $\delta^{26}Mg$. The accuracy of these analytical methods is confirmed by measurement of inter-laboratory standards. Mg isotope ratios are reported relative to the standard DSM-3. For $Mg^{2+}$, $\delta^{26}Mg$ of the Cambridge-1 standard measured at −2.59 ± 0.06% agrees well with measurements of other laboratories (Galy, et al., 2002). As a check for mass-dependent variations in the measured $\delta^{26}Mg$ values, the results of the analyses were evaluated on a triple-isotope plot (e.g. $\delta^{25}Mg$ vs $\delta^{26}Mg$) and samples that deviated significantly from the terrestrial mass-dependent line were discarded.

# 3 RESULTS

In total, 66 samples were collected from boreholes, rivers and springs along the west coasts of South Africa and Namibia. For ease of analysis, the field area has been subdivided into three regions. The Berg, Olifants and Verloren Rivers comprise the southern region; Groen, Buffels and Orange Rivers the central region and Tsauchab, Tsondab and Kuiseb Rivers the northern region. This grouping is based primarily on the proximity of the catchments to one another. Catchments situated close to one another share similar features in terms of climate, geomorphology, geology and, presumably, hydrology. Surface and groundwater samples will also be compared in the analysis.

## 3.1 Field parameters

EC, pH, Oxidation-Reduction potential (ORP) and temperature were measured in the field. The surface water samples had on average higher pH and EC values and showed less variation than the groundwater samples. The average pH and EC values for the surface samples were 7.62 and 1800 µS/cm respectively. The highest recorded pH values were obtained for the Orange River samples, which all exceeded a pH of 8 (figure 13).

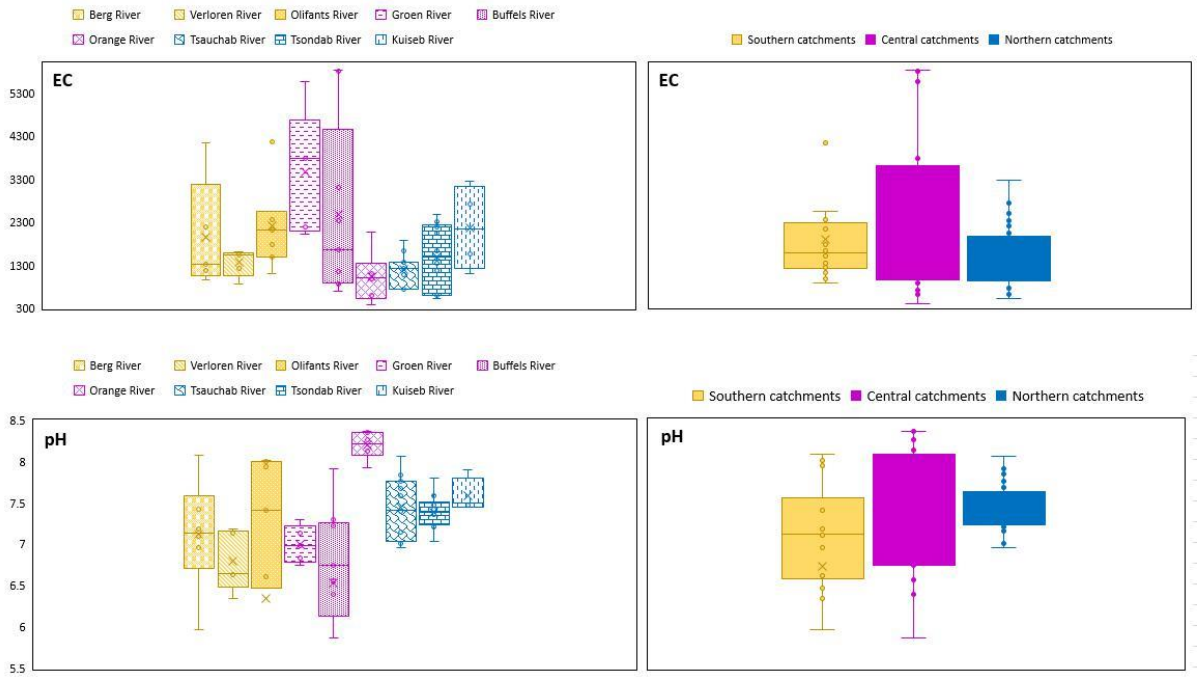


***Figure 13:*** *pH and EC values (µS) for both surface and groundwater samples from the three catchment regions (right) as well as the individual catchments (left).*

The temperatures of the surface water samples were lower than for the borehole samples, and did not exceed 25°C. A very narrow range was observed in the ORP values obtained for the surface water samples (132-196 mV) compared to the groundwater samples (73-237 mV), and overall the surface

water ORP values were higher (157 mV). The groundwater samples had pH values between 3.99 and 8 (Gvv04 and Gor04), EC values ranging between 511 µS/cm and 5840 µS/cm (B59 and Gbf07) and temperatures generally above 25°C. The highest temperatures were observed in groundwater samples obtained from boreholes in the Tsauchab River catchment, which all exceed depths of 100 meters. Groundwater samples from the Buffels and Groen River catchments had the highest EC values, mostly above 2000 µS/cm.

## 3.2 Hydrochemistry

### 3.2.1 Major ion chemistry

Sodium concentrations are generally lower in the surface water samples when compared to the groundwater samples, with values between 9 and 747 mg.L$^{-1}$. Surface water samples BR01 (collected from the mouth of the Berg River) and OG01 (collected from the mouth of the Orange River) are outliers with significantly higher concentrations of 9634 and 6903 mg.L$^{-1}$ respectively. The groundwater samples contain higher concentrations between 27 and 2857 mg.L$^{-1}$. The highest sodium concentrations were measured in the groundwater samples collected from the Groen River catchment, which all exceed 1000 mg.L$^{-1}$. Both magnesium and calcium show very similar trends to sodium. Higher magnesium concentrations between 9 and 1597 mg.L$^{-1}$ were measured in the groundwater samples while the surface water samples showed lower values between 1 and 830 mg.L$^{-1}$. For calcium, the concentration range for the groundwater samples was 8 and 629 mg.L$^{-1}$, and for the surface water samples between 1 and 117 mg.L$^{-1}$. BR01 is again an outlier and contains significantly high magnesium and calcium concentrations of 1147 and 417 mg.L$^{-1}$ respectively. Samples collected from both the Buffels and Groen River catchments have the highest magnesium and calcium concentrations for the sample set. Potassium concentrations are relatively uniform throughout the surface and groundwater samples with concentrations between 0.06 and 83 mg.L$^{-1}$, with BR01 and OG05 as outliers.

The chloride concentrations are significantly higher in the groundwater samples compared to the surface water samples, with concentrations ranging between 32 and 4285 mg.L$^{-1}$. Groundwater samples Gbf05 and Gbf07, both collected from the Buffels River catchment, are outliers with very high chloride values of 6405 and 8841 mg.L$^{-1}$ respectively. The surface water samples have much lower chloride concentrations between 4 and 511 mg. L$^{-1}$, except for the outliers OR03 (1055 mg.L$^{-1}$) and OR04 (1326 mg.L$^{-1}$), collected from the Olifants River, and OG01 (3830 mg.L$^{-1}$), from the Orange River. As for chloride, higher sulphate concentrations between 23 and 836 mg.L$^{-1}$ are observed in the groundwater samples compared to the surface water samples, which vary from below the detection limit of 2 to 374 mg.L$^{-1}$. Surface water sample BR01 is an outlier with an exceptionally high sulphate concentration of 2483 mg.L$^{-1}$. Boron concentrations are also higher in the groundwater samples, particularly those collected from the Groen River catchment, which have values ranging from 7 to 13 mg.L$^{-1}$. For the rest of the groundwater samples, the boron concentrations are relatively low, varying from 0.21 to 3 mg.L$^{-1}$. For the surface water samples, only two samples (both from the Olifants River catchment) displayed boron concentrations above the detection limit, with values of 3.26 mg.L$^{-1}$ (OR03) and 4.09 mg.L$^{-1}$ (OR04). The only samples containing any significant nitrate concentration were those collected from the Tsauchab catchment (both ground and surface water samples were collected) and the Tsondab catchment, with concentrations ranging

from 3 to 36 $mg.L^{-1}$ and 3 to 40 $mg.L^{-1}$ respectively. Nitrate concentrations were also recorded in only four other samples: Gvv01 (24 $mg.L^{-1}$) and Gvv04 (32 $mg.L^{-1}$), both collected from the Verloren River; Gor04 (from the Olifants River catchment) with a concentration of 32 $mg.L^{-1}$ and Gbf06 (obtained from a borehole next to the water treatment ponds at Spektakel mine, Buffels River) which recorded the highest nitrate concentration of 44 $mg.L^{-1}$ for the sample set.

Total alkalinity ($mg.L^{-1}$ $HCO_3^-$) was calculated based on titration measurements obtained in the laboratory. Higher average alkalinity concentrations are observed in surface water samples, with values ranging between 2.9 and 184.6 $mg.L^{-1}$. Sample OR04, from the Olifants River catchment, is an outlier for the sample set, with an anomalously high alkalinity concentration of 533.5 $mg.L^{-1}$. The groundwater samples have alkalinity values between 12.3 and 203.2 $mg.L^{-1}$. Samples collected from the Olifants River catchment show the highest alkalinity concentrations overall (26-203 $mg.L^{-1}$), while groundwater sample B71 from the Tsauchab catchment represents an outlier for the groundwater samples, with a relatively high alkalinity of 462.4 $mg.L^{-1}$.

Several molar ratios were assessed for the catchment samples (figure 14). The Na/Ca ratios were on average the lowest for the groundwater samples, although they show a greater range from 0.4 to 13.15. For the surface water samples, the Na/Ca ratios vary between 0.73 and 8.84, with samples BR01 (collected from the Berg River) representing an outlier with a value of 23.11. This same trend is observed for K/Na molar ratios. For Mg/Ca, both the groundwater and surface water samples show similar trends, with groundwater samples ranging between 0.17 and 1.97.and surface water samples from 0.12 to 1.53. The groundwater samples also recorded higher Na/Cl ratios when compared to the surface water samples, with values between 0.02 and 12.50. The surface water samples range from 0.07 to 3.07 with two outliers, VV02 (taken from the Verlorenvlei catchment) with a value of 8.35, and OG03 (collected from the Orange River) which recorded an anomalously high value of 23. There is a considerable overlap for Cl/Br ratios between all the groundwater and surface water samples ranging from 72.15 to 524.9 mg/L.

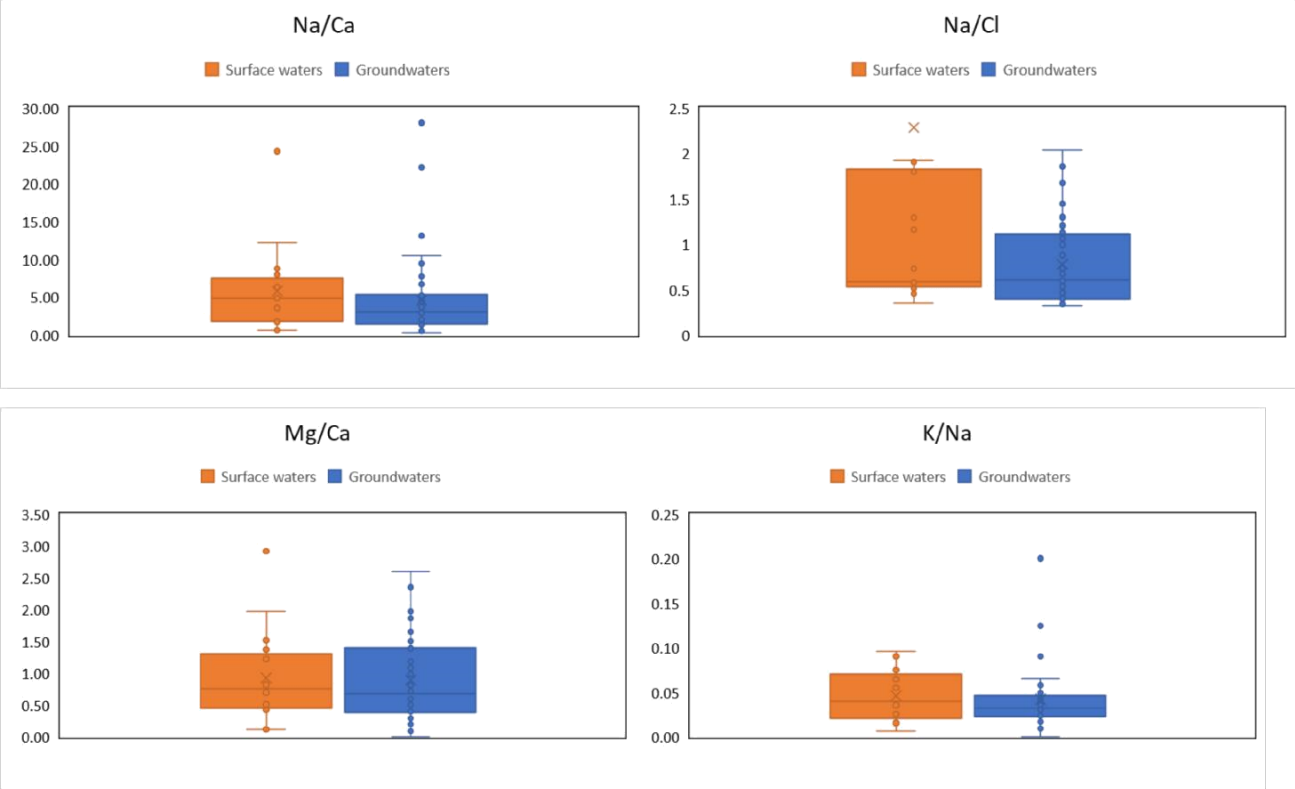


***Figure 14**: Box-and-whisker diagrams indicating variability in the molar ratios discussed: Na/Ca, Na/Cl, Mg/Ca and K/Na. Surface water samples are indicated in orange and groundwater samples in blue.*

### 3.2.2 Trace elements

Of the twenty-one trace elements analysed, only three (Li, B and Sr) showed any trends between the surface and groundwater samples, with the exception of all trace element concentrations measured for sample Gbf06. For this sample, which was obtained from a borehole next to the Spektakel mine water treatment pools in the Buffels River catchment, the concentrations of many of the elements analysed was high enough to warrant them as major elements. In addition to the high Li (1.40 mg/L), Sr (6 mg/L) and B (2.35 mg/L) concentrations measured for Gbf06, anomalously high concentrations of Al (57 mg/L), Mn (76 mg/L) and Fe (465 mg/L) were also detected.

Surface and groundwater samples are well differentiated in lithium concentrations with higher concentrations observed in the groundwater samples (2.46 and 436 µg/L), in particularly the Groen (15-436 µg/L), Tsauchab (80-316 µg/L) and Tsondab (7-188 µg/L) River catchments. The surface water samples contained much lower concentrations of Li, with values ranging between 0.3 and 131 µg/L. However, surface water samples from the Tsauchab catchment are outliers with relatively higher Li concentrations (211 to 264 µg/L). Boron is present in significantly higher concentrations in the groundwater samples when compared with the surface water samples. The groundwater samples have concentrations between 48 and 2409 µg/L, while the surface water samples contain lower concentrations between 8 and 252 µg/L. Samples BR01 (from the mouth of the Berg River - 4 mg/L), OG02 (from the mouth of the Orange River – 3 mg/L), OR03 (a surface water sample from the Olifants River – 1.6

mg/L) and OR04 (a surface water sample from the Olifants River – 1.7 mg/L) are all outliers for the surface water samples because of their significantly higher boron concentrations. Like lithium and boron, strontium concentrations are higher in the groundwater samples when compared with the surface water samples.

Strontium concentrations for the groundwater samples range between 86.39 µg/L and 6 mg/L, while the surface water samples vary from 2.93 µg/L and 3.6 mg/L. Apart from two outliers with anomalously high Sr concentrations compared with the other samples collected from their respective catchments (BR01 from the Berg River –7 mg/L; OG01 from the Orange River mouth – 5 mg/L), Sr shows a relatively good differentiation among the various catchments. For both surface and groundwater samples, very high concentrations were observed in the Tsauchab catchment. Additionally, Sr was present as a major element in all the groundwater samples collected from the Groen, Buffels and Tsondab River catchments (no surface water samples were collected) with concentrations exceeding 1000 µg/L.

## 3.3 Stable isotopes

### 3.3.1 $\delta^{18}O$ and $\delta D$ Ratios

The standard $\delta D$ versus $\delta^{18}O$ plot displaying the results from both the groundwater and surface water samples collected throughout the field area in reference to the Global Meteoric Water Line (GMWL) and the Local Meteoric Water Line (LMWL) for southern Africa is displayed in Figure 15. The results obtained for this study correlate well with both the GMWL and the LMWL.

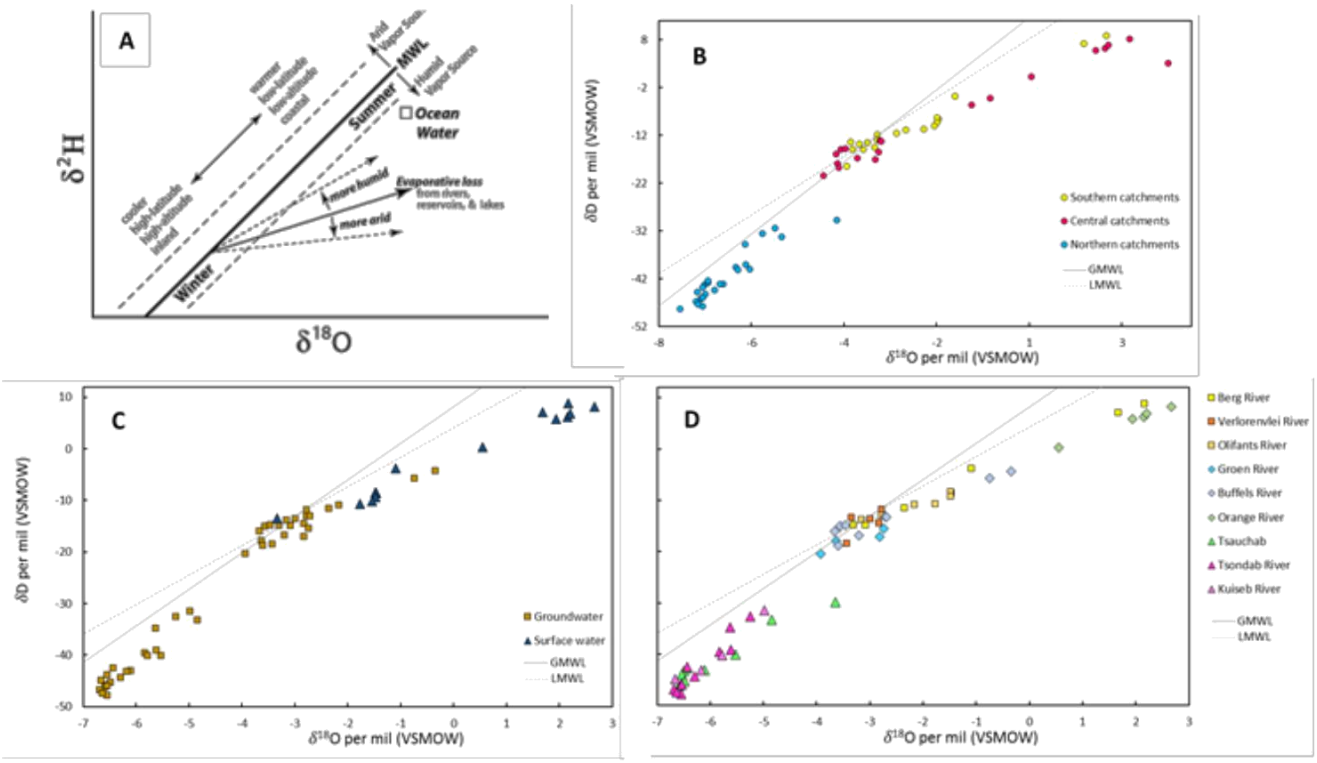


***Figure 15:*** *(A) Summary diagram of the various hydrologic processes affecting the oxygen and hydrogen isotopic composition of water. (B-D) The relationship between $\delta^{18}O$ and $\delta^{2}H$ with the GMWL and LMWL for (B) the three catchment regions, (C) surface and groundwater samples and (C) the individual catchment areas.*

Comparison of the δD and $\delta^{18}O$ values shows that samples from catchments in the northern region (Tsauchab, Tsondab and Kuiseb) are depleted in the heavy isotopes relative to the samples from catchments in the southern and central regions. The Northern catchments have $\delta^{18}O$ values between -7.03 and -3.65‰ and δD values ranging from -48.40 to -29.80‰. Samples from these catchments are well distributed along the GMWL. The southern and central catchments plot higher up on the GMWL and display a considerably wider range in δD and $\delta^{18}O$ values (δD: -3.43 to 2.17‰; $\delta^{18}O$: -18.50 to 8.80‰). Samples collected from the central catchments have δD values between -20 and 8.20‰ and $\delta^{18}O$ values between -3.93 and 3.51‰. Samples from the Verlorenvlei, Buffels and Groen River catchments are clustered about the intersection of the GMWL with the LMWL, with a narrow range of $\delta^{18}O$ (-2.7 to -4‰) and δD (-12 to -20‰) values; while samples collected from Olifants, Berg and Orange River catchments record a wider range of $\delta^{18}O$ and δD between -2 to 4‰ and -11 to 9‰ respectively. A prominent evaporation trend is also observed by the samples in comparison to the LMWL. Samples collected from the Orange River catchment were the most enriched in the heavy isotopes relative to the other samples in the sample set, with only positive $\delta^{18}O$ and δD values observed.

### 3.3.2 $\delta^{13}$C-DIC

The $\delta^{13}$C-DIC values for all the samples vary between -17.7‰ and -3.8‰. Only one of the samples, obtained from a borehole on the banks of the Tsondab River, recorded a positive value of 1.75‰. The

$\delta^{13}$C-DIC values for groundwater samples collected from the southern region catchments show on average lower values (-11‰) than the central (-8.7‰) and northern region catchments (-8.2‰). Most of the groundwater samples recorded more negative values than the surface water samples. Only the northern catchment samples from the carbonate-hosted Tsauchab and Tsondab aquifers showed $\delta^{13}$C-DIC values higher than -7‰, consistent with values measured in the surface water samples.

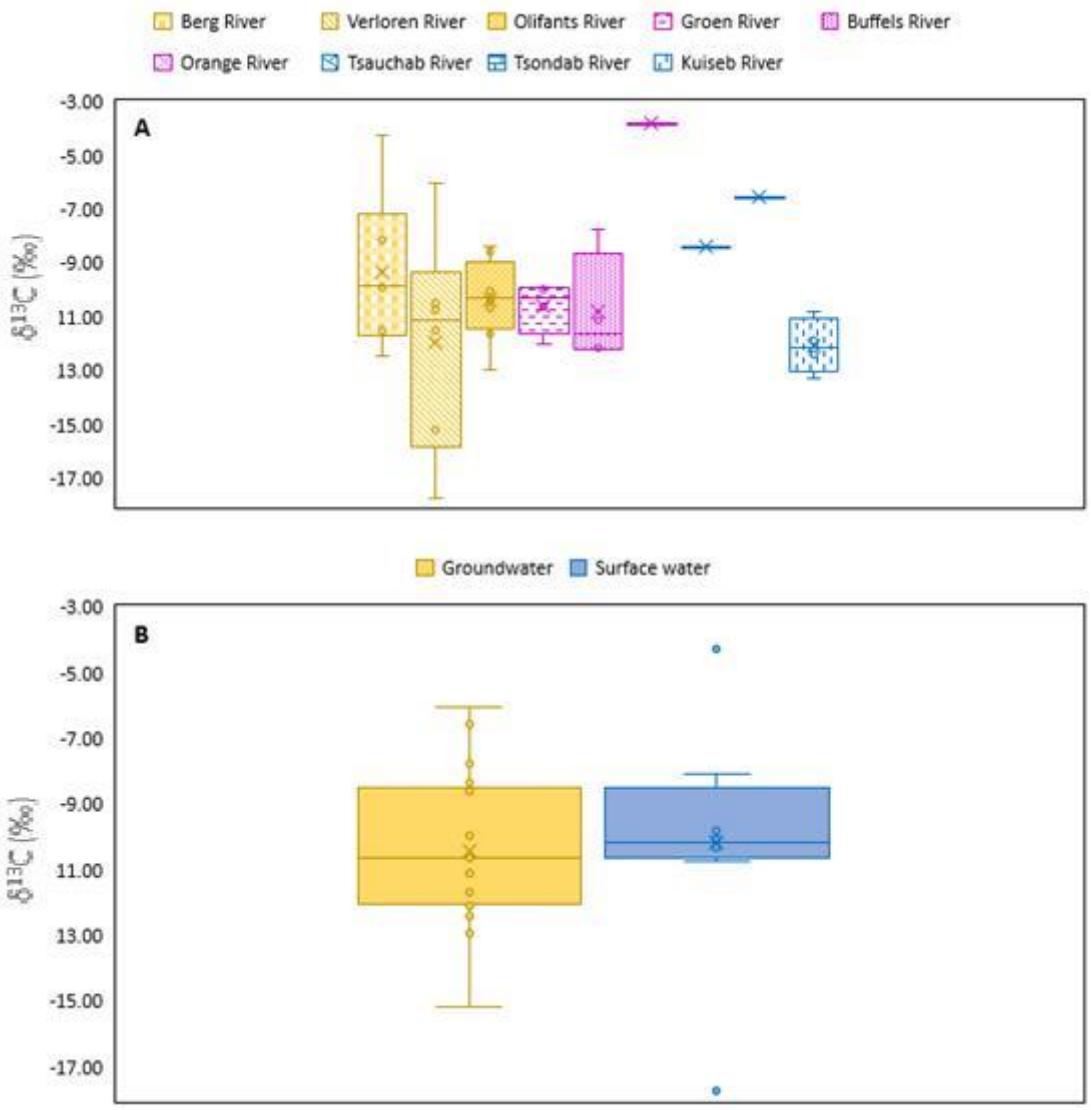


***Figure 16:*** *$\delta^{13}$C, given in ‰ relative to VPDB, for (a) all the samples collected from the field area (b) Surface and groundwater samples separately.*

### 3.3.3 $\delta^{26}$Mg Ratios

When plotted as $\delta^{26}$Mg versus $\delta^{25}$Mg (figure 17), all data yield a line with a slope of 0.5125, in good agreement with the theoretical equilibrium slope of 0.521 (Young & Galy, 2004). Hereafter, only $\delta^{26}$Mg is discussed.

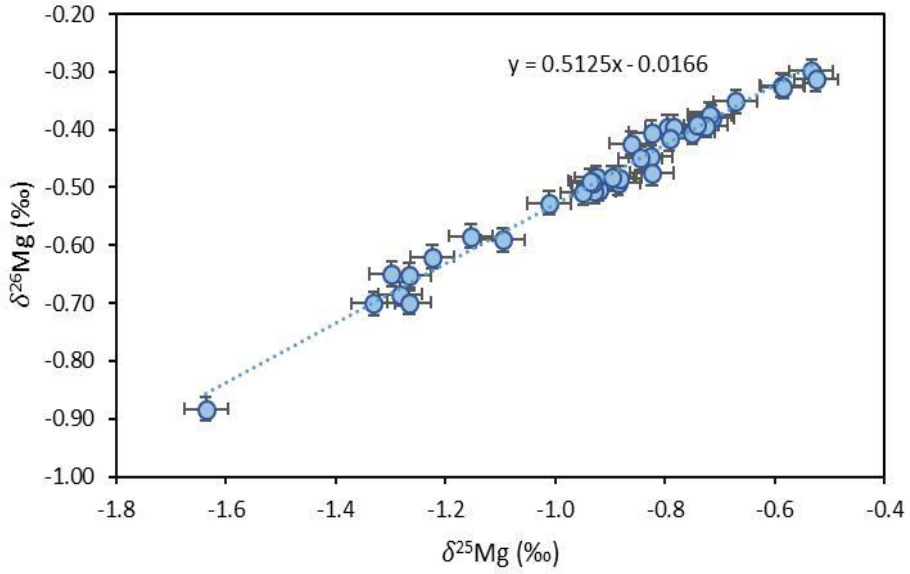


***Figure 17:*** *$\delta^{26}Mg$ versus $\delta^{25}Mg$ for the catchment samples analysed. The samples plot predominately on a straight line, thereby showing mass dependent fractionation, with negligible scatter.*

Figure 18 shows a clear distinction between waters draining carbonates and waters draining silicates. Because of their widespread variation, silicate rocks have been subdivided to identify possible trends that exist for the silicate catchment waters. West coast waters draining predominately basic and intermediate silicate rock have a $\delta^{26}Mg$ of -0.83‰ (n=17). Groundwater draining granitic and gneissic silicate bedrock (Namaqualand catchments) have a $\delta^{26}Mg$ of 0.81‰ (n=8). Waters draining carbonate rocks, from the Tsauchab & Tsondab catchments in Namibia, display the most negative values, with a $\delta^{26}Mg_{average}$ = -1.22‰ (n=9). The Orange River, which consists of a predominately siliciclastic geology with minor volcanic interaction, showed the heaviest $\delta^{26}Mg$ for the dataset, with an average value of -0.74‰. Only one of the samples, a groundwater sample from the Olifants River, recorded an anomalously negative value (-1.3‰) than would be expected for waters draining silicate rocks.

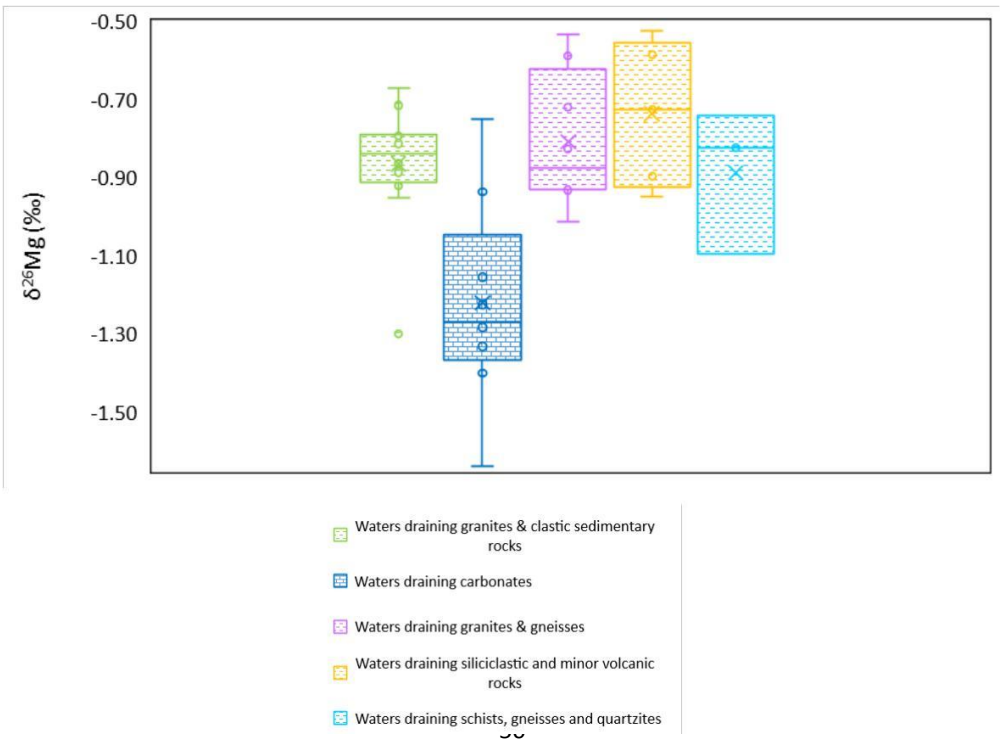

*Figure 18: $\delta^{26}$Mg (‰) for the catchment waters based on prominent lithologies that are drained. Silicate rocks have been subdivided into granites, gneisses, schists, quartzites and siliciclastic rocks.*

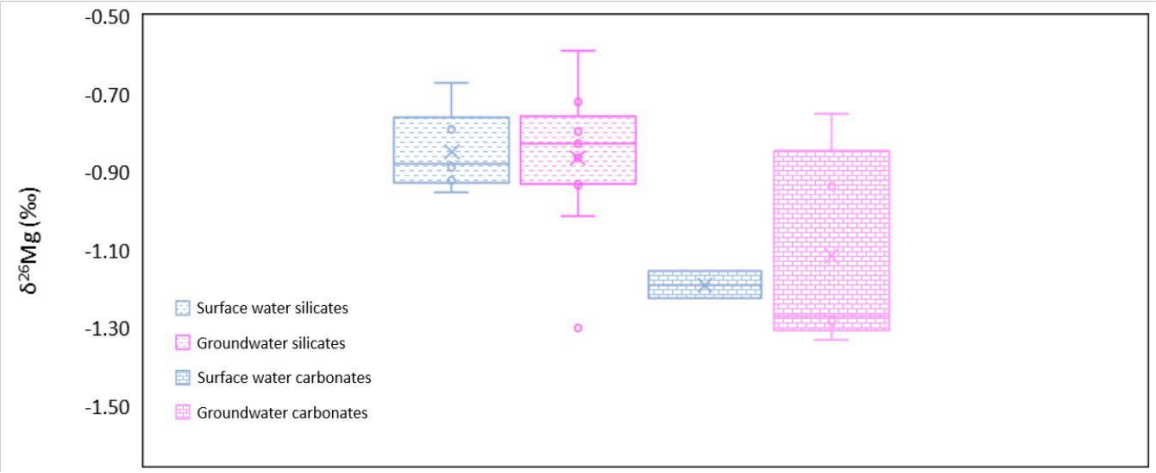


*Figure 19: Variation in $\delta^{26}$Mg for surface waters and groundwaters draining silicate rocks and surface waters and groundwaters draining carbonates.*

The range in $\delta^{26}$Mg for groundwaters and surface waters draining silicate rock is small at 0.7‰ and are indistinguishable in their $\delta^{26}$Mg composition. For the catchments draining carbonate rocks, surface water samples were collected from the Tsauchab catchment only, which shows a relatively large $\delta^{26}$Mg variation of 0.6‰ in the groundwater samples. However, the range of $\delta^{26}$Mg for the two surface water samples (-1.15‰ and -1.22‰) fall within the range of $\delta^{26}$Mg for the groundwater samples (-0.75‰ to -1.33‰) and are therefore also indistinguishable from groundwater in their $\delta^{26}$Mg composition.

## 3.4 Radiogenic Sr isotopes

$^{87}Sr/^{86}Sr$ ratios were analysed for selected samples from the study area. All the samples, except those from the Buffels River catchment, displayed relatively uniform radiogenic strontium values varying between 0.70998 and 0.74804. The samples from the Buffels River catchment however, which were collected from boreholes intersecting basic igneous rocks, had relatively high radiogenic $^{87}Sr/^{86}Sr$ ratios ranging between 0.71303 and 0.74804 (figure 20). Consequently, the highest $^{87}Sr/^{86}Sr$ ratios were observed for the central catchments, with a median value of 0.73024. The southern and northern catchments measured lower values of 0.71425 and 0.71686 respectively. On average, the groundwater samples displayed higher $^{87}Sr/^{86}Sr$ ratios (0.72167) than the surface water samples (0.71849). The results of $^{87}Sr/^{86}Sr$ is given separately for each catchment/catchment region below:

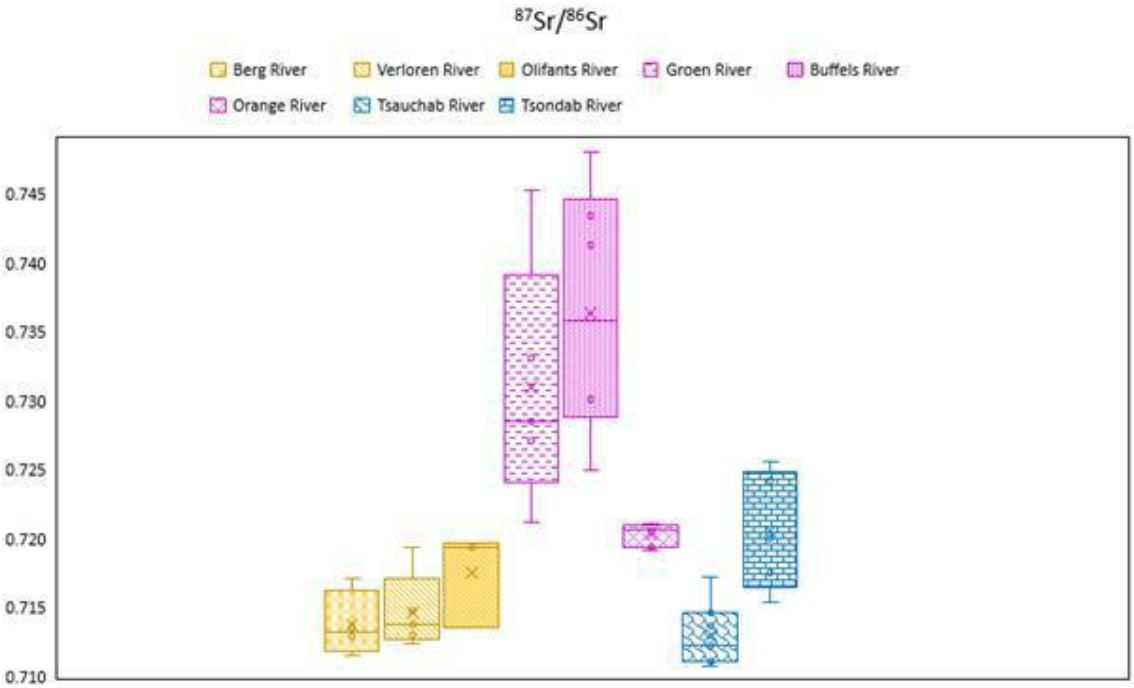


***Figure 20:*** *$^{87/86}$Sr ratios measured in samples from all nine catchments, from left to right: Berg (pink); Verlorenvlei (light brown); Olifants (purple); Groen (light green); Buffels (dark green); Orange (orange) Tsauchab (light blue); Tsondab (dark blue).*

### *The southern catchments*

All three of the southern catchments fall within a similar geological region, where the dominant rock formations are Malmesbury shales, Cape granites and sandstones and quartzites of the Cape Fold Belt. These south-western Cape rock groups are pre-Cambrian to Cambrian in age, and are therefore enriched in $^{87}$Sr, owing to the higher rate of $^{86}$Rb decay with increased time. The southern catchment

$^{87}$Sr/$^{86}$Sr ratios display considerable variation, with values correlating to the distance of the sampling points from the ocean (figure 21). Samples situated closer to the shoreline recorded smaller $^{87}$Sr/$^{86}$Sr ratios, which steeply increase further inland. Because most of the coastal plain is covered with recent marine sands, which will reflect $^{87}$Sr/$^{86}$Sr compositions close to the marine average (0.70923), waters infiltrating the coastal portions of the catchments would show relatively depleted $^{87}$Sr/$^{86}$Sr ratios. The inland samples, from approximately sixty kilometres from the river mouth, all display markedly higher values ranging from 0.7171 to 0.7207. It is therefore evident that the strontium isotopic nature of the coastal resource zone is distinguishable from that from that of the inland area, with underlying Cambrian and pre-Cambrian rocks. This trend was not observed in any of the other catchments.

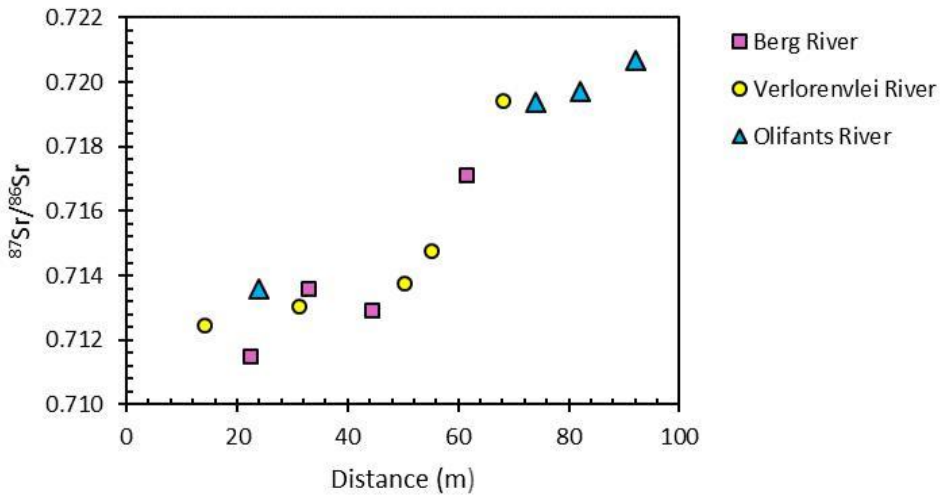


*Figure 21: $^{87/86}Sr$ vs. distance from the ocean for each of the samples collected from the Berg, Verlorenvlei and Orange River catchments. Samples collected closer to the ocean recorded smaller $^{87/86}Sr$ ratios, which showed a marked increase further inland.*

### *The Groen and Buffels River catchments*

The water samples collected from the Groen and Buffels River catchments showed the highest $^{87}Sr/^{86}Sr$ ratios for the sample set, ranging from 0.7212 to 0.7480. Previous ground and surface water studies in Namaqualand have focused extensively on the Buffels River catchment owing to prominent groundwater salinisation and small-scale copper mining in the region (Adams, et al., 2004; Titus, et al., 2009; Fersch, 2007; Benito, et al., 2010; Leshomo, 2011). Little is known about the hydrology and hydrogeology of the Groen River catchment (Meyer, et al., 2014).

Groundwater in the Buffels River Valley is saline to very saline (Adams, et al., 2004). Water in this catchment is hosted in one of two aquifers: (i) The Spektakel aquifer, a deep basement aquifer, and (ii) shallow perched aquifers within the river bed, which are used to supply water to the small towns of Buffels River and Kommagas (Adams, et al., 2004). Four samples were collected from boreholes situated in the Spektakel aquifer, and five from boreholes in the Buffels River bed.

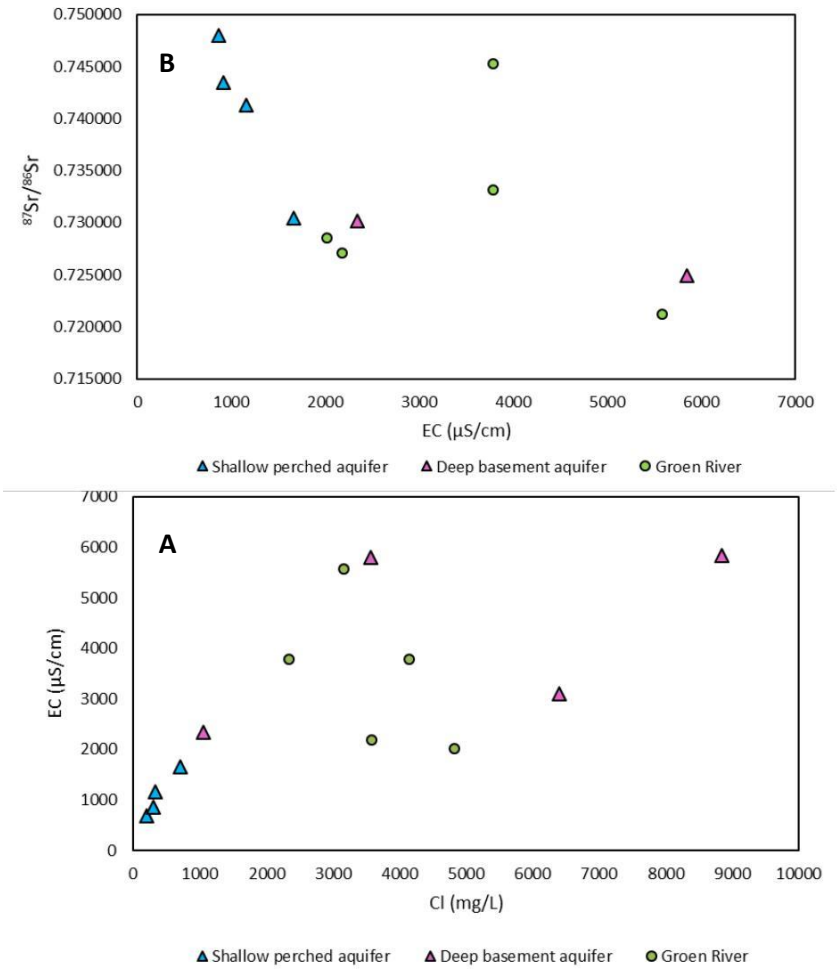


***Figure 22:*** *EC vs. Cl (left) and $^{87}Sr/^{86}Sr$ vs. EC (right) for samples collected from the Groen and Buffels Rivers (deep basement aquifer samples are separated from shallow perched aquifer samples).*

Figure 22 shows the correlation between EC, $Cl^-$ and $^{87}Sr/^{86}Sr$ for the shallow perched and deep basement aquifer samples collected from the Buffels River catchment. An increase in the $Cl^-$ concentration of these shallow waters corresponds to an increase in EC, and a decrease in the $^{87}Sr/^{86}Sr$ ratio. Chloride ions are the main constituents in waters that directly affect the EC values, and the lack of relationship between $Cl^-$ and EC in Groen River samples and deep basement aquifer samples from the Buffels River indicate two separate radiogenic Sr components.

*The Orange River catchment*

All the water samples collected from the Orange River catchment show enriched radiogenic Sr signatures, ranging between 0.7191 and 0.7211, with an average ratio of 0.7203. These values may represent the influence of igneous basement on riverine $^{87}Sr/^{86}Sr$ ratios or may be inherited from further upstream. Massive rivers that flow for hundreds of kilometres, such as the Orange River, will show only average Sr isotope ratios as opposed to primary rivers in actively-eroded areas, which exhibit a much closer relationship with the local geology (de Villiers, et al., 2000). In a study of the Orange River basin by Jordaan et al (2015), $^{87}Sr/^{86}Sr$ ratios of water samples increased from 0.715 at

the confluence of the Vaal and Orange Rivers to 0.720 in the Lower portion of the Orange River, and was attributed to the variation in stratigraphy along the river's flow path, originating in the Drakensberg basalts, then flowing into older successions of the Karoo sedimentary sequence and basement lithologies (Jordaan, et al., 2016).

*The northern catchments*

The Tsauchab and Tsondab river samples are confined mainly to the Namib aquifer, which is composed of gravels, sandstone, conglomerate, dune sand and fluvial sediments. The tributaries of these two rivers emanate from the Naukluft Mountains as well as from basement highs, where associated Naukluft Nappe Thrust limestones and dolomites range in $^{87}Sr/^{86}Sr$ values between 0.70844 and 0.71405 (Miller, et al., 2008). It is possible that some of the more depleted $^{87}Sr/^{86}Sr$ samples from the Tsauchab river are influenced by these carbonate lithologies, however, because waters in contact with carbonate host rocks isotopically equilibrate in a very short period, it is evident that the Namib aquifer host rocks have a more profound influence on the Tsauchab $^{87}Sr/^{86}Sr$ signatures.

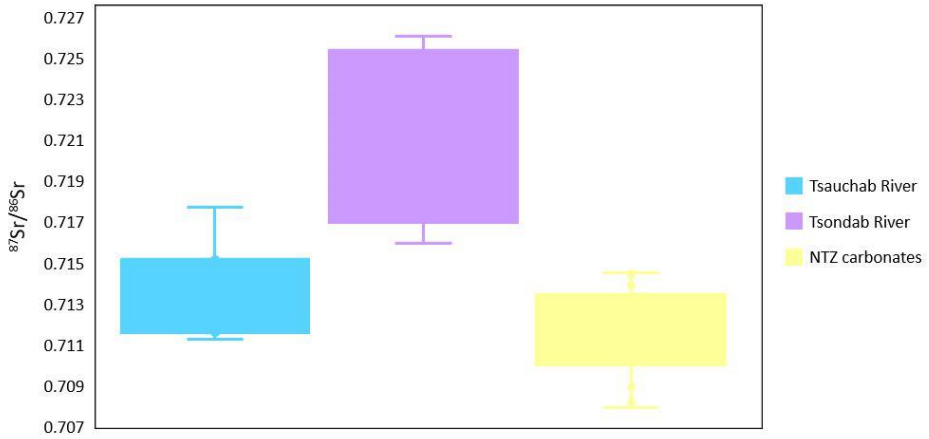


***Figure 23:*** *Sr isotopic data for the Tsauchab and Tsondab River catchment samples, as well as for selected dolomite and limestone samples associated with the Naukluft Thrust Zone (Miller, et al., 2008).*

The Tsondab catchment samples recorded elevated $^{87}Sr/^{86}Sr$ ratios compared to the Southern catchment and Tsauchab catchment samples. These high values indicate possible water-rock interactions with basement units carrying a high radiogenic Sr component; a greater contribution from tributaries draining basement highs; or, as proposed by Miller et al, (2008), the result of regional-scale hypersaline fluid flow overprinted by episodes of fluid–rock interaction involving basement-derived fluids (Miller, et al., 2008).

# 4 DISCUSSION

Ground and surface water samples collected for this project are subdivided into regions based on the proximity of catchments to one another: southern catchment region, central catchment region and northern catchment region. Hydrochemical and isotopic parameters will then be compared, contrasted and discussed within each region. If significant trends exist, groundwater and surface water samples are also compared to one another. Differences observed between the three catchment regions are likely controlled by the various geological and environmental processes taking place in each catchment/catchment region. A general overview of the main characteristics of and differences between the southern, central and northern catchment region surface and groundwaters, in addition to potential explanations for these differences, are discussed in the sections below

## 4.1 Characterisation of ground and surface water

For each catchment, where possible, both surface water and groundwater samples were collected. Sampling took place at regular distance intervals starting from the mouths of the respective rivers moving inland for approximately thirty kilometers. This sampling strategy aimed to provide the most representative assessment of the river catchments as a whole. For the $\delta^{18}O$, $\delta D$, $\delta^{13}C$-DIC, $^{87}Sr/^{86}Sr$ and $\delta^{26}Mg$ isotope systems, processes occurring in each catchment affect the specific isotopic compositions of the respective waters. Because hydrochemical parameters are also a natural tracer, for example of groundwater origin, residence times, water-rock interactions and mixing, combining their use with that of environmental isotopes may prove valuable for delineating processes occurring in each catchment. A holistic overview of the hydrochemical and isotopic parameters for each of the catchment regions is given below.

### 4.1.1 Southern region catchments

The geology of the southern region catchments is similar to one another, and there is minimal variation between catchments for both isotopic and hydrochemical parameters. The southern catchment waters show a dominant $Na^+$ type cation, and although some scatter exists among the anion concentrations, most of the samples show a $Cl^-$ dominance. The southern catchment region is therefore comprised of NaCl-type waters. The average $\delta^{18}O$ and $\delta D$ composition of the waters is -2.0‰ and -9.8‰ respectively. The range in $\delta^{13}C$-DIC values is -17‰ to -4‰, with more negative values measured in groundwater samples compared to surface water samples. The $^{87}Sr/^{86}Sr$ ratios were the lowest measured ratios for the sample set, with a median value of 0.71348. $\delta^{26}Mg$ ratios recorded in southern catchment waters range between -1.3‰ and -0.7‰.

### 4.1.2 Central region catchments

Both the Groen and Buffels Rivers drain predominately granites and gneisses of the Namaqua Metamorphic Belt, and hence waters sampled from these catchments show similarities in their hydrochemical and isotopic characters. The Orange River, situated further north, drains predominately basement igneous rocks and some volcanic lithologies. Furthermore, while mainly groundwater samples were collected from the Groen and Buffels River catchments, none were collected from the Orange River catchment. The dominant water-facies type for the Buffels and Groen River catchments is NaCl-type. For the Orange River, anion concentrations show considerable scatter, ranging from sulfate-type to bicarbonate-type. The cation concentrations show less scatter, and show a trend towards $Na^+$ enrichment. Overall, the Orange River samples also indicate a NaCl-type dominance. The average $\delta^{18}O$ and $\delta D$ composition for the central region catchments is -2.7‰ and - 9.3‰ respectively. The range in $\delta^{13}C$-DIC values is -12‰ to -4‰, with more negative values measured in groundwater samples compared to surface water samples. For $\delta^{26}Mg$, values measured in the water samples range from -1‰ to -0.5‰. The $\delta\ ^{18}O$, $\delta D$, $\delta^{13}C$-DIC and $\delta^{26}Mg$ compositions of the central catchment waters are relatively similar to those of the southern catchment but bear no correlation to the northern catchment samples. $^{87}Sr/^{86}Sr$ ratios for the Buffels and Groen River samples are the highest for the samples set, averaging 0.73024.

### 4.1.3 Northern region catchments

The northern region catchments refer to the carbonate Tsauchab and Tsondab River catchments, with the Kuiseb River catchment to the north draining predominately silicate lithologies. The northern catchment waters show considerable scatter with regard to major ion chemistry. The anions are distributed between sulfate and bicarbonate type waters, while the cation concentrations for most of the samples show no dominant type. The average $\delta^{18}O$ and $\delta D$ compositions for the northern catchment samples are the most negative for the samples set, with median values of -6‰ and -42‰ respectively. The $\delta^{13}C$-DIC values for the northern catchment samples range between -10‰ and 1.75‰, and therefore represent the most enriched $\delta^{13}C$-DIC compositions for the samples set. $^{87}Sr/^{86}Sr$ ratios average 0.715063. For $\delta^{26}Mg$, samples from the Tsauchab and Tsondab catchment range from -1.6‰ to -1.2‰, considerably more negative than the $\delta^{26}Mg$ compositions for the other seven catchments. The Kuiseb River samples recorded more enriched $\delta^{26}Mg$ ratios similar to that of the southern and northern catchments, with a median $\delta^{26}Mg$ value of -0.9‰.

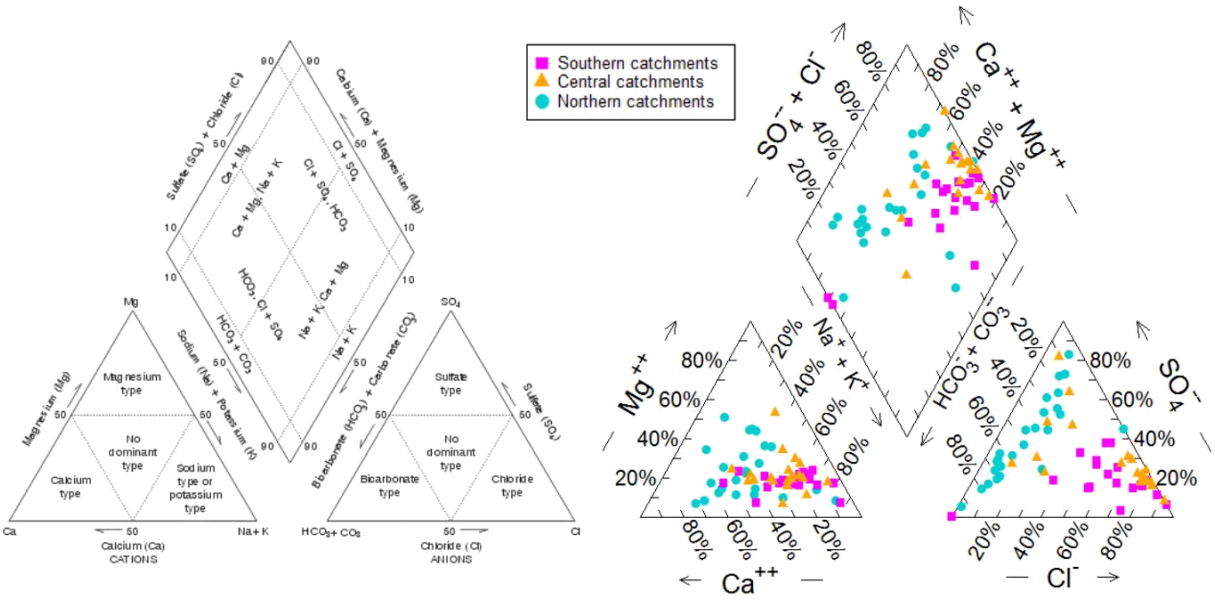


***Figure 24:*** *(L) Piper classification diagram for anion and cation facies in the form of major-ion percentages. Water types are designed according to the domain in which they occur on the diagram segments (Black, 1966); (R) Piper diagram showing the dominant facies for the three catchment regions.*

## 4.2 Mechanisms controlling geochemical character of west coast waters

There are several factors controlling groundwater chemistry which can be related to the physical situation of the aquifer, bedrock mineralogy and weather condition (Narany, et al., 2014). Gibbs (1970) suggested TDS versus $Na^+/Na^+ + Ca^{2+}$ for cations and TDS versus $Cl^-/Cl^- + HCO_3^-$ for anions to illustrate the natural mechanisms controlling water chemistry. These mechanisms are atmospheric precipitation, rock dominance, and evaporation-crystallisation (Gibbs, 1970).

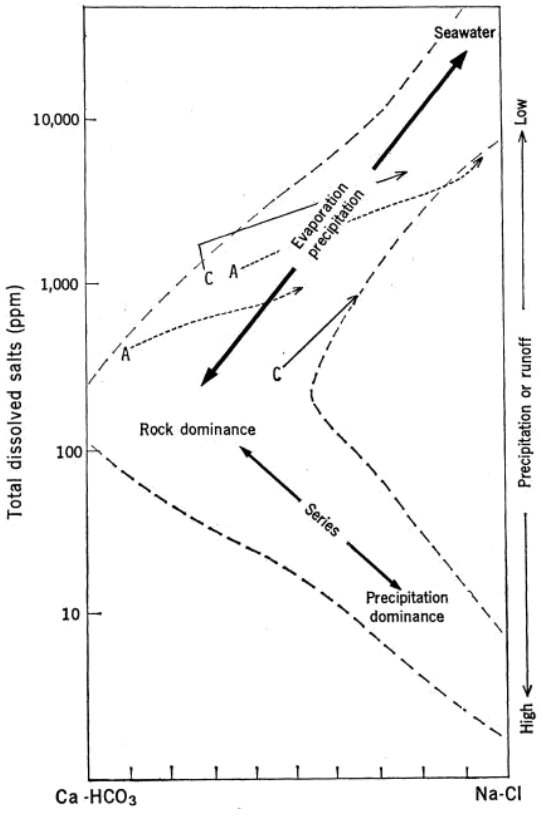


***Figure 25:*** *The Gibbs diagram uses the TDS concentration as a function of the ratio between $Cl^-$ and $Cl^- + HCO_3^-$ and $Na^+$ and $Na^+ + Ca^{2+}$ to determine the main the mechanisms affecting the chemistry of waters (Gibbs, 1970).*

Separate Gibbs diagrams were plotted for ground and surface waters. For groundwater, most of the samples plotted in the rock dominance group. This implies that the rocks and soils of these catchments serve as the dominant source of salts to the groundwater systems (Gibbs, 1970). For the Groen and Buffels River catchments, there is a strong evaporative control on the water chemistry (figure 26).

Waters plotting in the evaporation-crystallisation group are typically situated in hot, arid regions. Furthermore, these waters tend to show distinctive evolutionary flow paths with processes of evaporation and seaward intrusion driving their compositions towards the Na-rich, high salinity end-member (Gibbs, 1970).

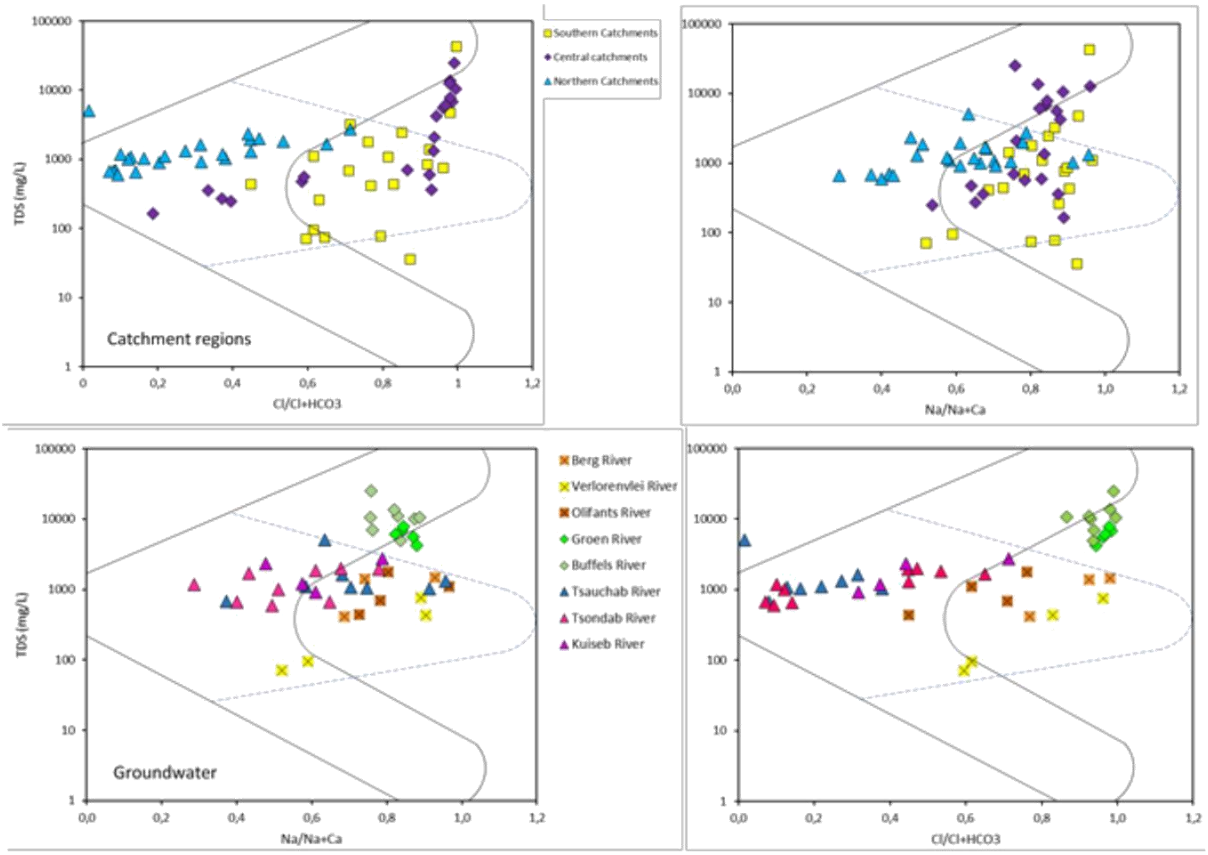


***Figure 26:*** *Gibbs diagrams representing the TSD to $Cl^-/Cl^- + HCO_3^-$ and TDS to $Na^+/Na^+ + Ca^{2+}$ ratios for the groundwater samples (bottom two diagrams) and the groundwater and surface water samples separated into the three catchment regions (top two diagrams).*

The surface waters show a similar trend, with 65% of the samples plotting in the rock dominance group. Three of the surface water samples – BR01 (Berg River), OR04 (Olifants River) and OG01 (Orange River) – fall within the evaporation-crystallisation dominance group. BR01 and OG01 were both sampled at the mouths of the rivers, very close to the sea. Evaporation rates are typically high at river mouths, and that coupled with incoming seawater into these two rivers are the most likely causes of the high TDS compositions. Sample OR04 was collected from a portion of the Olifants river flowing past a campsite. The water was murky and muddy, and regular camping activity coupled with extreme summer temperatures experienced in this area have most likely resulted in the high concentration of minerals. Both the Orange and Berg Rivers, along with the Verloren River, also produced samples plotting in the precipitation dominance group. BR03 (Berg River), VV01 (Verloren River) and OR01 (Olifants River) were sampled at locations along the respective rivers situated furthest away from the ocean, high up in the mountainous areas of these catchments. Sample BR03 was collected from the portion of the river flowing through Piketberg, a small town inland from Veldrif surrounded by high-rising peaks of Table Mountain Sandstone. Sample OR01 was sampled form the Olifants River where it flows through the Cederberg mountains before making its way to the sea, and collection of sample VV02 was preceded by a 30-minute hike into the mountains to a small tributary of the Verloren River, producing cold, fresh mountain water. The chemical compositions of these low salinity waters in the high-relief sections of

these catchments are most likely furnished by atmospheric precipitation, supplying low rates of dissolved solids to these rivers (Gibbs, 1970).

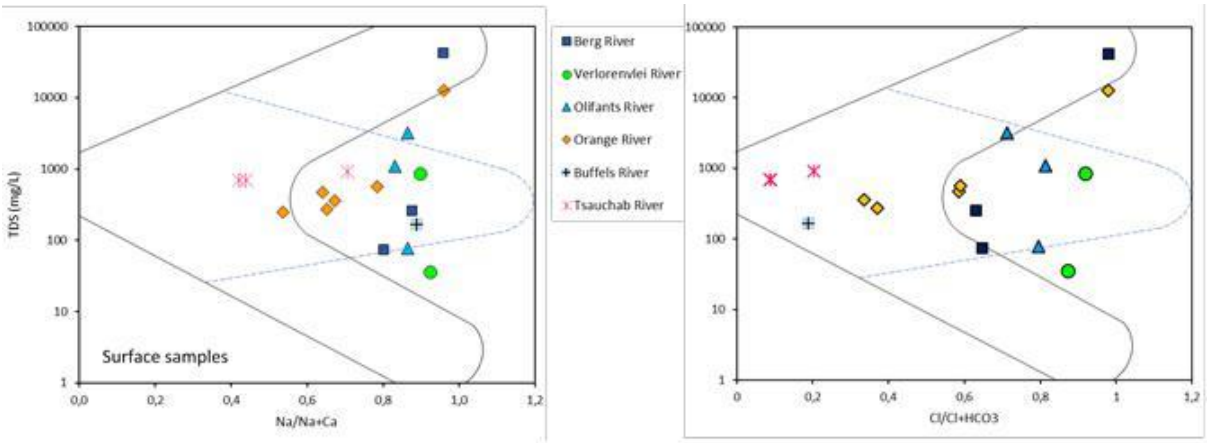


***Figure 27:*** *Gibbs diagrams representing the TSD to $Cl^-/Cl^- + HCO_3^-$ and TDS to $Na^+/Na^+ + Ca^{2+}$ ratios for the surface water samples. As most of the rivers were dry at the time of sampling, less surface water samples were collected compared to groundwater samples.*

## 4.3 Controls of recharge on $\delta^{18}O$ and $\delta D$ ratios

### 4.3.1 Recharge to southern catchments

Stable isotope compositions of rainfall in the Cederberg, Olifants River Mountains (Diamond, 2017) and Verlorenvlei catchment (Sigidi & Eilers, 2017) collected over a period of 2-3 years were averaged and plotted against $\delta^{18}O$ and $\delta D$ values measured for both the ground and surface water samples from the southern catchments to determine the source of aquifer recharge:

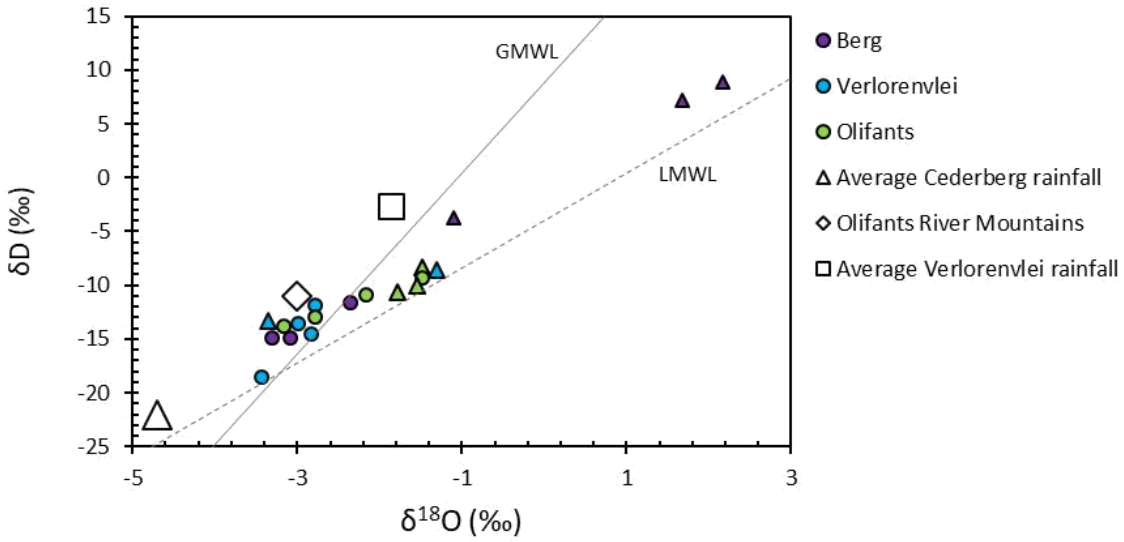


***Figure 28:*** *Stable isotope compositions for both surface (coloured triangles) and groundwater (coloured circles) samples collected from the Berg, Verlorenvlei and Olifants Rivers catchments (purple, blue and green circles respectively) and averaged stable isotope compositions of rainfall in the region, collected from the Cederberg (triangle) (Diamond, 2017), Olifants River Mountains (Diamond, 2017) and Verlorenvlei catchment (square) (Sigidi & Eilers, 2017) over a period of 2-3 years.*

80% of the groundwater samples are clustered about the averaged $\delta^{18}O$ and $\delta D$ compositions obtained for the Olifants River Mountains precipitation (figure 28). It is unlikely that neither precipitation from the Verlorenvlei catchment nor the Cederberg Mountains is infiltrating groundwater systems in this region. However, the similarity in $\delta^{18}O$ and $\delta D$ compositions of the southern catchment waters to one another suggest a connectivity of regional aquifers, promoting regional groundwater movement, which is recharging aquifers from the same source (the Olifants River Mountains). The minor discrepancy that exists between the groundwater samples which are slightly more depleted in $\delta^{18}O$ and $\delta D$ than the mean for Olifants River Mountain rainfall is most likely the result of heavier winter rains (more intense rainfall results in more negative isotopic compositions) recharging groundwater to a more significant extent. The surface water samples generally plot along the LMWL, suggesting mixed contributions from both the Olifants River Mountains and Verlorenvlei catchment rainfalls, with an additional influence of evaporation. The two outliers with relatively high values, both surface water samples collected within a one-kilometre radius of the mouth of the Berg River, are influenced to a much greater extent by evaporation than

the other southern catchment samples. This is further supported by low d-excess values measured in these two samples.

## 4.3.2 Recharge to central catchments

### *4.3.2.1 Buffels River and Groen River:*

Figure 29 shows the $\delta^{18}O$ vs $\delta D$ for samples collected for this project plotted along with the $\delta^{18}O$ vs $\delta D$ for precipitation in the Buffels River region from 2015-2017 (Sigidi & Eilers, 2017) (Nakwafila, 2015). The lack of correlation indicates that recent rainfall events have not recharged the groundwater systems. Alternatively, very high rates of evaporation in these two catchments have driven stable isotopic composition away from the GMWL. In the second figure, $\delta^{18}O$ vs $\delta D$ for groundwater samples alone are plotted relative to the GMWL and LMWL, and show a considerable scatter for the Buffels and Groen River catchments:

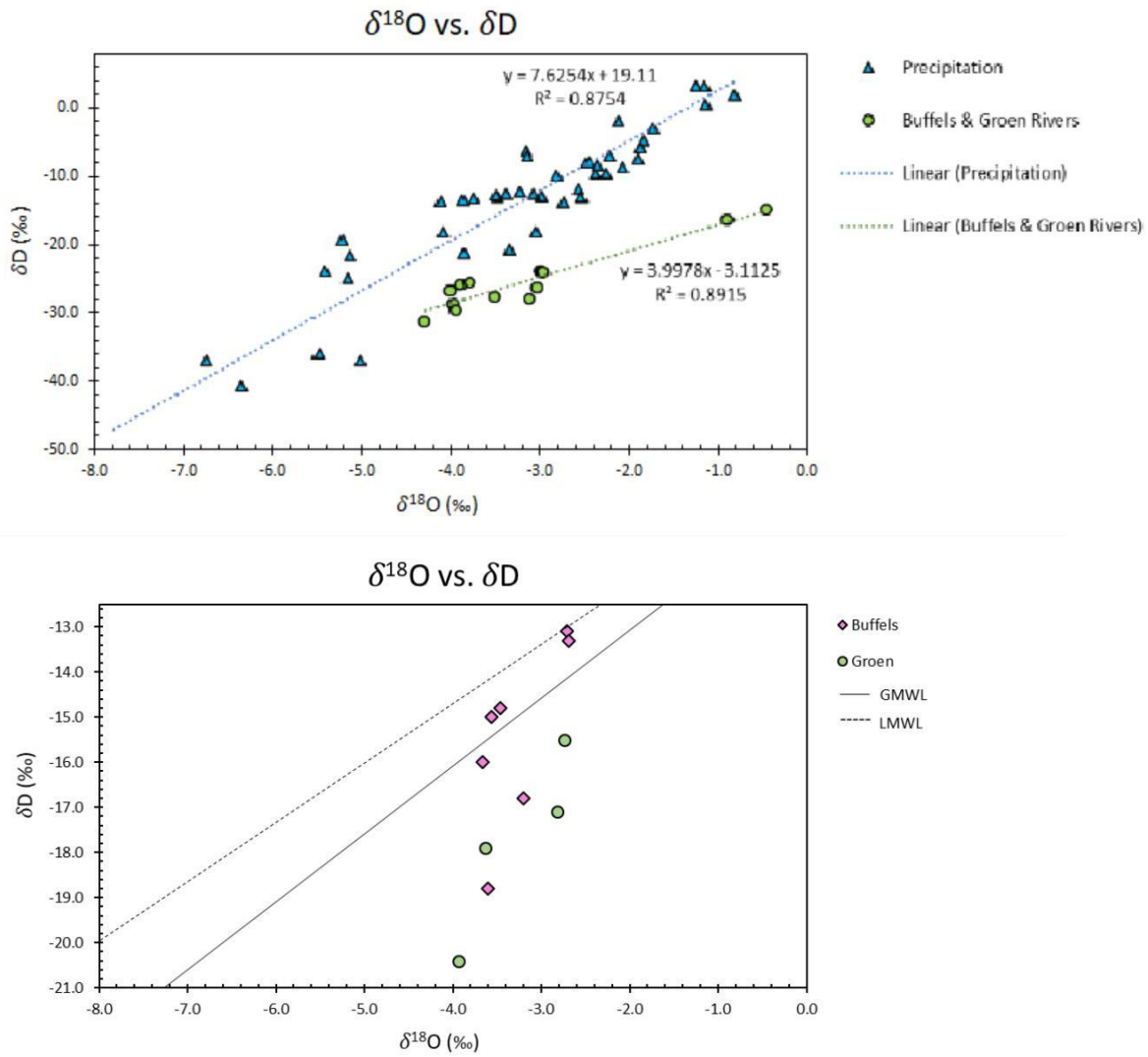


***Figure 29:*** *(Top): $\delta^{18}O$ vs $\delta D$ for samples collected from the Buffels and Groen River catchments are plotted along with $\delta^{18}O$ vs $\delta D$ for precipitation samples collected over numerous sampling seasons (2015-2017) (Sigidi & Eilers, 2017) (Nakwafila, 2015). (Bottom): $\delta D$ vs $\delta^{18}O$ for the Buffels and Groen River samples are plotted relative to the GMWL (Craig, 1961) and the LMWL for the Namaqualand region, where $\delta D = 7\,\delta^{18}O + 8$ (Adams, et al., 2004).*

The groundwater samples from these two catchments generally lie on the lines:

$$\delta D = \mathbf{3.8}\ \delta^{18}O - 3 \textit{ (Buffels)} \qquad (5)$$

$$\textit{δD = } \mathbf{\textit{3.1}}\ \textit{δ}^{18}\textit{O – 7 (Groen)} \qquad (6)$$

The groundwater for the Buffels and Groen River catchments have general slopes of 3.8 and 3.1 respectively, confirming that in fact most of the water has undergone some degree of evaporation. This is expected, as the current potential evapotranspiration rates are 12-15 times that of precipitation (Adams, et al., 2004).

#### *4.3.2.2 Orange River*

The Orange River samples recorded the heaviest $\delta^{18}O$ and δD values for the samples set, and do not correlate with either the GMWL or LMWL (figure 30). Because river water flows on the ground surface, it is easily influenced by evaporative concentration, particularly in arid and semi-arid regions (Yamanaka & Yabusaki, 2017). Furthermore, rivers with immense drainage areas, such as the Orange River with a catchment size of 892 000 $km^2$, are expected to be strongly influenced by evaporative concentration (Heath & Brown, 2007).

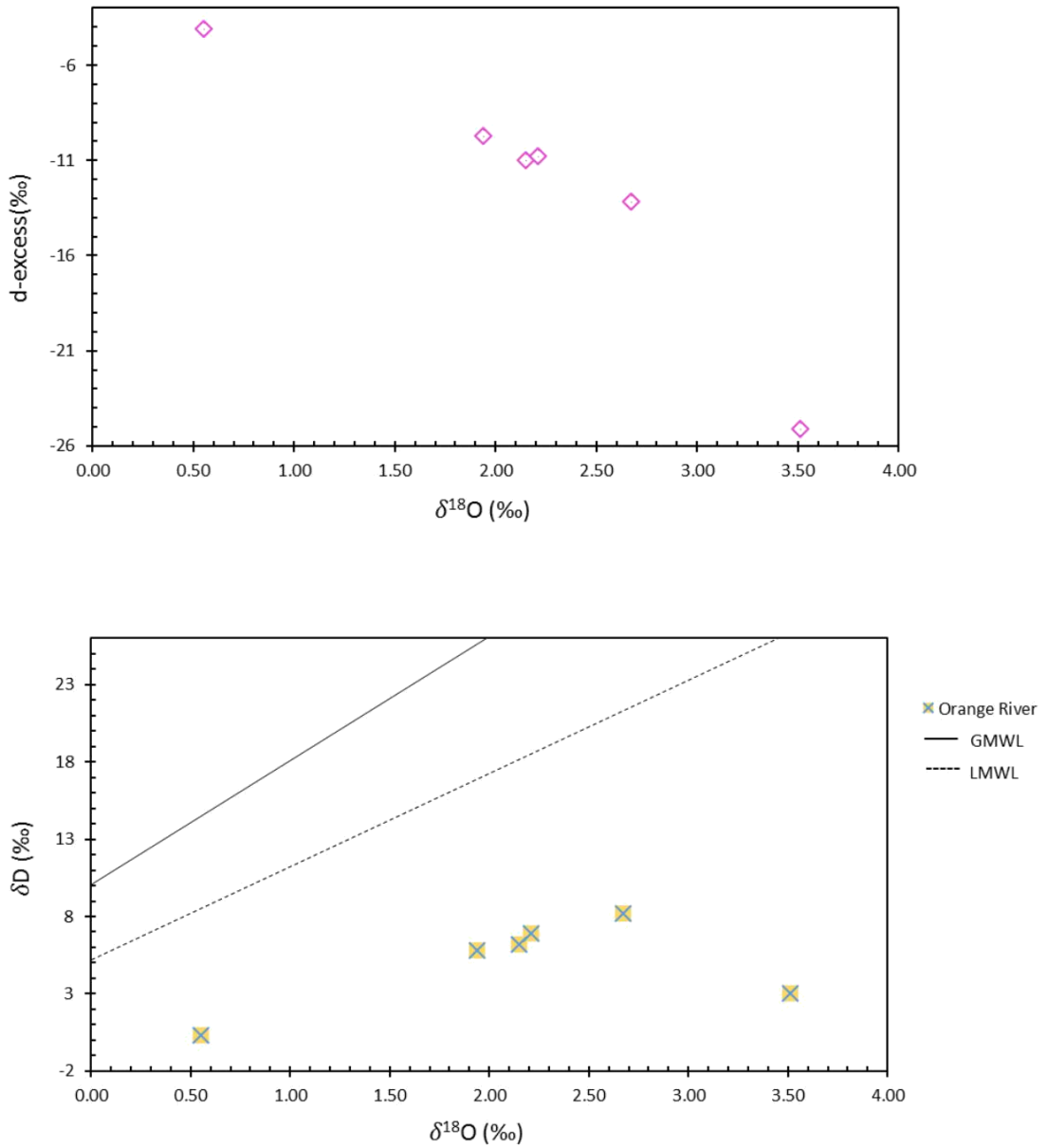


***Figure 30:*** *(Top) d-excess, defined by d = δD -8 $\delta^{18}O$ (Dansgaard, 1964), showing a negative correlation with $\delta^{18}O$. (Bottom) δD vs $\delta^{18}O$ for the Orange River samples in relation to the GMWL and LMWL.*

For evaluating the influence of evaporation, deuterium excess (d-excess) is a more useful index than isotopic composition ($\delta^{18}O$ and δD) (Yamanaka & Yabusaki, 2017), and several studies have effectively used d-excess values to evaluate evaporation processes in arid and semi-arid regions (Tsujimura, et al., 2007; Meredith, et al., 2009; Huang & Pang, 2014; Yamanaka & Yabusaki, 2017). The Orange River samples showed a negative correlation between d-excess and $\delta^{18}O$, which is attributed to the effect of evaporation on the water after precipitation has occurred (Pfahl & Sodemann, 2014).

## 4.3.3 Recharge to the Northern catchments waters

In figure 31, stable isotope compositions for the northern catchments are plotted along with that of rainfall, based on a compilation by Kaseke, et al, for Namibia for a 53-year period (1960-2013) (Kaseke, et al., 2016), as well as the values measured for precipitation by Naude (2010) for the Naukluft region.

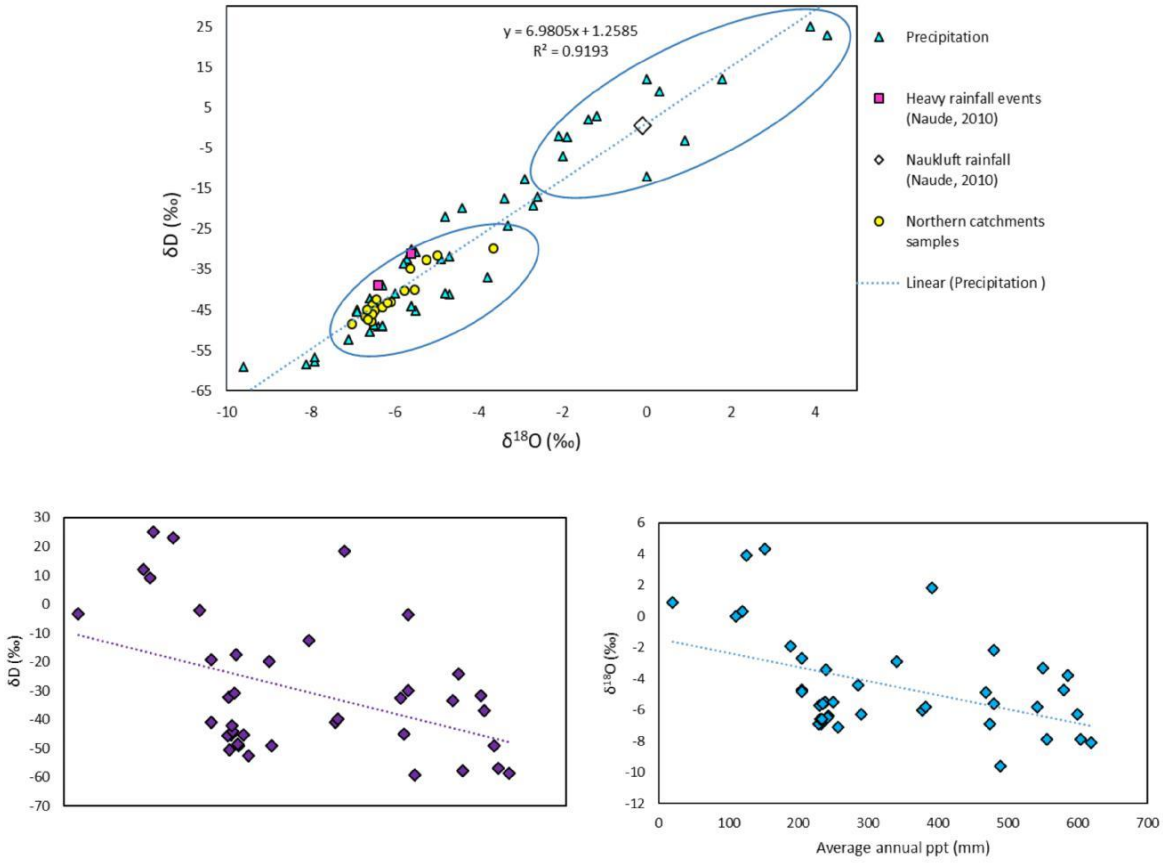


***Figure 31:*** *(1) δD vs $\delta^{18}O$ for: the samples collected from the northern catchments (yellow dots), average annual precipitation over the entire country from 1960-2013 (blue triangles), precipitation in the Naukluft for a period of 2 years (Naude, 2010) and for heavy rainfall events in the Naukluft region (pink squares) (Naude, 2010) The circles indicate δD vs $\delta^{18}O$ of precipitation for the Naukluft region only. δD vs $\delta^{18}O$ for samples collected for this project (yellow) are also encircled. (2&3) δD and $\delta^{18}O$ vs average annual precipitation for Namibia showing the amount effect on the stable isotope composition of rainfall.*

Figure 31 (2) displays the correlation between the decrease in $\delta^{18}O$ and δD for the rainfall compilation and an increase in average annual precipitation, indicating the amount effect (negative correlation between isotopic values and rainfall amount (Dansgaard, 1964) on the stable isotopic composition of Namibian rainfall. Stable isotope compositions of groundwater and spring water samples collected from the Tsauchab, Tsondab and Kuiseb catchments averaged -6‰ and -42‰ for $\delta^{18}O$ and δD respectively, and show no correlation to local Naukluft precipitation, which is comparatively enriched in δD and $\delta^{18}O$ (the average δD and $\delta^{18}O$ for Naukluft precipitation is -0.1‰ and 0.4‰ respectively) (Naude, 2010). This suggests that local precipitation is not integrated into the groundwater systems.

However, in semi-arid regions such as Namibia, generally only large storm events will recharge aquifers, resulting in a stable isotope composition of those rain events that differs from the overall average (Sklash & Farvolden, 1979; Frederickson & Criss, 1999). The δD and $\delta^{18}O$ values measured for the heavy rainfall events that occurred in the Naukluft (Naude, 2010) show distinctly more negative values when compared to the Naukluft precipitation samples, closer in range to the values obtained for the groundwater samples.

δD and $\delta^{18}O$ values measured for rainfall beyond the eastern edge of the study area plots in the same range as the samples and coincides with the narrow region of isotopic depletion for the Namib Escarpment (Kaseke, et al., 2016). The isotopic depletion in this rainfall can attributed to steep elevation changes from the Namib Desert to the Namib Escarpment, causing orographic uplift and rapid rainout of the heavy isotopes of $\delta^{18}O$ and δD (Kaseke, et al., 2016; Dansgaard, 1964). The elevation of the Escarpment, at 1700 meters, can possibly produce a hydraulic head sufficient enough to drive lateral subsurface flow to the Namib west coast aquifers.

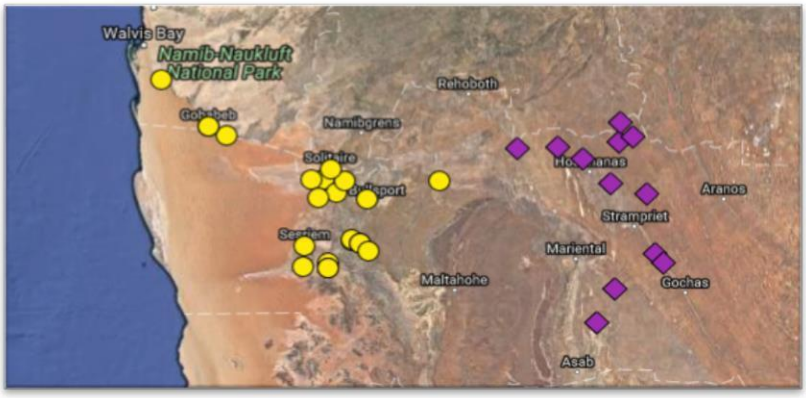


***Figure 32:*** *Location of the samples collected from the northern catchments (yellow) in relation to the occurrence of rainfall further inland (purple) showing a distinctly similar isotopic signature. This may indicate lateral flow of recharge from inland to west coast aquifers.*

Alternatively, the discrepancy between the isotopic compositions of groundwater and precipitation may be explained by aquifer recharge occurring during ancient pluvial periods when meteoric precipitation had different values and a lower deuterium excess than today (Frederickson & Criss, 1999).

## 4.4 Factors controlling the $\delta^{13}$C-DIC composition of West coast waters

### 4.4.1 Ground waters

The two primary sources of dissolved inorganic carbon (DIC) in groundwaters are (i) $CO_2$ derived from decaying organic matter (soil $CO_2$) and (ii) carbonate rock dissolution (Sharma, et al., 2013). The contribution of atmospheric $CO_2$ to groundwater systems has been found to be negligible in most environments but may be important in dry-climate areas or in cases of thin soil cover, such as in Alpine systems (Clark & Fritz, 1997). The carbon isotope composition of these two major contributions are generally distinct, notably as most carbonate derived from rocks is of marine origin (Schobben, et al., 2017). The average $\delta^{13}$C of soil $CO_2$ in areas dominated by $C_4$ vegetation, which applies to the central and northern region catchments, is expected to be approximately −12‰ VPDB (Aravena, et al., 1992), while for the southern region catchments, which fall in the winter rainfall area of South Africa, terrestrial flora is largely $C_3$, producing soil $^{13}CO_2$ values of approximately -23‰ VPDB (Sharma, et al., 2013). In contrast, the $\delta^{13}$C of most carbonate rocks is around 0 ± 2‰ (Aravena, et al., 1992). Groundwater typically receives an equal contribution from both these end members, as one mol of $CO_2$ will produce 1 mol of $H_2CO_3$, that can dissolve 1 mol of $CaCO_3$ (if it is present). This results in $\delta^{13}$C-DIC values ranging between −10‰ and −14‰ for mixed $CO_2$ derived from $C_3$ vegetation and from marine carbonate rocks, and -11‰ to -16‰ for mixed $CO_2$ derived from $C_4$ vegetation and from marine carbonate rocks (Mook & Tan, 1991). In purely silicate bedrock terranes, the DIC does not evolve much beyond the conditions established in the soil and hence has values in the lower range of -14‰ to -18‰. However, for carbonate bedrock, calcite dissolution provides an additional source of carbon to the DIC pool (Clark & Fritz, 1997). Groundwater typically seeps through the soil zone prior to aquifer infiltration, becoming progressively $^{13}$C-depleted due to soil respiration. As the water moves further into the ground, water-rock interaction increases the $^{13}$C content of the DIC, if marine carbonates are present in the infiltration profile (Pitkänen, et al., 2004).

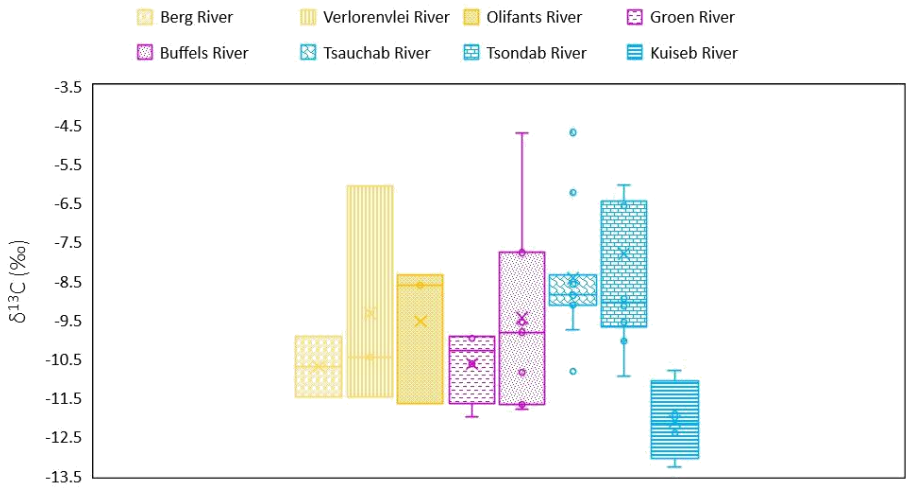


***Figure 33:*** *$\delta^{13}$C-DIC values for groundwater samples from each catchment (no groundwater samples were collected in the Orange River catchment). Each region is denoted by a different colour, where yellow indicates catchments in the southern region, Pink for central region catchments, and blue for the northern region catchments. Within each region, each catchment is represented by a different pattern.*

The $\delta^{13}$C-DIC values for most of the groundwater samples are consistent with these trends, with samples collected from the southern region catchments, draining silicate lithologies and $C_3$ vegetation, showing on average lower values (-11‰) than the central (also draining silicate lithologies but $C_4$ vegetation) (-8.7‰) and northern region catchments (draining carbonate lithologies and $C_4$ vegetation) (-8.2‰). All the groundwater samples recorded more negative values than the surface water samples, generally <-7‰. However, $\delta^{13}$C-DIC values higher than -7‰ were recorded for six of the borehole samples, four of which occur in the carbonate Tsauchab and Tsondab aquifers. These waters show less negative $\delta^{13}$C-DIC compositions because they drain carbonate lithologies, which provide an additional source of isotopically enriched carbon to the DIC pool.

Two samples, Gvv01 (Verlorenvlei catchment) and Gbf07 (Buffels River catchment), show distinctly less negative $\delta^{13}$C-DIC values (-6‰ and -4‰ respectively) than would be expected for waters draining silicate lithologies. In such cases where carbonates do not form a significant part of the regional geology, localised $\delta^{13}$C-DIC outliers, such as these two samples, can be attributed to calcite present as fracture minerals, or as carbonate grains, cobbles or cement in clastic aquifers (carbonate minerals in igneous and metamorphic rocks have $\delta^{13}$C values of 0 to -10‰) (Clarke, 2015). In the case of the Buffels River catchment, atmospheric $CO_2$ is an important contributor to the DIC budget because the contribution of soil-respired $^{13}CO_2$ is limited in areas with sandy soils and low vegetation covers. For the samples collected from the Kuiseb River catchment in Namibia, which drains a predominately silicate geology and $C_4$ vegetation (although sparse), $\delta^{13}$C-DIC values lower than −12‰ were measured. It is likely that these deep groundwaters, whose $\delta^{13}$C-DIC composition reflect a significant addition of carbon from isotopically lighter sources, are interacting with organic matter in the form of coals and/or petrified

carbon within shale lithologies, which would drive $\delta^{13}$C-DIC compositions towards more negative values.

### 4.4.2 Surface waters

In general, the three primary sources of dissolved inorganic carbon (DIC) in rivers and streams are: (i) the infiltration of shallow groundwater; (ii) soil respiration (soil $^{13}CO_2$) and (iii) exchange with atmospheric $^{13}CO_2$ ($\delta^{13}$C of -8.6‰ is measured for today's atmosphere. With fractionation, this value would end up closer to 0‰, as is the case for sea water) (Clark & Fritz, 1997). On average, the $\delta^{13}$C-DIC values for the surface water in this study samples are only slightly more enriched in $^{13}$C compared to the groundwater samples. Because of the lack of rainfall along the west coast during the sampling season, and in general, it is unlikely that the infiltration of groundwater is the most important process controlling surface water $\delta^{13}$C-DIC. The similarity in surface water and groundwater $\delta^{13}$C-DIC values within each catchment suggest that the same processes are controlling both surface and groundwater $\delta^{13}$C-DIC within each catchment. For the silicate-draining rivers (southern and central catchments, and Kuiseb River catchment) this process is soil $CO_2$ from $C_3$ (southern catchments) or $C_4$ (central and northern catchments) vegetation. In the Tsauchab catchment, the only northern region catchment from which surface water samples were collected, carbonate lithologies provide an additional source of carbon, driving the $\delta^{13}$C-DIC composition to more positive values. Samples collected from the Orange River show distinctly more enriched $\delta^{13}$C-DIC compositions (figure 29) and have the highest pH values for the sample set. Along the section of the Orange River where most of the samples were collected, the geology consists predominately of igneous basement and volcanic lithologies. However, it is possible that Orange River water has derived its hydrochemical character from further upstream, from carbonate lithologies that it had already passed over.

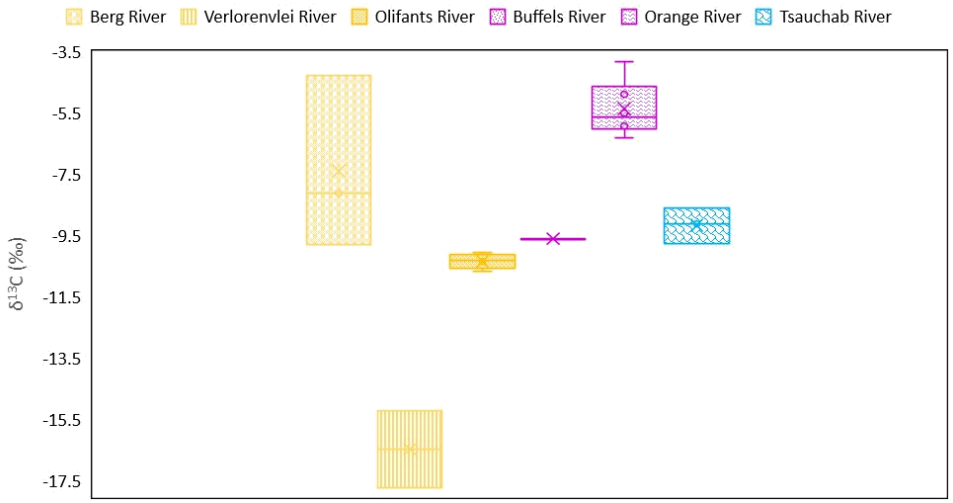


***Figure 34:*** *$\delta^{13}$C-DIC values for surface water samples from each catchment (no surface water samples were collected in the Groen, Buffels, Tsondab or Kuiseb catchments as the rivers were not flowing). Each region is denoted by a different colour, where yellow indicates catchments in the Southern region, Pink for Central region catchments, and blue for the Northern catchment regions. Each catchment is represented by a different pattern. No groundwater samples were collected in the Orange River catchment.*

Alternatively, several processes may be responsible for the high-pH less negative-$\delta^{13}$C-DIC values observed in Orange River waters. Periods of intense photosynthetic activity, particularly during the summer months, drives $\delta^{13}$C-DIC to less negative values as algae and macrophytes in the water column preferentially consume $^{12}CO_2$ (Aravena, et al., 1992). Secondly, in large rivers with extensive surface areas, continued exchange with atmospheric $CO_2$ will increase the $\delta^{13}$C-DIC. This occurs because of a steep $pCO_2$ gradient that exists between surface waters and the atmosphere, whereby the $pCO_2$ of rivers and streams is typically an order of magnitude or more below atmospheric $pCO_2$, owing to $CO_2$-oversaturation. Continued exchange with surface water systems accentuates the $pCO_2$ in the water column, leading to an increase in $\delta^{13}$C-DIC, which may eventually approach an equilibrium value depending on pH and temperature conditions (Clarke, 2015). Thirdly, high surface water temperatures, a common phenomenon observed in west coast rivers, lead to an increase in pH as $CO_2$ is actively degassed (Bade, et al., 2004). At higher pH values, $CO_3^{2-}$ becomes the more dominant carbonate species, and undergoes larger positive fractionation. This would result in the less negative $\delta^{13}$C-DIC values observed in the Orange River samples (Bade, et al., 2004).

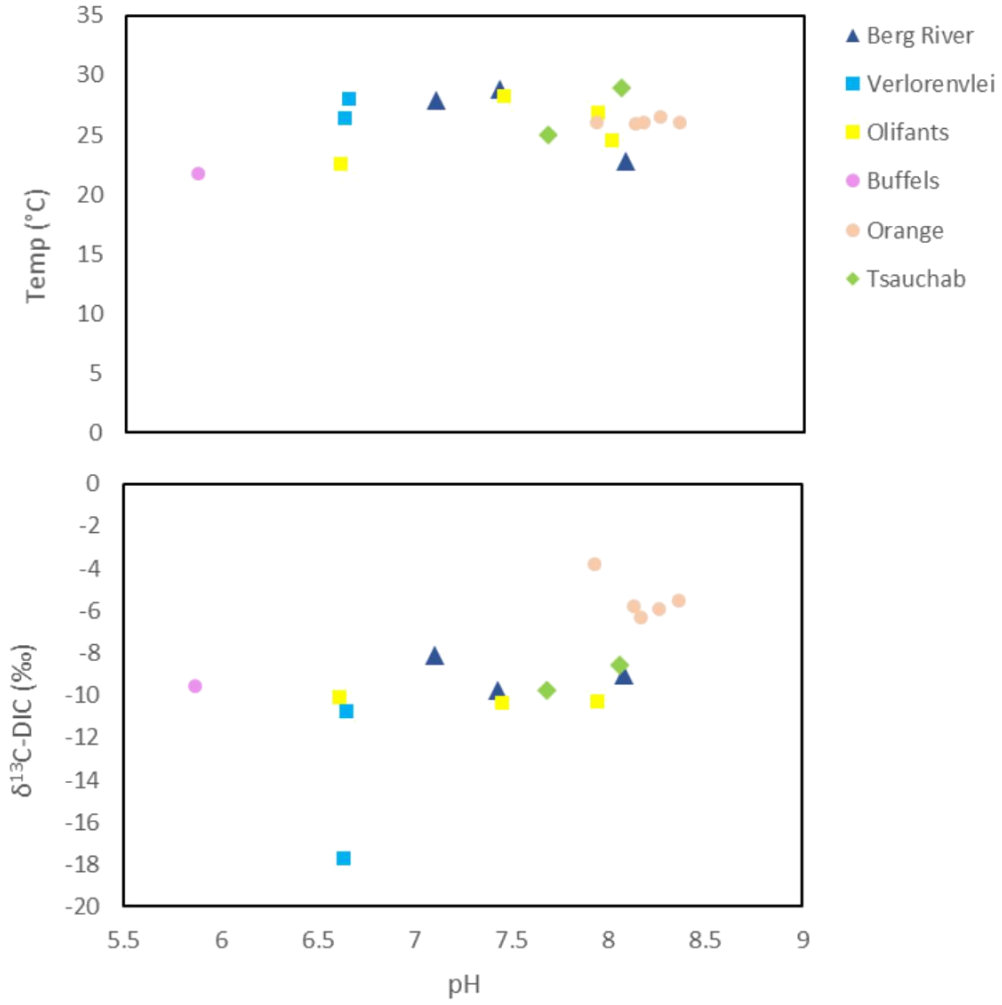


***Figure 35:*** *Temperature and $\delta^{13}$C-DIC vs. pH. No relationship is observed for temperature vs. pH conditions for the surface water samples. However, for $\delta^{13}$C-DIC vs. pH, the Orange River samples display a trend of high pH and more enriched $\delta^{13}$C-DIC values.*

Despite the numerous possible causes for the higher $\delta^{13}$C-DIC values measured for the Orange River samples, several studies have suggested that high bioactivity within surface waters is the most important process influencing the $\delta^{13}$C-DIC (Bass, et al., 2010; Hanson, et al., 2006; Mybro & Shapley, 2006; Trojanowska, et al., 2008; Bade, et al., 2004; Finlay, 2003). This could explain the lack of correlation between temperature and pH conditions for the surface water samples. Future studies in this field area should aim to monitor the $\delta^{13}$C-DIC and dissolved oxygen at different intervals during the day and night to determine responses to changes in the relative rates of aquatic photosynthesis and respiration.

## 4.5 The role of water-rock interaction and seawater intrusion

$^{87}Sr/^{86}Sr$ ratios were assessed relative to several major ion molar ratios to determine the influence of water-rock interactions and seawater intrusions on west coast water chemistry. $^{87}Sr/^{86}Sr$ vs Na/Cl and $^{87}Sr/^{86}Sr$ vs Ca/Mg produced the most significant trends, showing two distinct signals in the form of trajectories (figure 33). The first exists for the Orange River catchment, showing a variation in Na/Cl molar ratios, with very subtle variations in the $^{87}Sr/^{86}Sr$ ratio. Apart from the Buffels and Groen Rivers, all the other catchment waters show a similar trend, however with a less well-defined trajectory. For the Buffels and Groen River samples, this trend is reversed, with samples reflecting a smaller variation in the molar Na/Cl ratio and a significantly larger variation in the $^{87}Sr/^{86}Sr$ ratio. The occurrence of a number of Buffels and Groen River data points above the ocean water line indicates that process other than sea water intrusion are influencing the $^{87}Sr/^{86}Sr$ ratios in these waters (Vengosh, 2003). The basement lithologies of these two catchments are dominated by Mesoproterozoic gneisses and granites, which are characterised by high Na/Cl molar ratios and high $^{87}Sr/^{86}Sr$ ratios (Adams, et al., 2004). The groundwaters in these two catchments are also characterised by high Na/Cl molar ratios and high $^{87}Sr/^{86}Sr$ ratios, resulting from water-rock interactions. Similar trends are observed for $^{87}Sr/^{86}Sr$ ratios vs. Ca/Mg molar ratios (figure 33). For all the samples, the changes that occur in the major cation and anion ratios of the waters, albeit minimal, are partnered by variations in the $^{87}Sr/^{86}Sr$ ratio, suggesting a link between water chemistry and ion exchange reactions with local lithologies (Shand, et al., 2009).

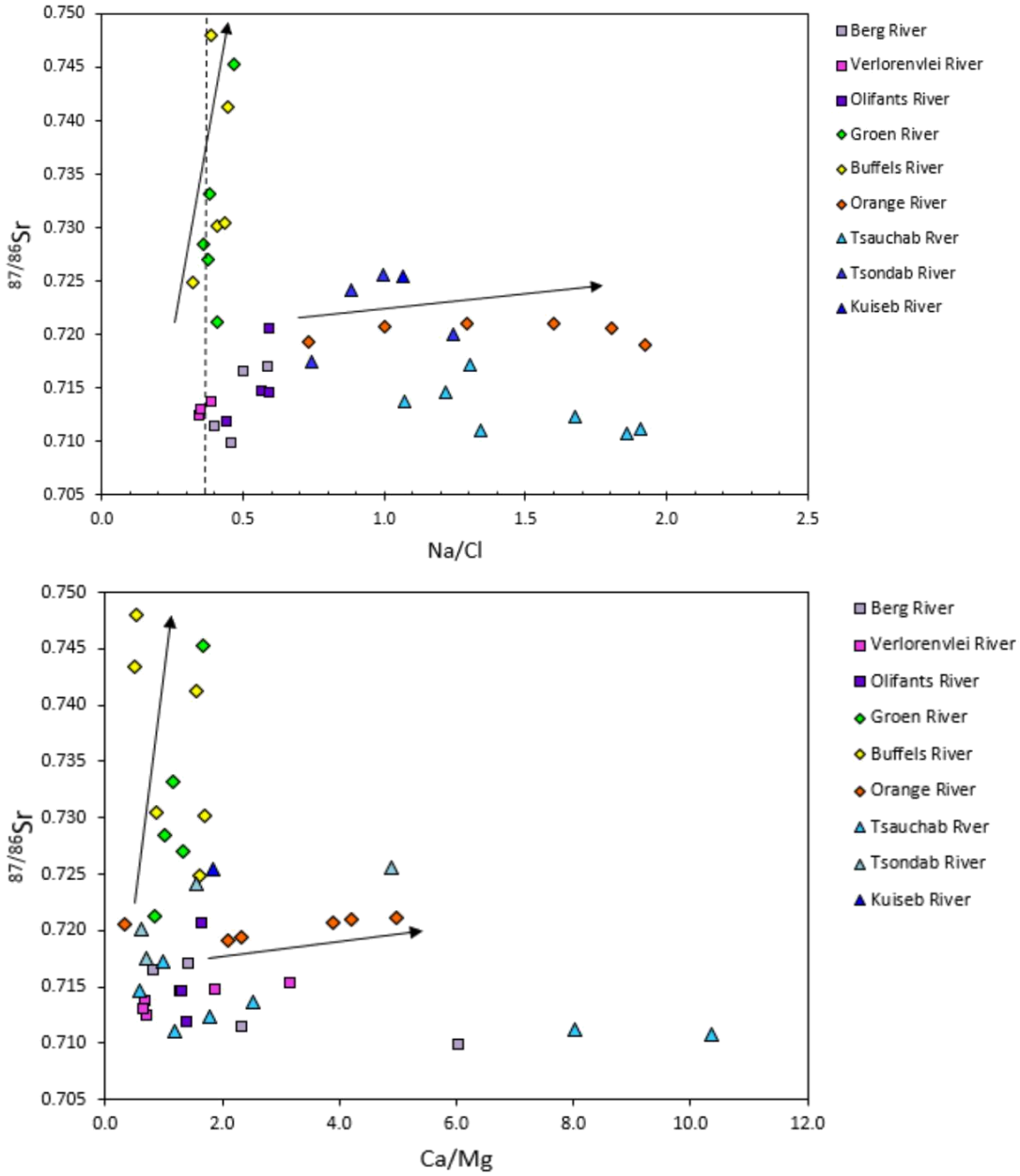


***Figure 36**: Variations in the $^{87}Sr/^{86}Sr$ ratios of the water samples with molar Na/Cl and Ca/Mg ratios. Black arrows indicate: (1) The Buffels & Groen Rivers' trajectory with characteristically high $^{87}Sr/^{86}Sr$ ratios, and (2) The Orange River trajectory with distinctly variable Na/Cl and Ca/Mg ratios and similar $^{87}Sr/^{86}Sr$ ratios. The Na/Cl ocean water line is also indicated in the first plot.*

## 4.6 Controls on the Mg isotopes of West coast catchments

The $\delta^{26}$Mg values analysed for this project, together with $\delta^{26}$Mg values for global Mg isotope data published for groundwaters, rivers and rocks (Galy & France-Lanord, 1999; Galy, et al., 1999; Galy, et al., 2002; Jacobson, et al., 2010; Teng, 2017; Tipper, et al., 2006; Tipper, 2006; Tipper, et al., 2008), are shown in Figures 38 and 39, and listed in appendix 2. To date, Tipper's compilation (Tipper, 2006) remains the most robust dataset of Mg isotope compositions in fresh water sources, albeit for rivers only (Teng, 2017).

Mg isotopic data for groundwater is limited and displays a large variation with $\delta^{26}$Mg ranging from -1.70‰ to 0.23‰, with an average value of -1.23‰ (n=16) (Teng, 2017). For the West coast sample set, $\delta^{26}$Mg ranges between -1.64‰ and -0.59‰, and averages -0.98‰, higher than the global average for groundwater.

### 4.6.1 Waters draining predominately silicate lithologies

The range in $\delta^{26}$Mg values for groundwaters and surface waters draining silicate rocks is small at ~0.7‰. Only one sample, groundwater from the Olifants River, recorded a $\delta^{26}$Mg value that is substantially lower (-1.3‰) than would be expected for waters draining silicate rocks though the average $\delta^{26}$Mg value for the sample suite (-0.82‰) is demonstrably lower than global $\delta^{26}$Mg value of bulk silicate Earth ($\delta^{26}$Mg = -0.3 per mil) (Teng, 2017), consistent with fractionation of Mg during clay formation in soils (with the heavy isotope preferentially retained in the clay; (Tipper, et al., 2006).

It is possible in sufficiently dilute samples that a significant portion of the Mg may be derived from cyclic input of precipitation (Tipper, 2006). As no rainfall samples were collected and analysed for $\delta^{26}$Mg, it is not possible to correct for this contribution.

### 4.6.2 Waters draining predominately limestone and dolomite lithologies

Overall, the $\delta^{26}$Mg values of the water samples from the carbonate terranes are lower than the $\delta^{26}$Mg values from those weathering silicate terrains, consistent with expectations based on the estimated $\delta^{26}$Mg values of the primary rock. Limestones and dolomites of the Naukluft Nappe Complex in western Namibia form a significant part of the geology of both the Tsauchab and Tsondab River catchments. To a lesser extent, dolomitic limestones of the Karibib formation form part of the Kuiseb River catchment geology (situated to the north of the Tsauchab and Tsondab Rivers). However, major ion chemistry and radiogenic Sr signatures suggest that the influence of carbonate rocks on Kuiseb catchment water is secondary to that of silicates. In the figure below (figure 37), Mg isotope ratios measured for the Tsauchab and Tsondab catchment samples in Namibia are plotted along with a compilation of the $\delta^{26}$Mg values for global rivers draining limestones and dolostones (Tipper, 2006; Teng, 2017).

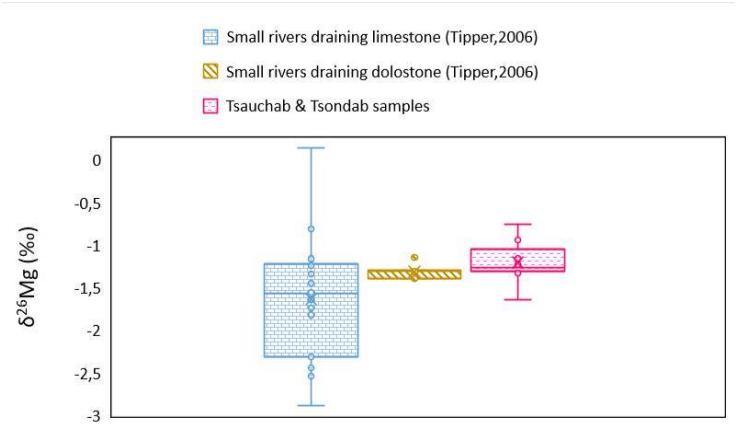


***Figure 37:*** *Mg isotope ratios measured for the Tsauchab and Tsondab catchment samples in Namibia (pink) plotted against a compilation of $\delta^{26}$Mg values for global rivers draining limestones (blue) and dolostones (brown), compiled by Tipper (Tipper, 2006).*

Although overall the $\delta^{26}$Mg values of the rivers draining purely limestone or dolostone rocks are lower than those draining silicate rocks, the Tsauchab and Tsondab groundwater and spring samples are not quite as low as many of the rivers included in the Tipper (2006) compilation. This discrepancy likely results from the fact that in the Tsauchab catchment, groundwater is hosted in deep-seated aquifers in contact with igneous basement rocks, and relatively high EC values coupled with low pH values suggest a dominant silicate-rock interaction for these waters. Because Mg is only found in trace amounts in calcite minerals, the Mg budget of waters can be significantly influenced by small amounts of silicate minerals or dolomite in which Mg is a major component (Tipper, 2006). Furthermore, Na concentrations in the Tsauchab River samples were higher than in the Tsondab River samples, with low Mg/Ca ratios, confirming the contribution of Mg from mostly silicate material in three of the seven samples collected from this catchment.

When samples only close to the Naukluft Mountains are considered, the Mg isotopic composition of the Tsauchab samples are indistinguishable to that of dolomite. These results imply that Mg isotope ratios are not fractionated during dolomite dissolution. However, the $\delta^{26}$Mg of dolomite reported below represents a large range from different samples sites across the globe, and therefore this theory would be more accurately supported if measurements were restricted to local dolomite lithologies. Neither radiogenic Sr signatures nor Mg/Ca ratios indicate a significant presence of dolomite in these catchments (apart from being enriched in Mg, the Sr ratios are higher than that of limestones, ranging between 0.710 and 0.717). This suggests that either trace amounts of dolomite are significant enough to fractionate Mg isotopes in this catchment or Mg is fractionated by both dolomite and silicate weathering mechanisms, hence producing lower $\delta^{26}$Mg values than for the other catchment samples.

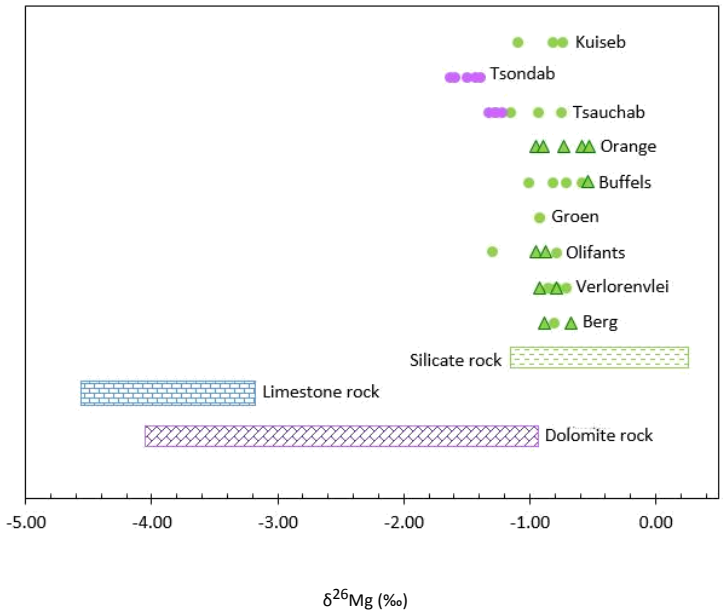


***Figure 38:*** *The correlation between $\delta^{26}Mg$ of the water samples and $\delta^{26}Mg$ of the three $\delta^{26}Mg$ -contributing rock-types. The $\delta^{26}Mg$ values of both the surface water (triangles) and groundwater (circles) samples show little variation within each catchment. Catchment-scale waters will differ in their $\delta^{26}Mg$ values from those of the rocks, with offsets varying with rock-type (Tipper, et al., 2008).*

### 4.6.3 What is controlling the $\delta^{26}Mg$ values of rivers and groundwater along the west coast?

The similarity between $\delta^{26}Mg$ measured for the water samples and $\delta^{26}Mg$ values of lithologic units suggests that, to a first order, river $\delta^{26}Mg$ values are controlled by lithology. However, figure 39 indicates a general lack of correlation between $\delta^{26}Mg$ and $^{87}Sr/^{86}Sr$, with Sr typically being used as a "lithological tracer" (Brenot, et al., 2008).

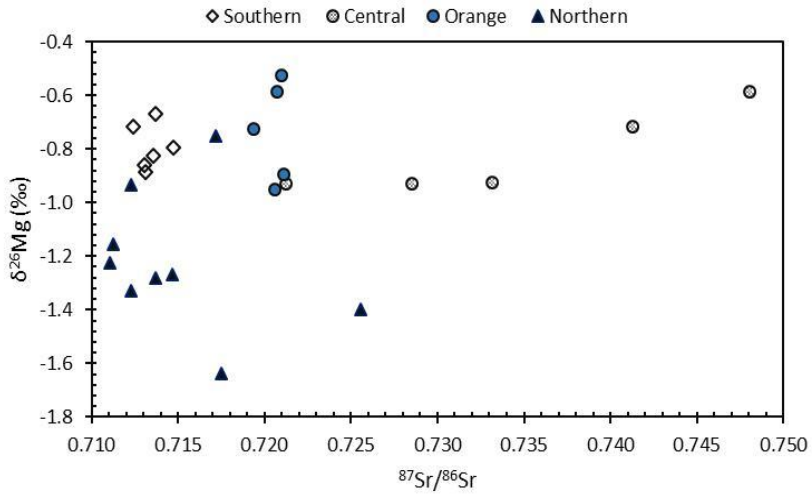


***Figure 39:*** *$\delta^{26}Mg$ vs $^{87}Sr/^{86}Sr$ for both the surface and groundwater samples. The Orange River samples have been separated from the Buffels & Groen River samples (Central region) because they do not fall within the Namaqua Metamorphic Belt, which displays distinctly high $^{87}Sr/^{86}Sr$ signatures.*

If lithology is not the major control, then it is possible that alternative processes known to fractionate Mg isotope ratios, such as precipitation of clay phases and secondary carbonate, may be of significance (Tipper, 2006). Furthermore, numerous studies have reported fractionations in the weathering environment, whereby light isotopes are preferentially released during bedrock dissolution leading to enriched residues, as the major source of $\delta^{26}$Mg variability (Galy, et al., 2002; Schmitt, et al., 2003; Tipper, 2006; Brantley, et al., 2001; Ziegler, et al., 2006). For the Groen and Buffels River catchments, a positive correlation exists between $\delta^{26}$Mg and $^{87}Sr/^{86}Sr$, which could be explained by a coupled leaching of Mg and Sr from primary rocks and minerals (primary Mg-minerals such biotite also have high $^{87}Sr/^{86}Sr$ values) (Brenot, et al., 2008).

As previously mentioned, Mg isotope ratios are known to be fractionated by (i) secondary carbonate formation; (ii) precipitation of clay phases during incongruent weathering; and (iii) the incorporation of Mg into biomass, which is typically only observed in catchments with dense vegetation (de Villiers, et al., 2005; Tipper, et al., 2006; Pogge von Strandmann, et al., 2008). These mechanisms result in isotopic compositions which are shifted away from those of the weathered parent rock (Teng, 2017).

#### *4.6.3.1 Secondary carbonate formation*

Tipper (2006) used fractionation factors measured for groundwater and travertine deposits to model, by means of Rayleigh distillation, the isotopic evolution of water and calcite interaction in a closed system, where Mg is removed from the system and incorporated into travertine deposits for a catchment in the Himalayas (Tipper, 2006). This catchment, the Bhote Kosi, was selected for the model because of its lack of vegetation and monolithological terrane, thereby eliminating additional possible mechanisms of Mg isotope fractionation to determine the effect of secondary carbonate precipitation (Tipper, 2006).

Only two of the catchments sampled for this project drain carbonate rocks, namely the Tsauchab and Tsondab catchments along the West coast of Namibia. It has been suggested based on the similarity of $\delta^{26}$Mg values of some of the samples from the Tsauchab to global average $\delta^{26}$Mg of silicate rocks that the Tsauchab groundwaters may be influenced to an extent by the presence of granitic basement rocks. However, the Tsondab catchment is comparable to that of the Bhote Kosi. Vegetation is very scarce owing to the catchment's proximity to the Namib Desert, and as observed by other chemical parameters ($^{87}Sr/^{86}Sr$, Mg/Ca ratios) the local geology, consisting of the carbonate Naukluft Nappes, is a significant contributor to Tsondab groundwater. In addition, travertine deposits associated with the Naukluft Nappe Complex are a commonly occurring phenomenon in this region.

The Rayleigh distillation curve for the Bhote Kosi catchment predicts that very little change in $\delta^{26}$Mg occurs during the precipitation of calcite, because so little Mg is incorporated into this mineral. Figure 40 below shows that within each catchment, variation exists in the $\delta^{26}$Mg values measured, with no discernible patterns between $\delta^{26}$Mg and distance along flowpaths. For the Tsondab

catchment, the measured range is relatively small (0.24‰). Although not significant globally, these variations may be important on a catchment-scale. However, because the Rayleigh fractionation model predicts very little to no change in $\delta^{26}$Mg, the precipitation of Mg-poor limestone cannot account for the observed variations in Mg isotopes in these catchments. It is therefore more likely that the dissolution of silicate minerals affects the dissolved Mg budget of West coast waters. Furthermore, in catchments where limestone represents a significant part of the local geology, Mg is only present as a trace element, whilst Mg is a major element in silicate rock (Hoefs, 2009).

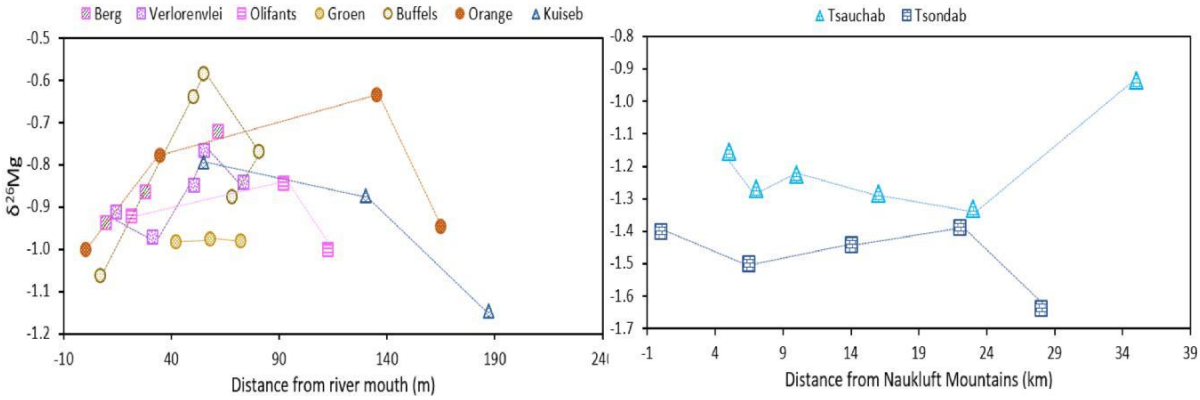


***Figure 40:*** *The relationship of δ26Mg in the catchment samples with distance from the river mouth (left) and the Naukluft Mountains (right). All the samples except those collected from the Groen River show considerable variation in their respective catchments.*

### *4.6.3.2 Precipitation of clay phases during incongruent weathering*

Additional evidence supports the theory that the precipitation of clay phases during incongruent dissolution of silicates fractionates Mg isotopes. Firstly, all of the samples collected for this project (including from the Tsondab River catchment, in which, apart from the dominant cabonate lithologies, minor siliciclastic rocks also occur) have $\delta^{26}$Mg values lighter than global $\delta^{26}$Mg averages obtained for silicate bedrocks (figure 35, appendix 2). Although cyclic and tributary input of Mg may affect $\delta^{26}$Mg signatures (Hoefs, 2009), most of the samples collected are groundwater samples, owing to the aridity of the West coast coupled with the effects of drought, and therefore it is likely that the effects of these inputs are negligible.

Furthermore, although no bedrock or soil samples were collected for analyses from the field area, when compared to global averages, $\delta^{26}$Mg of silicate soil is 0.03‰ (Teng, 2017; Tipper, 2006), which is 0.9‰ heavier than the average $\delta^{26}$Mg (-0.87‰) for the water samples draining silicate lithologies. This suggests that during the weathering of silicate rock to soil in West coast catchments, the heavy isotopes of Mg are preferentially retained in the soil residue, thereby enriching companion waters in the light isotopes of Mg.

#### *4.6.3.3 Influence of vegetation on $\delta^{26}Mg$*

Two studies have suggested that Mg isotope ratios may be fractionated by the uptake of vegetation (Schmitt, et al., 2003; Wiegand, et al., 2005). Plants preferentially uptake the heavy isotope of $\delta^{26}Mg$, and therefore should lead to a depletion $^{26}Mg$ in the dissolved load of companion solutions (Galy, et al., 2002). The west coasts of South Africa and Namibia are classified as semi-desert and desert regions respectively, and consequently in areas where vegetation does occur, it is confined to scatterings of shallow-rooted, short-lived succulent shrubs (Cowling, et al., 1999). Only the southern catchments showed any significant plant coverage, however the average $\delta^{26}Mg$ values measured for these waters (-0.86‰) are very similar to those obtained for the other silicate-dominated catchments (Central catchments: -0.80‰; Kuiseb River catchment: -0.89‰), and do not correspond to the $\delta^{26}Mg$ depletion expected in companion solutions where plants are fractionating Mg isotopes (published results of $\delta^{26}Mg$ for plants indicate average values of -0.34‰ (Hoefs, 2009; Tipper, et al., 2012), which would result in an average $\delta^{26}Mg$ of the catchment waters of around -1.2‰, which was not observed). Therefore, it is unlikely that nutrient utilisation of Mg by plants along southern African West coasts are affecting the $\delta^{26}Mg$ of waters.

### 4.6.4 Chemical evolution by dedolomitization

Dedolomitization is used to describe the process whereby waters saturated with calcite and dolomite will experience additional dissolution of dolomite and concurrent precipitation of calcite (Back and others, 1983). Only one case of groundwater dedolomitization is reported in literature and based on the similarity of the behaviour of Madison Aquifer groundwaters to Tsauchab groundwaters, it is possible that groundwater in the Tsauchab catchment also chemically evolves by dedolomitization. According to this reaction pathway, the dissolution of dolomite results in the precipitation of calcite, following the generalised reaction:

$$CaMg(CO_3)_2 \rightarrow CaCO_3 + Mg^{2+} + CO_3^{2-} \qquad (7)$$

Figure 41 (below) indicates that if dedolomitization is occurring, it is only significant until a distance of approximately 16 kilometers from the Naukluft Mountains. Along the initial 14 kilometer-flowpath, Mg concentrations decrease from 84 mg/L to 35mg/L. This corresponds to an increase in $Na^+$ from 116 mg/L to 143mg/L, an increase in $Cl^-$ from 96mg/L to 133mg/L, and an increase in $Ca^{2+}$ from 49mg/L to 102mg/L. These trends suggest that along this reaction pathway, halite dissolution also occurs, resulting in Mg-for-Na exchange (Jacobson, et al., 2010). Alternatively, $Na^+$ may be sourced from other silicate minerals present in the Tsauchab catchment.

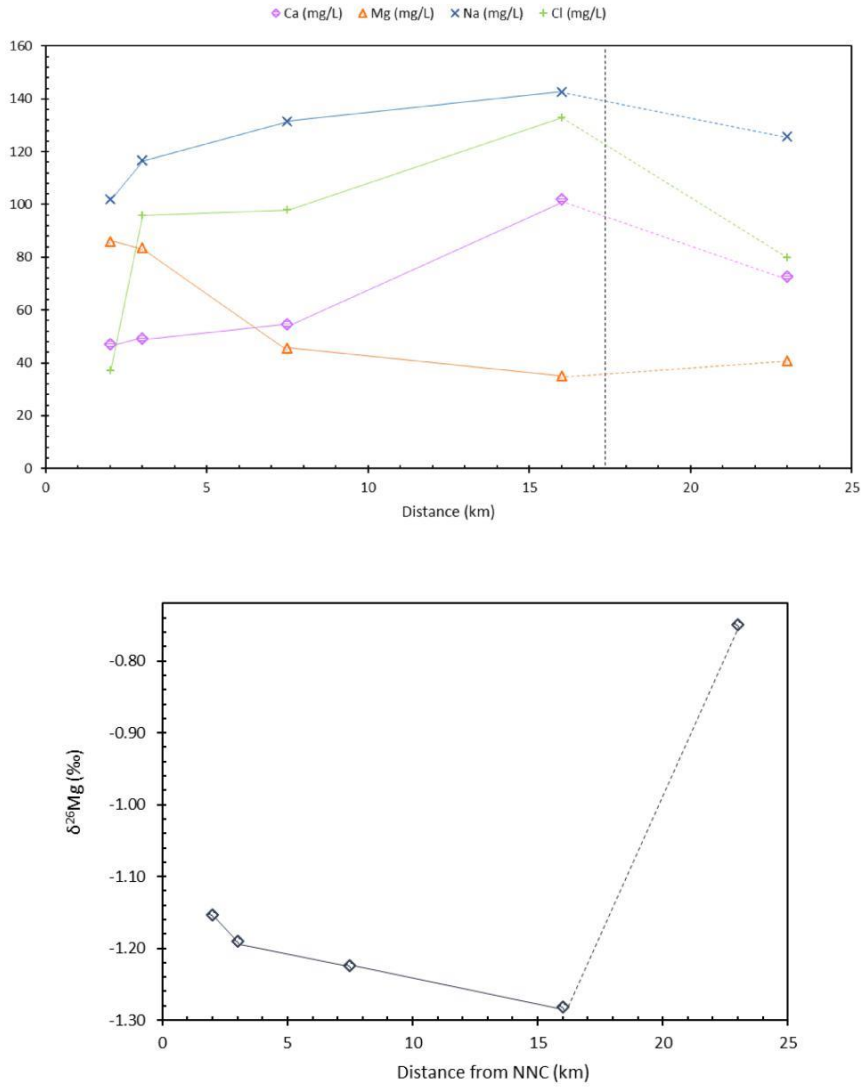


***Figure 41:*** *(1) Change and correlation in chemical parameters ($Ca^{2+}$, $Mg^{2+}$, $Na^{+}$, $Cl^{-}$) with distance from the Naukluft Nappe Complex (Naukluft Mountains). (2) $\delta^{26}Mg$ values decrease with an increase in distance from the Naukluft Mountains, with samples situated further away from the Nappes in the desert-portion of the Tsauchab catchment showing a drastic increase in $\delta^{26}Mg$, consistent with that of silicate bedrock.*

During dedolomitization, fractionation by Mg-for-Na ion exchange preferentially removes $^{26}Mg$ over $^{24}Mg$, with a fractionation factor of -0.6‰. The effects of calcite precipitation on Mg fractionation is estimated to be negligible because calcite is not a significant sink of Mg (Jacobson, et al., 2010). The result of this fractionation is a decrease in $\delta^{26}Mg$ along the flowpath, away from the Naukluft Mountains. Samples situated closer to the Namib Desert exhibit relatively more enriched $\delta^{26}Mg$ compositions, and the chemistry of the water no longer indicates the occurrence of dedolomitization (figure 43). Abundant silicates situated in this portion of the catchment are most likely responsible for fractionation of the Mg isotope ratios further along the Tsauchab River flowpath. These trends were not observed in the Tsondab catchment, where is has been established that fractionation of Mg isotopes by secondary carbonate formation and the precipitation of clay phases are most likely responsible for the observed $\delta^{26}Mg$ variation.

Plotting $\delta^{26}Mg$ against several major ion ratios shows evidence of processes taking place which may influence the $\delta^{26}Mg$ of the catchment waters and support the theory of dedolomitization occurring in the Tsauchab catchment. Once again, two distinct groups emerge from the dataset. For Na/Mg molar ratios, waters in the carbonate Tsauchab and Tsondab River catchments show low ratios corresponding with more negative $\delta^{26}Mg$ values, while waters draining predominately silicate lithologies trend towards higher Na/Mg ratios and less negative $\delta^{26}Mg$ values. These trends are consisting with the dominant lithologies occurring in each catchment, whereby carbonate-draining waters are depleted in $Na^+$ and more enriched in $Mg^{2+}$, and silicate-draining waters are enriched in $Na^+$ and depleted in $Mg^{2+}$. Two of the samples from the Tsauchab catchment, TS07 and B32, both collected from the Namib Desert (furthest away from the carbonate Naukluft Mountains), consistently outlie the trends observed for the other Tsauchab and Tsondab catchment samples and fall within the range of both $\delta^{26}Mg$ and major ion ratios consistent with silicate-draining waters (figure 44).

For Na/Ca, the same trends are observed, where the bulk of Tsauchab and Tsondab catchment waters draining carbonate lithologies show low ratios, the result of low $Na^+$ and high $Ca^{2+}$ concentrations, while silicate-draining waters and samples TS07 and B32 display higher ratios, corresponding to high $Na^+$ and low $Ca^{2+}$ concentrations measured in the samples. These trends are also observed in the plots of $\delta^{26}Mg$ vs. K/Ca and K/Mg.

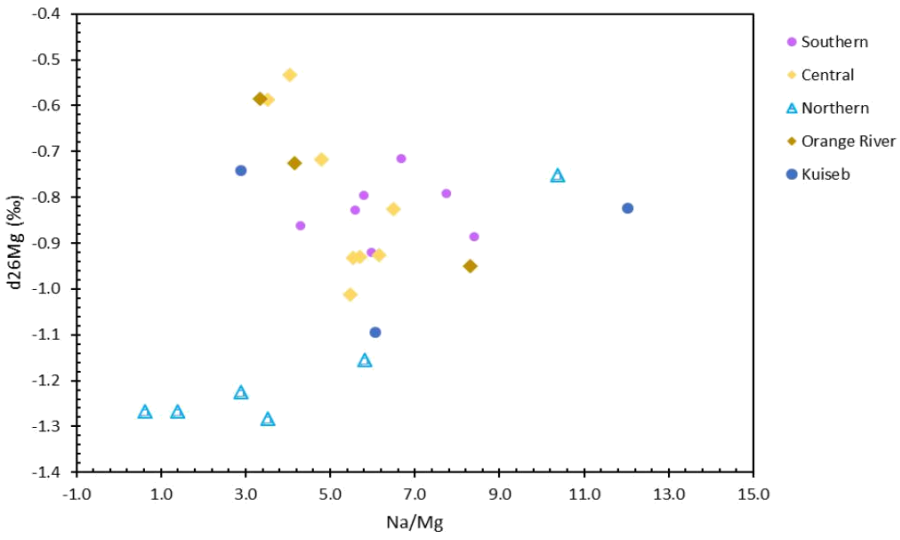


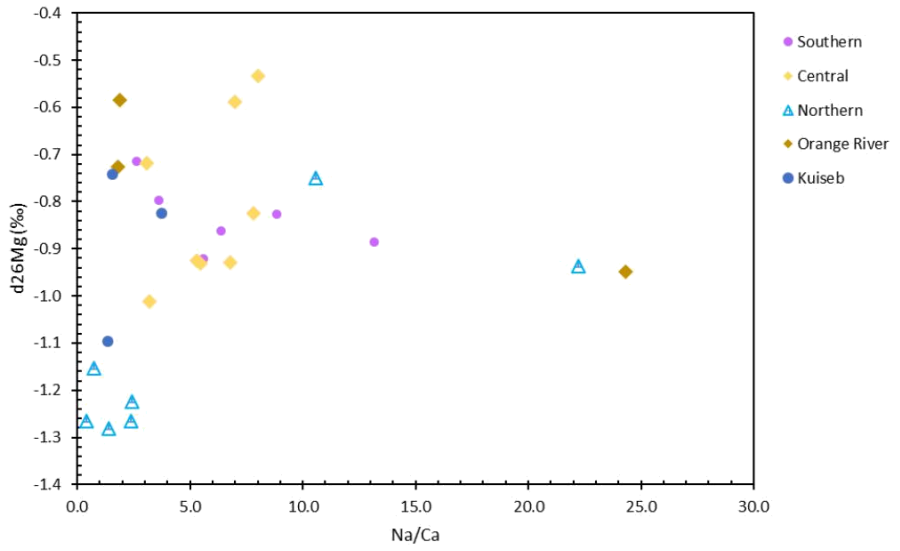


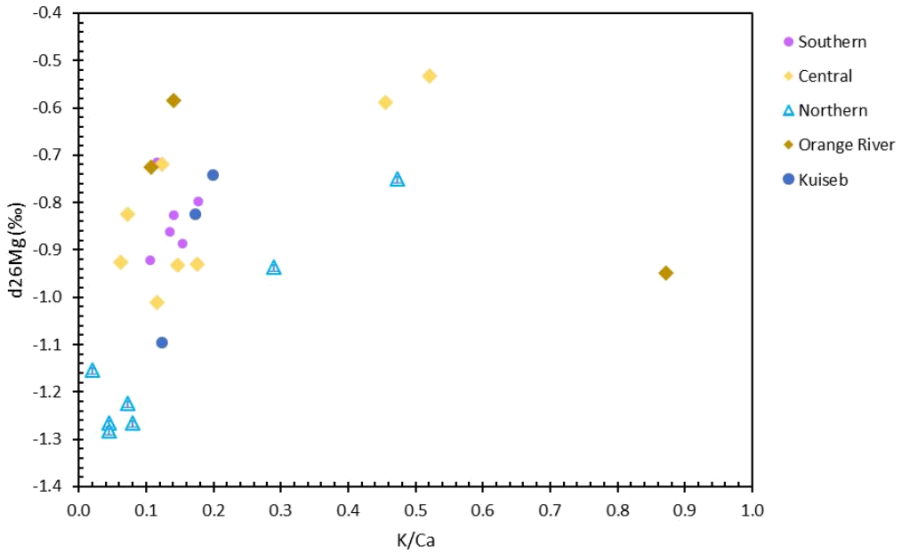

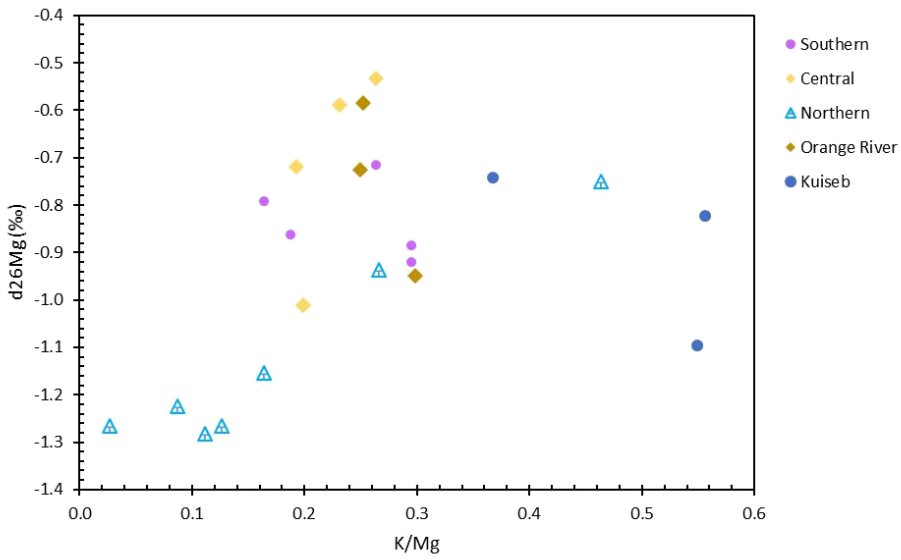


***Figure 42**: $\delta^{26}Mg$ vs. several major ion ratios showing trends in these two parameters for the various catchments/catchment regions, showing two distinct groups: carbonate-draining waters and silicate-draining waters. Samples Ts07 and B32, both collected from the Namib Desert portion of the Tsauchab catchment, consistently outlie the trends observed for the rest of the carbonate-draining Tsauchab and Tsondab catchment samples.*

## 4.6 Viability of Mg isotopes as a hydrological tool in southern Africa?

In this study, the use of $\delta^{26}Mg$ has allowed for the processes controlling Mg isotope fractionation in west coast waters to be constrained. The insight provided by this isotope system allows for a more comprehensive understanding of hydrological systems. However, because the characteristics that determine the $\delta^{26}Mg$ values of waters are not necessarily unique to one catchment (geology, vegetation-type), $\delta^{26}Mg$ alone cannot be used to differentiate groundwater and surface water catchments. However, when used in conjunction with other isotope systems and hydrochemical parameters, a more robust understanding of hydrological systems can be established, which is essential for the formulation of sustainable resource development and management strategies.

In a southern African context, the only setback to analysing $\delta^{26}Mg$ in waters is a lack of analytical facility. Otherwise, the collection and storage of waters for $\delta^{26}Mg$ analysis is straight forward and follows the same protocol as oxygen and hydrogen stable isotopes and radiogenic strontium. Because droughts are a major feature of the southern African climate, and South Africa (in particular, the Western Cape) is expecting to suffer from the increasing occurrence of drought, the need to improve the countries abilities to prepare and mitigate against such climatic events in the future is of vital importance. Mg isotopes contribute to bridging information gaps that exist on hydrological systems in southern African countries and can ultimately prove to be regularly used isotopic tool contributing to the implementation of effective water management strategies.

## 4.7 Can west coast catchments be distinguished based on isotopes alone?

Several isotopic analyses were performed for this project and have proved useful in indicating specific processes taking place in west coast catchments. As previously mentioned, for water management purposes, $\delta^{26}Mg$ compositions are best used in conjunction with hydrochemistry and other isotope systems to fully characterise ground and surface waters. The purpose of this section is to assess the capability of isotopes alone to delineate isotopically distinct regions within the study area, and relate processes controlling the individual isotope system compositions to one another to gain a comprehensive understanding of the water systems to which they are applied.

Figure 45 represents an attempt to conceptualise the relationship between the isotopic characters of the ground and surface waters sampled for this project. $^{87}Sr/^{68}Sr$ ratios are represented by patterns, whereby blue dashes are silicate-draining waters and pink blocks are carbonate-draining waters.

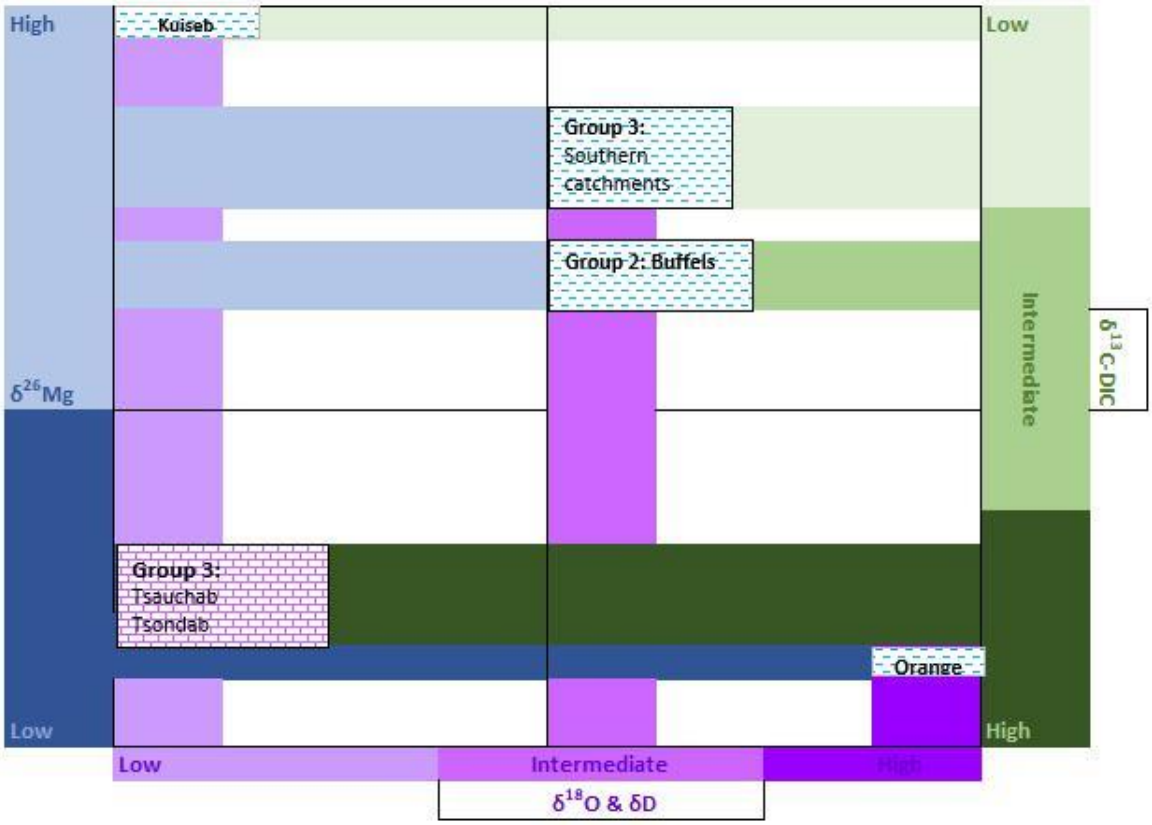


***Figure 43:*** *Diagram representing the relationship between the isotopic characters of the ground and surface waters sampled for this project using the isotope systems discussed thus far: $\delta^{18}O$ & $\delta D$, $\delta^{13}C$-DIC, $^{87}Sr/^{86}Sr$ and $\delta^{26}Mg$, $^{87}Sr/^{86}Sr$ is represented by patterns, whereby dashes represent silicate-draining waters and bricks represent carbonate-draining waters. 'High' indicates values trending towards less negative values while 'low' indicates values becoming progressively more negative. These descriptions are only for the samples in this study, relative to one another (i.e. Low ratios relative to the other catchment samples).*

Three distinct groups emerge from this diagram: (1) Waters from the southern region catchments (Berg, Olifants and Verloren Rivers), which drain silicates of the TMG group, (2) groundwaters from the Buffels and Groen Rivers which drain granites and gneisses of the Namaqua Metamorphic Belt,

and (3) waters sampled from the carbonate-draining Tsauchab and Tsondab River catchments. Two outliers of the dataset are the Kuiseb and Orange Rivers. The isotopic characters of the three groups can be described as the following:

**Group 1** – waters drain predominately silicate lithologies, the geology of all three catchments is similar, producing $^{87}Sr/^{68}Sr$ ratios in the range of 0.70999 to 0.72065. $\delta^{13}$C-DIC values for this group are low, averaging -11‰, and are derived from soil $CO_2$ in a $C_3$-vegetated region. $\delta^{18}O$ and δD values for this group fall in the intermediate range for the sample set, with values ranging from - 3.5‰ to -1‰ for $\delta^{18}O$ and -15‰ to -5‰ for δD. Some of the samples plot off the LMWL, indicating an influence of evaporation on group 1 waters. The $\delta^{26}$Mg compositions are relatively high, but not unique to this group. These values indicate a dominant process of preferential retainment of $^{26}$Mg in soil clays inducing fractionation of Mg isotope ratios.

**Group 2** – groundwater samples collected from the Buffels and Groen River catchments comprise the second isotopically characteristic zone in the study area. Group 2 and group 1 are similar in isotopic values. However, samples from group 2 show very high $^{87}Sr/^{68}Sr$ ratios owing to the granitic and gneissic terrane in which these catchments are situated. Secondly, $\delta^{13}$C-DIC values for these waters are less negative than group 1 waters and fall within an intermediate range for the sample set. These values (-8.7‰ on average) are attributed to the influence of atmospheric $CO_2$ on the groundwater-$\delta^{13}$C-DIC, owing to the sparse vegetation and sandy soils in these regions.

**Group 3** – The catchments in this group, namely the Tsauchab and Tsondab River catchments, are isotopically different to groups 1 and 2, and hence plot oppositely in figure 45. Group 3 waters are characterised by $^{87}Sr/^{68}Sr$ ratios in the range of 0.71076 to 0.72557, which is consistent with $^{87}Sr/^{68}Sr$ ratios in local lithologies. $\delta^{13}$C-DIC values are the highest for the sample set and are the result of carbonate dissolution occurring in these catchments. $\delta^{18}O$ and δD values for group 3 waters are the most depleted for the sample set, ranging between -5‰ and -7‰ for $\delta^{18}O$ and -30‰ to -50‰ for δD. $\delta^{26}$Mg values for most of the group 3 samples are low, and reflect a greater contribution from carbonate lithologies.

**Outliers** – The Kuiseb and Orange River waters represent outliers in this study, and do not show isotopic characteristics that categorise them into one of the three groups. The Orange River catchment is unique to this project because it represents the only catchment in which surface water samples alone were collected and was one of few rivers on the west coast that was in full-flow. As a result,

most of the surface water samples constituting this study are from this catchment. If these samples were compared to those of larger rivers in a surface water study, it is more likely that groups of isotopically similar zones could be characterised. The Kuiseb River further north from the two other northern region catchments. Also, due to time constraints, only four samples were collected from

this catchment. A more accurate study would incorporate more samples, as well as catchments in a closer proximity, to distinguish isotopic zones.

The aim of this section was to isotopically characterise the catchments sampled for this project and determine whether groups of similar isotopic character can be delineated. The end goal would be a set of isotopic criteria to characterise processes taking place in catchment waters to obtain a more robust understanding of hydrological systems. Based on the groups described above, it is evident that in this study, mechanisms occurring in west coast catchment waters can be constrained to sufficient precision using isotope systems alone.

# 5 CONCLUSIONS

Prior to this study, no published measurements of Mg isotope ratios in rivers and groundwater systems exists for southern Africa. This thesis has presented 40 new measurements of Mg isotope ratios in major rivers and their corresponding groundwater catchments from the west coast of South Africa and Namibia. Analysis of $\delta^{26}$Mg has provided an understanding of the mechanisms that control riverine and groundwater $\delta^{26}$Mg in West coast aquifers. Riverine and groundwater Mg on a global scale is mainly derived from the weathering of silicates and dolostones (Tipper, 2006). On the west coast of southern Africa, Mg isotope ratios are interpreted in the context of processes inferred from $^{87}Sr/^{86}Sr$, $\delta^{13}$C-DIC, $\delta$D and $\delta^{18}$O isotope ratios and major element chemistry.

West coast waters draining predominately basic and intermediate silicate rock have a $\delta^{26}$Mg of -0.83‰ (n=17). Groundwater draining granitic and gneissic silicate bedrock (Namaqualand catchments) have a $\delta^{26}$Mg of 0.81‰ (n=8). When compared to the global $\delta^{26}$Mg average for silicate bedrock (-1.24‰) (Tipper, 2006), waters draining silicate rock are enriched in the light isotopes of Mg by approximately 0.42‰. This suggests that Mg isotope ratios are fractionated during silicate weathering. Furthermore, global bulk silicate soils record an average $\delta^{26}$Mg of 0.03‰, which is around 0.4‰ more enriched in the heavy isotopes of Mg compared to the silicate rocks from which it formed (Tipper, 2006). This value is consistent with the retention of $^{26}$Mg in soil minerals, which would enrich companion solutions in the light isotopes of Mg, as is observed in the silicate catchment waters. Nine Groundwater and three spring samples collected from the catchments of the Tsauchab and Tsondab Rivers, which drain predominately carbonate rocks, have an average $\delta^{26}$Mg of -1.21‰ (n=11), which fall within the global $\delta^{26}$Mg range for dolostones and dolomite-rich rocks (Teng, 2017). These results suggest that Mg isotope ratios are not fractionated during the dissolution of dolomite. However, it is difficult to extrapolate this average to a global scale because of the ~3‰ $\delta^{26}$Mg variation that has been documented for dolomites (Tipper, 2006; Teng, 2017).

This study has attempted not only to assess the natural Mg isotopic variation in west coast catchments and identify processes responsible for this variation, but also to quantify the effectiveness of Mg isotopes as a routine tool for isotope hydrology. As mentioned previously, Mg isotopes are a potentially strong lithological source tracer and provide a reliable means of studying geological and environmental processes (Brenot, et al., 2008). The large scale of this project presented well constrained and contrasting lithologies, and this is reflected in both the hydrochemical and isotopic parameters measured in the water samples. The results of these analyses illustrate that the use of Mg isotopes coupled with other isotope tracers and major element chemistry can be used to better constrain sources of riverine and groundwater magnesium. A potential setback in this study was the

limitation of Mg isotopic measurement to water systems only. Future hydrological Mg-isotope studies in southern africa should be used in conjunction with measurements obtained from soils and parent rocks representative of the main lithologies, and local precipitation where possible.

# 6 REFERENCES

Adams, S., Titus, R. & Xu, Y., 2004. *Groundwater Recharge Assessment of the Basement Aquifers of Central Namaqualand ,* Belville: Water Research Commission.

Adelana, S., 2005. Summary of Isotopes in Contaminant Hydrogeology. In: J. Lehr & J. Keeley, eds. *Water Encyclopedia .* s.l.:John Wiley & Sons, Inc., pp. 1-12.

Adelana, S. & Olasehinde, P., 2005. *Isotope Techniques as Tools for Sustainable Groundwater Development and Management.* Pretoria, Biennial Groundwater Conference.

Aggarwal, P., 2011. *Using isotopes effectively to support comprehemsive groundwater management.*

Vienna, International Atomic Energy Agency (IAEA).

Aggarwal, P., Froehlich, K. & Kulkarni, K., 2009. Environmental Isotopes in Groundwater Studies. In: L.

Silveria & J. Usunoff, eds. *Groundwater Volume 2.* Oxford, United Kingdom: EOLSS , pp. 69-92.

Albat, H., 1984. *The Proterozoic granulite facies terrane around Kliprand, Namaqualand Metamorphic Complex,* Cape Town: University of Cape Town, Dept. of Geology, Chamber of Mines Precambrian Research Unit.

Alvaradoa, J. et al., 2011. Reconstruction of past climate conditions over central Europe from groundwater data. *Quaternary Science Reviews,* 30(23-24), p. 3423–3429.

An, Y. & Huang, F., 2014. A Review of Mg Isotope Analytical Methods by MC-ICP-MS. *Journal of Earth Science,* 25(5), pp. 822-840.

An, Y. & Huang, F., 2014. A Review of Mg Isotope Analytical Methods by MC-ICP-MS. *Journal of Earth Science,* 25(5), p. 822–840.

Aravena, R. et al., 1992. Evaluating Dissolved Inorganic Carbon Cycling in a Forested Lake Watershed Using Carbon Isotopes. *Radiocarbon,* 34(3), pp. 636-645.

Backstrom, M. et al., 2003. Speciation of heavy metals in road runoff and roadside total deposition.

*Water, Air & Soil Pollution,* Volume 147, pp. 343-366.

Bade, D. et al., 2004. Controls of S13C-DIC in lakes: Geochemistry, lake metabolism, and morphometry.

*Limnology and Oceanography,* 49(4), pp. 1160-1172.

Baker, J. et al., 2005. Earth planetesimal melting from an age of 4.5662 Ga Gyr for differentiated meteorites.. *Nature,* Volume 436, pp. 1127-1131.

Barker, J. & Fritz, P., 1981. Carbon isotope fractionation during microbial methane oxidation. *Nature,* Volume 293, pp. 289-291.

Bass, A. et al., 2010. Temporal and spatial heterogeneity in lacustrine δ13CDIC and δ18ODO signatures. *Journal of Limnology,* 69(2), pp. 341-349.

Baxter, A. & Meadows, M., 1996. Evidence for Holocene sea level change at Verlorenvlei,. *Quaternary International,* Volume 56, p. 66.

Benito, G. et al., 2010. Rainfall-runoff modelling and palaeoflood hydrology applied to reconstruct centennial scale records of flooding and aquifer recharge in ungauged ephemeral rivers. *Hydrology and Earth System Science,* Volume 15, pp. 1186-1187.

Benito, G. et al., 2009. Management of Alluvial Aquifers in Two Southern African Ephemeral Rivers: Implications for IWRM. *Water Resour Manage,* Volume 24, p. 641–667.

Berner, A., Lasaga, A. & Garrels, R., 1983. The carbonate–silicate geochemical cycle and its effect on atmospheric carbon-dioxide over the past 100 million years. *American Journal of Science,* Volume 283, p. 641–683.

Black, J., Yin, Q. & Casey, W., 2006. An experimental study of magnesium-isotope fractionation in chlorophyll-a photosynthesis. *Geochimica et Cosmochimica Acta,* Volume 70, pp. 4072-4079.

Black, W., 1966. *Hydrochemical facies and ground-water flow patterns in northern part of Atlantic Coastal Plain: U.S. Geological Survey Professional Paper 498-A,* Washington : United States Geological Survey.

Blättler, C., Miller, N. & Higgins, J., 2015. Mg and Ca isotope signatures of authigenic dolomite in siliceous deep-sea sediments. *Earth and Planetary Science Letters,* Volume 419, pp. 32-42.

Blum, J. & Erel, Y., 2005. Radiogenic Isotopes in Weathering and Hydrology. In: J. Drever, ed. *Surface and Ground Water, Weathering and Soils: Treatise on Geochemistry. .* s.l.:Elsevier, pp. 365-392.

Böhlke, J. & Horan, M., 2000. Strontium isotope geochemistry of groundwaters and streams affected by agriculture, Locust Grove, MD. *Applied Geochemistry ,* 15(5), pp. 599-609.

Booth, D., 1991. Urbanization and the Natural Drainage System - Impacts, Solutions and Prognoses. *The Northwest Environmental Journal,* 7(1), pp. 93-118.

Bouillon, S., Connolly, R. & Gillikin, D., 2011. Use of Stable Isotopes to Understand Food Webs and Ecosystem Functioning in Estuaries. In: E. Wolanski & D. McLusky, eds. *Treatise on Estuarine and Coastal Science.* s.l.:Waltham: Academic Press, pp. 144-165.

Bowen, G., 2008. Spatial analysis of the intra-annual variation of precipitation isotope ratios and its climatological corollaries. *Journal of Geophysical Research,* 113(D5).

Brantley, S., Liermann, L. & Bullen, T., 2001. Fractionation of Fe isotopes by soil microbes and organic acids. *Geology,* Volume 29, p. 535–538.

Brenot, A. et al., 2008. Magnesium isotope systematics of the lithologivally varied Moselle river basin, France. *Geochimica et Cosmochimica Acta ,* Volume 72, pp. 5070-5089.

Brook, G., Srivastava, P. & Marais, E., 2006. Characteristics and OSL minimum ages of relict fluvial deposits near Sossus Vlei, Tsauchab River, Namibia, and a regional climate record for the last 30 ka. *Journal of Quarternary Science ,* 21(4), p. 349.

Buhl, D. et al., 2007. Time series δ26Mg analysis in speleothem calcite: Kinetic versus equilibrium fractionation, comparison with other proxies and implications for palaeoclimate research. *Chemical Geology,* 244(3-4), pp. 715-729.

Bullen, T. & Kendall, C., 1998. Tracing of weathering reactions and water flowpaths: a multi-isotope approach. In: C. Kendall & J. MacDonnell, eds. *Isotope Tracers in Catchment Hydrology.* Amsterdam: Elsevier, p. 611–646.

Burnett, W., Taniguchi, M. & Oberdorfer, J., 2001. Measurement and significance of the direct discharge of groundwater into the coastal zone. *Journal of Sea Research,* Volume 46, pp. 109-116.

Buttle, J., 1998. Fundamentals of Small Catchment Hydrology. In: C. Kendall & J. MacDonnell, eds. *Isotope Tracers in Catchment Hydrology.* Amsterdam: Elsevier, pp. 2-41.

Capo, R., Stewart, B. & Chadwick, O., 1998. Strontium isotopes as tracers of ecosystem processes: Theory and methods. *Geoderma,* Volume 82, pp. 197-225.

Carder, E. et al., 2005. Magnesium isotopes in bacterial dolomites: A novel approach to the dolomite problem. *Geochimica et Cosmochimica Acta,* Volume 69, p. A213.

Cenki-Tok, B. et al., 2009. The impact of water–rock interaction and vegetation on calcium isotope fractionation in soil- and stream waters of a small, forested catchment (the Strengbach case). *Geochimica et Cosmochimica Acta,* 73(8), pp. 2215-2228.

Cerling, T., 1991. Carbon dioxide in the atmosphere: evidence from Cenozoic and Mesozoic paleosls. *American Journal of Science ,* 291(4), pp. 377-400.

Chesson, L. et al., 2012. Strontium isotopes in tap water from the coterminous USA. *Ecosphere,* 3(7), pp. 1-17.

Clarke, I., 2015. *Groundwater Geochemistry and Isotopes.* 1st ed. Milton Park, United Kingdom: Taylor & Francis.

Clark, I. & Fritz, P., 1997. *Environmental Isotopes in Hydrogeology.* New York: CRC Press.

Coat, S., Monti, D., Bouchon, C. & Lepoint, J., 2009. Trophic relationships in a tropical stream food web assessed by stable isotope analysis. *Freshwater Biology,* 54(5), pp. 1028-1041.

Coudray, C. et al., 2005. Stable isotopes in studies of intestinal adsorption, exchangeable pools and mineral status: the example of magnesium. *Journal of Trace Elements in Medicine and Biology,* Volume 19, pp. 97-103.

Cowling, R., Esler, K. & Rundel, P., 1999. Namaqualand, South Africa – an overview of a unique winter-rainfall desert ecosystem. *Plant Ecology,* 142(1-2), pp. 3-21.

Craig, H., 1961. Isotopic variations in meteoric waters. *Science ,* Volume 133, pp. 1702-1703.

Custudio, E., 1992. *Hydrogeological and hydrochemical aspects of aquifer over-exploitation. ,* Tenerife: International Congress of IAH.

Dansgaard, W., 1964. Stable isotopes in precipitation. *Tellus,* 16(4), p. 411–537.

Darling, W., Bath, A., Gibson, J. & Rozanski, K., 2006. Isotopes in Palaeoenvironmental Research. In: Ontario, ed. *Developments in Palaeoenvironmental Research.* Smol, J.P. : Springer, pp. 1-66.

Darling, W., Bath, A. & Talbot, J., 2003. The O & H stable isotopic composition of the British Isles.2. Surface waters and groundwater. *Hydrology and Earth System Sciences,* 7(2), pp. 183-195.

De Clercq, W., Fey, M. & Jovanovic, N., 2009. An overview of the salinization problem in the Berg river catchment (South Africa). *WIT Transactions on Ecology and the Environment,* Volume 127, pp. 379-389.

de Villiers, S., 2007. The deteriorating nutrient status of the Berg River, South Africa. *Water SA,* p. 660.

De Villiers, S. & Cadman, A., 2001. An analysis of the palynomorphs obtained from Tertiary sediments at Koingnaas, Namaqualand, South Africa. *Journal of African Earth Sciences,* 33(1), pp. 17-47.

de Villiers, S., Compton, J. & Lavelle, M., 2000. The strontium isotope systematics of the Orange River, Southern Africa. *South African Journal of Geology,* 103(3-4), pp. 237-248.

de Villiers, S., Dickson, J. & Ellam, R., 2005. The composition of the continental river weathering flux deduced from seawater Mg isotopes. *Chemical Geology ,* Volume 216, pp. 133-142.

de Villiers, S., Dickson, J. & Ellam, R., 2005. The composition of the continental river weatheringflux deduced from seawater Mg isotopes. *Chemical Geology,* Volume 216, p. 133–142.

Deines, P., 1980. The isotopic composition of reduced organic carbon. In: P. Fritz & J. Fontes, eds. *Handbook of Environmental Isotope Geochemistry Volume 1.* Amsterdam : Elsevier, p. 329–406.

Deodhar, A. et al., 2014. Isotope Techniques for Water Resources Management. *Barc Newsletter*, March-April, Issue 337, pp. 29-37.

Deodhar, A. et al., 2014. Isotope Techniques for Water Resources Management. *BARC News letter,* 35(337), pp. 29-35.

DePaolo, D., 2004. Calcium isotopic variations produced by biological, kinetic, radiogenic and nucleosynthetic processe. *Reviews in Mineralogy and Geochemistry,* Volume 55, p. 255–288.

Diamond, R., 2017. *Are farmers drying out the Cederberg? Deep groundwater flow and isotopes in the Table Mountain Group.* Stellenbosch , 15th Biennial Ground Water Division Conference.

Drake, H. et al., 2015. Extreme 13C depletion of carbonates formed during oxidation of biogenic methane in fractured granite. *Nature Communications,* Volume 6, pp. 1-9.

Dregne, H., 2002. Land degradation in the drylands. *Arid Land Researchand Management ,* Volume 16, pp. 99-132.

Eckardt, F., Livingston, I., Seely, M. & von Holdt, J., 2013. The surface geology and geomorphology around Gobabeb, Namib Desert, Namibia. *Physical geography,* Volume 95, p. 271–284.

Edmond, J. et al., 1979. Ridge crest hydrothermal activity and the balances of the major and minor elements in the ocean: The Galapagos data.. *Earth and Planetary Science Letters ,* Volume 46, pp. 1-18.

Edmunds, W., 2001. *Isotope techniques in water resource investigations in arid and semi-arid regions,* Vienna: IAEA.

Egli, M., Mirabella, A. & Sartori, G., 2008. The role of climate and vegetation in weathering and clay mineral formation in later Quaternary soils of the Swiss and Italian Alps. *Geomorphology,* Volume 102, pp. 307-324.

Elderfield, H. & Schultz, A., 1996. Mid-ocean ridge hydrothermal fluxes and the chemical composition of the ocean.. Volume 24, pp. 191-224.

Fairchild, I. & Baker, A., 2012. *Speleothem Science: From Process to Past Environments.* 1st ed. Hoboken, New Jersey, United States: Wiley-Blackwell.

Fantle, M. & Tipper, E., 2014. Calcium isotopes in the global biogeochemical Ca cycle: implications for development of a Ca isotope proxy. *Earth-Science Reviews,* Volume 129, p. 148–177.

Fan, Y., Chen, Y. H. Q., Li, W. & Wang, Y., 2016. Isotopic Characterization of River Waters and Water Source Identification in an Inland River, Central Asia. *Water,* 8(286), pp. 1-14.

Fersch, B., 2007. *Interactions between riparian phreatophytes and alluvial aquifers,* Freiburg: Universitat Freiburg.

Finlay, J., 2003. Controls of streamwater dissolved inorganic carbon dynamics in a forested watershed.. *Biogeochemistry,* Volume 62, pp. 231-252.

Fourie, J. & Steer, A., 1971. *Water Quality Survey of the Berg River for the Period 1963-1970,* Cape Town: Research Report of the National Institute of Water Research to the Provincial Administration of the Cape of Good Hope.

Frederickson, G. & Criss, R., 1999. Isotope hydrology and residence times of the unimpounded Meramec River Basin, Missouri.. *Chemical Geology,* Volume 157, pp. 303-317.

Froehlich, K., Rozanski, K. & Araguas, L., 1998. Isotope hydrology : Applied discipline in earth sciences. *Colloques et séminaires - Institut français de recherche scientifique pour le développement en coopération ,* pp. 56-72.

Galy, A., Bar-Matthews, M., Halicz, L. & O'Nions, R., 2002. Mg isotopic composition of carbonate: insight from speleothem formation. *Earth and Planetary Science Letters,* Volume 201, pp. 105-115.

Galy, A. & France-Lanord, C., 1999. Weathering processes in the Ganges-Brahmaputra basin and the riverine alkalinity budget.. *Chemical Geology,* Volume 159, p. 31–60.

Galy, A., France-Lanord, C. & and Derry, L., 1999. The strontium isotopic budget of Himalayan Rivers in Nepal and Bangladesh. *Geochim. et Cosmochim. Acta ,* Volume 63, pp. 1905-1925.

Gat, J., 1996. Oyxgen and Hydrogen Isotopes in the Hydrological Cycle. *Annual Review of Earth and Planetary Sciences,* Volume 24, pp. 225-262.

Gat, J. & Tzur, Y., 1967. *Modification of the isotopic composition of rainwater by processes which occur before groundwater recharge.* Vienna, IAEA.

Gaye, C., 2001. *Isotope techniques for monitoring groundwater salinization.* Vienna, s.n.

Geyh, M., 2000. Environmental Isotopes in the Hydrological Cycle: Principles and Applications. In: W. G. Mook, ed. *Groundwater Volume IV.* Hannover: Niedersächsisches Landesamt für Bodenforschung , pp. 1-185.

Gibbs, R., 1970. Mechanisms Controlling World Water Chemistry. *Science, New Series,* 170(3964), pp. 1088-1090.

Gore, J., King, J. & Hamman, K., 1991. Application of the instream flow incremental methodology to Southern African rivers: Protecting endemic fish of the Olifants River. *Water SA,* 17(3), pp. 225-236.

Gosz, J., Likens, G. & Bormann, F., 1973. Nutrient release from decomposing leaf and branch litter in the Hubbard Brook Froest, New Hampshire. *Ecological Monograms,* Volume 43, pp. 173-191.

Gourcy, L. & Aggarwal, P., 2005. Strengthening the use of Isotope techniques for a Sustainable Groundwater Management . In: E. Bocanegra, M. Hernandez & E. Usunoff, eds. *Groundwater and Human Development: IAH Selected Papers on Hydrogeology 6.* s.l.:CRC Press , pp. 41-48.

Graustein, W., 1989. 87Sr/86Sr Ratios Measure the Sources and Flow of Strontium in Terrestrial Ecosystems. In: P. Rundel, J. Ehleringer & K. Nagy, eds. *Stable Isotopes in Ecological Research.* Berlin: Springer , pp. 491-512.

Greshko, M., 2017. *Did This Mysterious Ape-Human Once Live Alongside Our Ancestors?,* Washington D.C.: National Geographic.

Gupta, S. & Deshpande, R., 2005. The need and potential applications of a network for monitoring of isotopes in waters of India. *Current Science ,* 88(1), pp. 107-118.

Gussone, N. et al., 2016. *Calcium Stable Isotope Geochemistry.* 1st ed. New York: Springer.

Hanson, P. et al., 2006. Lake dissolved inorganic carbon and dissolved oxygen: Changing drivers from days to decades. *Ecological Monographs ,* Volume 76, pp. 343-363.

Haper, C. et al., 2005. Increased rainfall variability and reduced rainfall amount decreases soil CO2 flux in a grassland ecosystem. *Global Change Biology,* Volume 11, pp. 322-334.

Hardie, L., 1996. Secular variation in seawater chemistry; an explanation for the coupled secular variation in the mineralogies of marine limestone and potash evaporites over the past 600 M.Y.. *Geology,* Volume 24, pp. 279-283.

Hayashi, M. & Rosenberry, D., 2002. Effects of Ground Water Exchange on the Hydrology and Ecology of Surface Water. *Groundwater,* 40(3), p. 309–316.

Heath, R. & Brown, C., 2007. *Orange River Integrated Water Resources Management Plan: Environmental Considerations Pertaining to the Orange River,* Botswana: WRP Consulting Engineers, Jeffares and Green, Sechaba Consulting, WCE Pty Ltd.

Herczeg, A., Simpson, H. & Mazor, E., 1993. Transport of soluble salts in a large semiarid basin: River Murray, Australia. *Journal of Hydrology,* Volume 144, pp. 59-84.

Hermoso, M., 2014. Coccolith-Derived Isotopic Proxies in Palaeoceanography: Where Geologists Need Biologists. *Cryptogamie, Algologie,* 38(2), pp. 323-351.

Hindshaw, R., 2011. *Chemical weathering and calcium isotope fractionation in a glaciated catchment,* Zurich: ETH.

Hippler, D. et al., 2009. Towards a better understanding of magnesium-isotope ratios from marine skeletal carbonates. *Geochimica et Cosmochimica Acta,* Volume 73, pp. 6134-6149.

Hoefs, J., 2009. Isotope fractionation processes of selected elements. In: *Stable Isotope Geochemistry.* Berlin: Springer, pp. 35-92.

Huang, T. & Pang, Z., 2014. The role of deuterium excess in determining the water salinization mechanism: A case study of the arid Tarim River Basin, NW China.. *Applied Geochemistry,* Volume 27, pp. 2382-2388.

Hughes, C. & Crawford, J., 2013. Spatial and temporal variation in precipitation isotopes in the Sydney Basin, Australia. *Journal of Hydrology,* Volume 489, p. 42–55.

IAEA, 2002. *Water for Development,* Vienna: International Atomic Energy Agency.

IAEA, 2011. *Using Isotopes Effectively to Support Comprehensive Groundwater Management,* Vienna: IAEA.

Immenhauser, A. et al., 2010. Magnesium-isotope fractionation during low-Mg calcite precipitation in a limestone cave - Field study and experiments. *Geochimica et Cosmochimica Acta,* Volume 74, pp. 4346-4364.

Ingraham, N., Caldwell, E. & Verhagen, B., 1998. Arid Catchments. In: C. Kendall & J. MacDonnell, eds. *Isotope Tracers in Catchment Hydrology.* Amsterdam : Elsevier, pp. 435-460.

Jacobson, A., Zhang, Z., Lundstrom, C. & Huang, F., 2010. Behaviour of Mg isotopes during dedolomitization in the Maidosn Aquifer, South Dakota. *Earth and Planetary Science Letters,* Volume 297, pp. 446-452.

Jacobson, P. J. K. S. M., 1995. *Ephemeral rivers and their catchments: sustaining people and development in western Namibia.* 1st ed. Windhoek : Desert Research Foundation of Namibia.

Jordaan, L., Wepener, V. & Huizenga, J., 2016. The strontium isotope distribution in water and fish within major South African catchments. *African Journals Online ,* 42(2), pp. 213-224.

Karasinski, J. et al., 2017. High precision direct analysis of magnesium isotope ratio by ion chromatography/multicollector-ICPMS using wet and dry plasma conditions. *Talanta,* Volume 165, pp. 64-68.

Kaseke, K. et al., 2016. An Analysis of Precipitation Isotope Distributions across Namibia Using Historical Data. *PLoS ONE 11(5),* Volume e0154598. doi:10.1371/, pp. 1-19.

Kebede, S., Puig, J. & Travi, Y., 2004. Groundwater Recharge, Circulation and Geochemical Evolution in the Source Region of the Blue Nile River, Ethiopia. *Colloque International en Education,* Volume 21,22 & 23, pp. 179-183.

Kemp, P., 1971. Chemistry of natural waters—III carbonic acid. *Water Research,* 5(8), pp. 611-619.

Kendall, C. & Caldwell, E., 1998. Fundamentals of Isotope Geochemistry. In: C. Kendall & J. McDonnell, eds. *Isotope Tracers in Catchment Hydrology.* Amsterdam: Elsevier Science B.V., pp. 51-86.

Kendall, C. & Doctor, D., 2003. Stable Isotope Applications in Hydrologic Studies. In: H. Holland & K. Turekian, eds. *Treatise on Geochemistry, Volume 5.* s.l.:Elsevier, pp. 319-364.

King, J., Cambray, J. & Impson, D., 1998. Linked effects of dam-released floods and water temperature on spawning of the Clanwilliam yellowfish Barbus capensis. *Hydrobiologia,* 384(1-3), pp. 245-265.

Knauth, L. & Beeunas, M., 1986. Isotope geochemistry of fluid inclusions in Permian halite with implications for the isotopic history of ocean water and the origin of saline formation waters.. *Geochimica et Cosmochimica Acta,* 50(3), p. 419–433.

Lancaster, N., 1984. Late Cenozoic fluvial deposits of the Tsondab Valley, central Namib Desert. *Madoqua,* 13(4), pp. 257-269.

Lancaster, N., 1984. Paleoenvironments in the Tsondab Valley, Central Namib Desert. *Palaeoecology of Africa,* Volume 16, pp. 411-419.

Lancaster, N. & Teller, J., 1988. Interdune deposits of the Namib sand sea. *Sedimentary Geology,* Volume 55, pp. 91-107.

Lasaga, A. et al., 1994. Chemical-weathering rate laws and global geochemical cycles. *Geochimica et Cosmochimica Acta,* Volume 58, p. 2361–2386.

Le Maitrea, D., Colvina, C. & Maherry, A., 2009. Water resources in the Klein Karoo: the challenge of sustainable development in a water-scarce area. *South African Journal of Science,* Volume 105, pp. 39-48.

Lebeau, O., Busigny, V., Chaduteau, C. & Ader, M., 2014. Organic matter removal for the analysis of carbon and oxygen isotope compositions of siderite. *Chemical Geology,* Volume 372, p. 54–61.

lee, S., Ryu, J. & Lee, K., 2013. Magnesium isotope geochemistry in the Han River, South Korea. *Chemical Geology,* 364(2014), pp. 9-19.

Lee, S., Ryu, J. & Lee, K., 2014. Magnesium isotope geochemistry in the Han River, South Korea. *Chemical Geology,* Volume 364, pp. 9-19.

Leibundgut, C., Maloszewski, P. & Kulls, C., 2009. *Tracers in Hydrology.* First ed. Chichester, United Kingdom: John Wiley & Sons Ltd.

Lemarchand, D., Wasserburg, G. & Papanastassiou, D., 2004. Rate-controlled calcium isotope fractionation in synthetic calcite. *Geochimica et Cosmochimica Acta,* 68(22), p. 4665–4678.

Leshomo, J., 2011. *Investigation of hydrochemistry and uranium radioactivity in the groundwater of Namaqualand, Northern Cape, South Africa,* Johannesburg: University of Witwatersrand.

Lovell, C., 2000. *Productive Water Points in Dryland Areas.* First ed. Great Britain: ITDG.

Lyons, W., Tyler, S., Gaudette, H. & Long, D., 1995. The use of strontium isotopes in determining groundwater mixing and brine fingering in a playa spring zone, Lake Tyrrell, Australia. *Journal of Hydrology,* Volume 167, pp. 225-239 .

Macpherson, G. & Townsend, M., 1998. Water Chemistry and Sustainable Yield. In: M. Sophocleous, ed. *Perspectives on Sustainable Development of Water Resources in Kansas.* Kansas: Kansas Geological Survey, pp. 117-154.

Maher, K., 2010. The dependence of chemical weathering on fluid residence time. *Earth and Planetary Science Letters,* Volume 294, pp. 101-110.

Marais, J., 1981. *Updated Technical Report on the Spektakel Water Scheme in the District of Springbok, Cape Province,* Nababeep: Unpublished report on the O'Okiep Copper Company Limited, South Africa.

Marais, J., Agenbacht, A., Prinsloo, M. & Basson, W., 2001. *The Geology of Sprinbok Area, Explanation: Sheet 2916. Scale 1:250 000. ,* Pretoria: Council for Geoscience.

Marker, M., 1979. Relict fluvial terraces on the Tsondab Flats, Namibia. *Journal of Arid Environments,* Volume 2, pp. 113-117 .

Marschner, H., 1995. *Mineral nutrition of higher plants.* 1st ed. London: Academic Press.

Martin, J., Vance, D. & Balter, V., 2014. Natural variation of magnesium isotopes in mammal bones and teeth from two South African trophic chains. *Geochimica et Cosmochimica Acta,* Volume 130, p. 12–20.

Martin, J., Vance, D. & Balter, V., 2014. Natural variation of magnesium isotopes in mammal bones and teeth from two South African trophic chains. *Geochimica et Cosmochimica Acta,* Volume 130, pp. 12-20.

McDowell, R., 2008. *Environmental Impacts of Pasture-Based Farming,* Oxfordshire: CAB International.

McNutt, R., 2000. Strontium isotopes. In: P. Cook & A. Herczeg, eds. *Environmental Tracers in Subsurface Geology.* Boston: Kluwer, pp. 234-260.

Meadows, M., Baxter, A. & Parkington, J., 1996. Late Holocene environments at Verlorenvlei, Western Cape. *Quaternary International,* Volume 33, p. 82.

Meredith, K. et al., 2009. Temporal variation in stable isotopes and manor ion concentrations within the Darling River between Bourke and Wilcannia due to variable flows, saline groundwater influx and evaporation.. *Journal of Hydrology,* Volume 378, pp. 313-324.

Meybeck, M., 1987. Global chemical weathering of surificial rocks estimated from river dissolved loas. *American Journal of Science ,* Volume 287, pp. 401-428.

Meybeck, M., 2003. Global analysis of river systems: From Earth system controls to Anthropocene syndromes. *Philosophical Transactions of the Royal Socitey Series B,* Volume 358, pp. 1935-1955.

Meyer, K. et al., 2014. Interpretation of speleothem calcite δ13C variations: Evidence from monitoring soil CO2, drip water, and modern speleothem calcite in central Texas. *Geochimica et Cosmochimica Acta,* Volume 142, pp. 281-298.

Meyer, S., Hansen, R., van Dyk, D. & Kruidenier, J., 2014. *Zandkopsdrift Mine Project, Northern Cape Province, South Africa.: Hydrogeological & Geochemical Specialist Study,* Johannesburg: AGES .

Mikova, J., 2012. Strontium isotopic composition as a tracer of weathering processes, a review with respect to James Ross Island, Antarctica. *Czech Polar Reports ,* 2(1), pp. 20-30.

Miller, J., Viola, G. & Mancktelow, N., 2008. Oxygen, carbon and strontium isotope constraints on the mechanisms of nappe emplacement and fluid–rock interaction along the subhorizontal Naukluft Thrust, central Namibia. *Journal of the Geological Society,* Volume 165, pp. 739-753.

Milner, A., Brown, L. & Hannah, D., 2009. Hydroecological response of river systems to shrinking glaciers. *Hydrological Processes ,* 23(1), p. 62–77.

Monjerezi, M., 2012. *Groundwater Salinity in lower Shire River valley (Malawi): Hydro-geochemical and isotope constraints on sources and evolution,* Oslo: s.n.

Mook, W. & Tan, F., 1991. Stable carbon isotopes in rivers and estuaries. In: E. Degens, S. Kempe & J. Richey, eds. *Biogeochemistry of Major World Rivers.* New York : John Wiley and Sons, pp. 245-264.

Moore, C. et al., 2003. Physical controls on phytoplankton physiology and production at a shelf sea front: a fast repetition-rate fluorometer based field study. *Marine Ecology Progress Series,* Volume 259, pp. 29-45 .

Morant, P., 1984. *Estuaries of the Cape: part2: Synopses of available information on individual systems.,* Stellenbosch: CSIR Research Report 406.

Morin, E. et al., 2009. Flood routing and alluvial aquifer recharge along the ephemeral arid Kuiseb River, Namibia. *Journal of Hydrology,* 368(1-4), pp. 262-275.

Mozley, P. & Burns, S., 1993. Oxygen and Carbon Isotopic Composition of Marine Carbonate Concretions: An Overview. *Journal of Sedimentary Petrology,* 63(1), pp. 73-83.

Mybro, A. & Shapley, M., 2006. Seasonal water-column dynamics of dissolved inorganic carbon isotopic compositions (δ13CDIC) in small hardwater lakes in Minnesota and Montana. *Geochimica et Cosmochimica Acta,* Volume 70, pp. 2699-2714.

Nakwafila, A., 2015. *Salinisation source(s) and mechanism(s) in shallow alluvial aquifers along the Buffels River, Northern Cape Province, South Africa ,* Stellenbosch : Stellenbosch University .

Narany, T. et al., 2014. Identification of the Hydrogeochemical Processes in Groundwater Using Classic Integrated Geochemical Methods and Geostatistical Techniques, in Amol-Babol Plain, Iran. *The Scientific World Journal ,* Volume PMC3913491.

Naude, K., 2010. *A Stable Isotope Study of the Hydrological Systems in the Naukluft Region in Namibia* , Cape Town : University of Cape Town .

Nielsen, L. et al., 2012. Calcium Isotopes as Tracers of Biogeochemical Processes. In: M. Baskaran, ed. *Handbook of Environmental Isotope Geochemistry. Advances in Isotope Geochemistry.* Berlin, Heidelberg: Springer, pp. 105-124.

Novara, et al., 2013. Carbon dynamics of soil organic matter in bulk soil and aggregate fraction during secondary succession in a Mediterranean environment. *Geoderma,* Volume 193-194, p. 213– 221.

Nyarko, B. et al., 2010. Use of isotopes to study floodplain wetland and river flow interaction in the White Volta River basin, Ghana. *Isotopes in Environmental and Health Studies ,* 26(1), pp. 91-106.

Palmer, M. & Edmond, J., 1992. Controls over the strontium isotope composition of river water. *Geochimica et Cosmochimica Acta,* 56(5), pp. 2099-2111.

Pang, H., Li, Y., Yang, J. & Liang, Y., 2010. Effect of brackish water irrigation and straw mulching on soil salinity and crop yields under monsoonal climatic conditions. *Agricultural Water Management* , 97(12), p. 1971–1977.

Parkington, J., 1976. Coastal Settlement between the Mouths of the Berg and Olifants Rivers, Cape Province. *The South African Archaeological Bulletin,* 31(123/124), pp. 127-140.

Park, S. et al., 2005. Regional hydrochemical study on salinization of coastal aquifers, western coastal area of South Korea. *Journal of Hydrology,* Volume 313, p. 182–194.

Pfahl, S. & Sodemann, H., 2014. What controls deuterium excess in global precipitation?. *Climate fo the Past,* Volume 10, p. 771–781.

Phillips, F., Hogan, J., Mills, S. & Hendrickx, J., 2003. Environmental tracers applied to quantifying causes of salinity in arid-region rivers: Preliminary results from the Rio Grande, Southwestern USA. *Developments in water science,* Volume 50, pp. 327-334.

Pickford, M., Eisenmannb, V. & Senutb, B., 1999. Timing of landscape development and calcrete genesis in northern Namaqualand, South Africa. *South African Joumal of Science,* Volume 95, pp. 357-359.

Pillsbury, A., 1981. The salinity of rivers. *Scientific American,* Volume 245, pp. 54-65.

Pitkänen, P., Partamies, S. & Luukkonen, A., 2004. *Hydrogeochemical Interpretation of Baseline Groundwater Conditions at the Olkiluoto Site,* Olkiluoto, Finalnd: Posiva Oy .

Pitman, W., Potgieter, D. & Middleton, B., 1981. *Surface water resources of South Africa ,* Johannesburg : University of Witwatersrand, Hydrological Research Department .

Pogge von Strandmann, P. et al., 2008. The influence of weathering processes on riverine magnesium isotopes ina basaltic terrain. *Earth and Planetary Science Letters,* Volume 276, pp. 187-197.

Pogge von Strandmann, P. et al., 2008. The influence of weathering processes on riverine magnesium isotopes in a basaltic terrain. *Earth and Planetary Sciences ,* Volume 276, pp. 187-197.

Pradeep, K., Aggarwal, K. & Kshitij, M., 2009. Environmental Isotopes in Groundwater Studies . In: L. Silveira & E. Usunoff, eds. *Groudnwater Volume 2: Encyclopedia of Life Support Systems.* s.l.:EOLSS Publications, p. 72.

Price, K., 2001. Effects of watershed topography, soils, land use, and climate on baseflow hydrology in humid regions: A review. *Progress in Physical Geography,* 35(4), p. 465–492.

Qiming, L. et al., 2014. Stable isotope geochemical characteristics of dissolved inorganic carbon in the Jiulong River Estuary, Fujian Province, China. *Chinese Journal of Geochemistry ,* Volume 33, pp. 178-182.

Raiber, M., Webb, J. & Bennets, D., 2009. Strontium isotopes as tracers to delineate aquifer interactions and the influence of rainfall in the basalt plains of southeastern Australia. *Journal of Hydrology,* 367(3-4), pp. 188-199.

Reitsema, R., 1980. Dolomite and nahcolite formation in organic rich sediments: isotopically heavy carbonates. *Geochimica et Cosmochimica Acta,* 44(12), pp. 2045-2049.

Rengasamy, P., 2006. World salinisation with emphasis on Australia. *Journal of Experimental Botany,* 57(5).

Rengasamy, P., 2006. World salinization with emphasis on Australia. *Journal of Experimental Botany,* 57(5), p. 1017–1023.

Retallack, G., 2005. Surface and Ground Water, Weathering, and Soils: Treatise on Geochemistry, Second Edition, Volume 5. In: J. Drever, ed. *Soils and Global Change in the Carbon Cycle over Geological Time.* Amsterdam: Elsevier, pp. 581-607.

Riechelmann, S., 2013. *Calibration and application of the new δ26Mg weathering proxy in speleothem research,* Bochum: Ruhr University Bochum.

Rindsberger, M., Jaffe, S., Rahamim, S. & Gat, J., 1990. Patterns of the isotopic composition of precipitation in time and space: data from the Israeli storm water collection program. *Tellus,* 42(3), p. 263–271.

Saenger, C. & Z., W., 2015. Magnesium isotope fractionation in biogenic and abiogenic carbonates: implications for paleoenvironmental proxies. *Quaternary Science Reviews,* Volume 90, pp. 1-21.

Salama, R., Otto, C. & Fitzpatrick, R., 1999. Contributions of groundwater conditions to soil and water salinization. *Hydrogeology Journal,* 7(1), pp. 46-64.

Sally, Z., Gaskin, S., Folifac, F. & Kometa, S., 2013. The effect of urbanization on community-managed water supply: case study of Buea, Cameroon. *Community Development Journal,* 49(4), pp. 524-540.

Santonia, S. et al., 2016. Strontium isotopes as tracers of water-rocks interactions, mixing processes and residence time indicator of groundwater within the granite-carbonate coastal aquifer of Bonifacio (Corsica, France). *Science of the Total Environment,* Volume 573, p. 233–246.

Scanlon, B. H. R. P., 2002. Choosing appropriate techniques for quantifying groundwater recharge. *Hydrogeology Journal,* Volume 10, pp. 18-39.

Schmitt, A., Chabaux, F. & Stille, P., 2003. The calcium riverine and hydrothermal isotope fluxes and the oceanic calcium mass balance. *Earth and Planetary Science Letters,* Volume 213, pp. 503-518.

Schmitt, A.-D., Chabaux, F. & Stille, P., 2003. The calcium riverine and hydrothermal isotopic fluxes and the oceanic calcium mass balance. *Earth and Planetary Science Letters,* 213(3-4), p. 503–518.

Schobben, M. et al., 2017. Latest Permian carbonate-carbon isotope variability traces heterogeneous organic carbon accumulation and authigenic carbonate formation. *Climate of the past Discussions (under review),* Volume 10.5194/cp-2017-66, 2017, pp. 1-35.

SEP, W. C. G., 2016. *Socio-economic Profile: West Coast District Municipality,* Cape Town: Western Cape Government.

Shand, P., Darbyshire, D., Love, A. & Edmunds, W., 2009. Sr isotopes in natural waters: Applications to source characterisation and water–rock interaction in contrasting landscapes. *Applied Geochemistry ,* Volume 24, p. 574–586.

Shanyengana, E., 2002. Supplementary sources of freshwater in arid environments—groundwater salinisation, solar desalination and fog collection. *PhD Dissertation, Stellenbosch University.*

Shanyengana, E., Henschela, J., Seelya, M. & Sandersonb, R., 2002. Exploring fog as a supplementary water source in Namibia. *Atmospheric Research,* 64(1-4), p. 251–259.

Sharma, S. et al., 2013. Isotope Approach to Assess Hydrologic Connections During Marcellus Shale Drilling. *Groundwater ,* pp. 1-10.

Shiferaw, B. et al., 2014. Managing vulnerability to drought and enhancing livelihood resilience in sub-Saharan Africa: Technological, institutional and policy options. *Weather and Xlimate Extremes,* Volume 3, pp. 67-79.

Silveria, L., 2009. Environmental Isotopes in Groundwater Studies. In: L. Silveira & E. Usunoff, eds. *Groundwater - Volume II.* s.l.:EOLSS Publications, pp. 69-93.

Sklash, M. & Farvolden, R., 1979. The role of groundwater in strom runoff. *Journal of Hydrology,* Volume 43, pp. 45-65.

Soderberg, K. & Compton, J., 2007. Dust as a Nutrient Source for Fynbos Ecosystems, South Africa. *Ecosystems ,* 10(4), pp. 550-561.

Sophocleous, M., 2002. Interactions between groundwater and surface water: the state of the science. *Hydrogeology Journal,* 10(1), p. 52–67.

Sophocleous, M., 2002. Interactions between groundwater and surface water: the state of the science. *Hydrogeology Journal,* 10(1), p. 52–67.

Sposito, G., 2008. *The Chemistry of Soils.* 1st ed. Oxford: Oxford University Press.

Srivastava, R., Ramesh, R. & Rao, T., 2014. Stable isotopic differences between summer and winter monsoon rains over southern India. *Journal of Atmospheric Chemistry,* Volume 71, p. 321–331.

Stengel, H., 1970. *Die Riviere van die Namib met hulle toelope na die Atlantiese Oseaan. Derde Deel: Tsondab, Tsams en Tsauchab,* Department of Water Affairs, S. FV. A. Branch: Unpublished Report.

Stewart, B., Capoa, R. & Chadwick, O., 1998. Quantitative strontium isotope models for weathering, pedogenesis and biogeochemical cycling. *Geoderma,* 82(1-3), pp. 173-195.

Talbot, M., 1990. A review of the palaeohydrological interpretation of carbon and oxygen isotopic ratios in primary lacustrine carbonates. *Chemical Geology,* Volume 80, pp. 261-279.

Tarr, P. & Tarr, J., 2009. *Southern Africa: An overview of the environment,* Windhoek: SAIEA.

Teng, F., 2017. Magnesium Isotope Geochemistry . In: F. Teng, J. Watkins & N. Dauphas, eds. *Non-Traditional Stable Isotopes.* Berlin: Walter de Gruyter GmbH & Co KG, pp. 219-278.

Tipper, E., 2006. *The isotopic fingerprint of calcium and magnesium: from the alteration of the continental crust to global budgets,* Cambridge: Department of Earth Sciences, Magdalene College, University of Cambridge.

Tipper, E. et al., 2006b. The short term sensitivity of carbonates and silicate weathering fluxes: insight from seasonal variations in river chemistry. *Geochimica et Comochimica Acta,* Volume 70, pp. 2737-2754.

Tipper, E., Galy, A. & Bickle, M., 2004. Isotopic composition of dissolved Mg in Himalayan river waters. *Geochimica et Cosmochimica Acta,* 68(11), p. 1.

Tipper, E., Galy, A. & Bickle, M., 2006. Riverine evidence for a fractionated reservoir of Ca and Mg on the continents: Implications for the oceanic Ca cycle. *Earth and Planetary Science Letters,* Volume 247, p. 267–279.

Tipper, E., Galy, A. & Bickle, M., 2008. Calcium and magnesium isotope systematics in rivers draining the Himalaya-Tibetan-Plateau region: Lithological or fractionation control?. *Geochemicia et Cosmochimica Acta,* Volume 72, pp. 1057-1075.

Tipper, E. et al., 2012. Seasonal sensitivity of weathering processes: Hints from magnesium isotopes in a. *Chemical Geology,* Volume 312-313, pp. 80-92.

Titus, R., Beekman, H., Adams, S. & Strachan, L., 2009. *The Basement Aquifers of Southern Africa,* Gezina: Water Research Commission.

Tooth, S. & McCarthy, T., 2004. Anabranching in mixed bedrock-alluvial rivers: the example of the Orange River above Augrabies Falls, Northern Cape Province, South Africa. *Geomorphology,* 57(3-4), pp. 236-237.

Towner, I., 1970. Schematic model calculations for 40K(β−)40Ca. *Nuclear Physics A,* 151(1), pp. 97-106.

Trček, B. & Zojer, H., 2009. Recharge of Springs . In: N. Kresic & Z. Stevanovic, eds. *Groundwater Hydrology of Springs: Engineering, Theory, Management and Sustainability.* Amsterdam: Elsevier, pp. 87-231.

Trojanowska, A. et al., 2008. Diurnal variations in the photosynthesis-respiration activity of a cyanobacterial bloom in a freshwater dam reservoir: An isotopic study.. *Isotopes in Environmental and Health Studies ,* Volume 44, pp. 163-175.

Trueman, C. & Tuross, N., 2002. Trace elements in recent and fossil bone apatite. *Reviews in Mineralogy and Geochemistry,* Volume 48, pp. 489-521.

Tsujimura, M. et al., 2007. Stable isotopic pic and geochemical characteristics of groundwater in Kherlen River basin, a semi-arid region in eastern Mongolia. *Journal of Hydrology,* Volume 333, pp. 47-57.

van Weert, F., van der Gun, J. & Reckman, J., 2009. *Global Overview of Saline Groundwater Occurrence and Genesis,* Utrecht: International groundwater resources assessment centre.

Van Weert, F., Van der Gun, J. & Reckman, J., 2009. *Global Overview of Saline Groundwater Occurrence and Genesis,* Utrecht: International Groundwater Resources Assessment Centre (IGRAC).

Vengosh, A., 2003. Salinization and Saline Environments. *Treatise on Geochemistry,* Volume 9, pp. 333-365.

Vitòria, L., Otero, N., Soler, A. & Canals, A., 2004. Fertilizer Characterization: Isotopic Data (N, S, O, C, and Sr). *Environmental Science & Technology ,* 38(12), p. 3254–3262.

Walker, J., Hays, P. & Kasting, J., 1981. A negative feedback mechanism for the long-term stabilization of Earth's surface-temperature. *Journal of Geophysical Research,* Volume 86, pp. 9776-9782.

Walvoord, M., Phillips, F., Tyler, S. & Hartsough, P., 2002. Deep arid system hydrodynamics 2. Application to paleohydrologic reconstruction using vadose zone profiles from the northern Mojave Desert. *Water Resources Research,* 38(12), p. 271–282.

Ward, J., 1988. Eolian, fluvial and pan (playa) facies of the Tertiary Tsondab Sandstone Formation in the central Namib Desert, Namibia. *Eolian Sediments ,* 55(1-2), p. 143.

Warner, N. et al., 2012. Geochemical evidence for possible natural migration of Marcellus Formation brine to shallow aquifers in Pennsylvania. *PNAS science Sessions ,* 109(30).

Werner, A. et al., 2013. Seawater intrusion processes, investigation and management: Recent advances. *Advances in Water Resources,* Volume 51, pp. 3-26.

White, A. & Blum, A., 1995. Effects of climate on chemical weathering in watersheds.. *Geochimica et Cosmochimica Acta,* 59(9), pp. 1729-1747.

WHO, 2003. Total dissolved solids in Drinking-water. In: *Guidelines for drinking-water quality.* Geneva : s.n.

Wiegand, B., Chadwick, O., Vitousek, P. & Wooden, J., 2005. Ca cycling and isotope fluxes in forested ecosystems in Hawaii. *Geophysical Research Letters,* Volume 32.

Wiegand, B., Chadwick, O., Vitousek, P. & Wooden, J., 2005. Ca cycling and isotopic fluxes in forested ecosystems in Hawaii. *Geophysical Research Letters ,* Volume 32, pp. 404-411.

Williams, W., 2001. Anthropogenic salinisation of inland waters. *Hydrobiologia,* 466(329-337).

Wimpenny, J., 2014. Investigating the behaviour of Mg isotopes during the formation of clay minerals. *Geochimica et Cosmochimica Acta,* Volume 128, pp. 178-194.

Wombacher, F. et al., 2009. Magnesium stable isotope fractionation in marine biogenic calcite and aragonite. *Geochimica et Cosmochimica Acta,* Volume 75, p. 5797–5818.

WRC, 2014. *Water resource management: WRC Knowledge Review,* s.l.: WRC.

Yamanaka, M. & Yabusaki, Y., 2017. Influence of Evaporation on River Water in Arid and Semi-arid Australia: Relationships between Stable Isotope Ratios and Climatic Factors. *Institute of Natural Science, Faculty of Arts and Science, Nihon University,* Volume 52, p. 225－ 236.

Young, E. & Galy, A., 2004. The Isotope Geochemistry and Cosmochemistry of Magnesium. *Reviews in Mineralogy & Geochemistry,* Volume 55, pp. 197-230.

Young, E. & Galy, A., 2004. The Isotope Geochemistry and Cosmochemistry of Magnesium. *Reviews in Mineralogy & Geochemistry,* Volume 55, pp. 197-230.

Zhao, M. et al., 2015. Response of dissolved inorganic carbon (DIC) and δ13CDIC to changes in climate and land cover in SW China karst catchments. *Geochimica et Cosmochimica Acta,* Volume 165, pp. 123-136.

Ziegler, K., Chadwick, O., Brzezinski, M. & Kelly, E., 2006. Natural variations of δ30Si ratios during progressive basalt weathering, Hawaiian Islands. *Geochim. et Cosmochim. Acta ,* Volume 69, pp. 4597-4610.

# 7. APPENDIX 1: Hydrochemistry

**Table 1:** Summary table of the hydrochemical parameters analysed and referred to in this thesis (cations and anions):

| | | | | Cation concentrations | | | | Anion concentrations | | | | | | | |
|---|---|---|---|---|---|---|---|---|---|---|---|---|---|---|---|
| | Sample Name | Sample Type | Location | Ca | K | Mg | Na | Cl | $NO_3$ | $PO_4$ | $SO_4$ | P | S | Br | $HCO_3^-$ |
| | | | | mg/L | | | | mg/L | | | | | | | |
| Berg | BR01 | River | Swartjiesbaai | 59.36 | 7.95 | 100.09 | 2601.31 | 28082 | 0 | 147 | 2483 | 0.21 | 806.20 | 87.78 | 80.60 |
| | Gbr01 | Borehole | Langrietvlei | 109.00 | 3.74 | 46.72 | 311.90 | 782 | 0 | 0 | 78 | 0.19 | 30.30 | 3.13 | 63.20 |
| | Gbr02 | Well | Kersefontein | 86.23 | 13.23 | 203.20 | 1133.96 | 3067 | 0 | 0 | 197 | 0.06 | 78.41 | 9.25 | 61.10 |
| | BR02 | River | Kersefontein | 10.03 | 2.85 | 12.31 | 70.82 | 142 | 0 | 0 | 19 | 0.01 | 7.17 | 0.50 | 83.30 |
| | Gbr03 | Borehole | Outside Hopefield | 42.42 | 1.86 | 7.03 | 93.12 | 204 | 0 | 0 | 4 | 0.36 | 2.15 | 0.59 | 61.40 |
| | BR03 | River | Outside Piketberg | 4.19 | 1.29 | 2.95 | 16.94 | 29 | 0 | 0 | 4 | 0.02 | 1.98 | 0.19 | 15.90 |
| Verlorenvlei | Gvv01 | Borehole | Skrikvanrondon | 20.82 | 4.95 | 31.32 | 169.60 | 439 | 24 | 0 | 53 | 0.01 | 18.49 | 1.10 | 17.40 |
| | Gvv02 | Borerhole | Valskuil | 70.97 | 4.03 | 37.64 | 103.10 | 0 | 0 | 0 | 0 | | | 0.99 | 200.80 |
| | Gvv03 | Borehole | Namaqausfontein | 95.86 | 2.55 | 30.37 | 101.80 | 0 | 0 | 0 | 0 | | | 0.79 | 185.20 |
| | VV01 | Stream | Moutonshoek | 0.74 | 0.06 | 1.02 | 9.12 | 20 | 0 | 0 | 2 | 0.04 | 0.72 | 0.12 | 2.90 |
| | VV02 | River | Outside Reydelingshuys | 20.24 | 2.84 | 30.91 | 178.90 | 511 | 2 | 0 | 53 | 0.01 | 17.78 | 1.11 | 45.00 |
| | GVV04 | Borehole | Fonteinjie | 8.70 | 3.27 | 12.40 | 82.90 | 242 | 32 | 0 | 49 | 0.02 | 5.77 | 0.54 | 49.90 |
| Olifants | OR01 | River | Surface | 2.67 | 1.56 | 3.29 | 17.18 | 31 | 0 | 10 | 4 | < 0.01 | 1.89 | 0.13 | 8.00 |
| | Gor01 | Borehole | Uitkyk | 44.04 | 7.83 | 26.57 | 158.50 | 269 | 0 | 6 | 69 | 0.01 | 26.56 | 0.82 | 110.00 |
| | Gor02 | Borehole | Jomar Boerdery | 89.60 | 14.68 | 64.43 | 365.09 | 828 | 3 | 0 | 151 | 0.03 | 56.98 | 2.33 | 260.00 |
| | Gor03 | Borehole | Jomar Boerdery | 41.87 | 4.84 | 25.82 | 110.90 | 203 | 0 | 0 | 52 | 0.02 | 20.40 | 0.69 | 249.00 |
| | OR02 | River | Jomar Boerdery | 52.68 | 5.29 | 40.92 | 260.28 | 459 | 0 | 0 | 169 | 0.02 | 61.39 | 1.20 | 104.50 |
| | OR03 | River | Outside Lutzville | 111.70 | 11.88 | 84.88 | 624.06 | 1055 | 0 | 0 | 374 | 0.03 | 128.80 | 3.26 | 184.60 |
| | Gor04 | Borehole | Koekenaap | 13.13 | 11.17 | 15.08 | 368.68 | 325 | 32 | 0 | 128 | 0.10 | 46.26 | 1.13 | 203.20 |
| | OR04 | River | Elrhyn | 117.30 | 15.79 | 96.51 | 747.30 | 1326 | 0 | 0 | 371 | 0.08 | 131.00 | 4.09 | 533.50 |
| Groen | Ggr01 | borehole | Unknown | 191.60 | 33.80 | 228.20 | 1300.00 | 3166 | 0 | 0 | 454 | 0.01 | 153.10 | 8.89 | 126.90 |
| | Ggr02 | borehole | Dikdoorn | 296.10 | 18.67 | 255.50 | 1573.00 | 4143 | 0 | 0 | 457 | 0.05 | 163.60 | 11.07 | 63.40 |
| | Ggr03 | Borehole | Perdekraal | 148.20 | 21.78 | 89.38 | 1089.62 | 2335 | 0 | 81 | 271 | < 0.01 | 103.80 | 6.87 | 138.40 |
| | Ggr04 | | Nooitvergeten | 316.40 | 46.51 | 311.80 | 1727.36 | 4825 | 0 | 33 | 455 | < 0.01 | 164.54 | 12.94 | 101.00 |
| | Ggr05 | Borehole | Groenriviersvallei | 291.80 | 23.99 | 218.50 | 1358.49 | 3589 | 0 | 0 | 431 | 0.18 | 149.35 | 10.03 | 122.00 |
| Buffels | Gbf01 | borehole | Kommagas | 60.59 | 13.21 | 69.53 | 311.42 | 712 | 9 | 0 | 108 | 0.01 | 42.64 | 2.50 | 48.60 |
| | Gbf02 | borehole | Kommagas | 11.45 | 5.22 | 22.58 | 79.82 | 199 | 6 | 0 | 23 | 0.01 | 8.04 | 0.70 | 15.00 |
| | Gbf03 | borehole | Kommagas | 23.75 | 7.10 | 44.38 | 115.00 | 298 | 9 | 0 | 72 | 0.01 | 25.31 | 0.91 | 24.10 |
| | Gbf04 | Borehole | Buffels River | 48.79 | 6.06 | 31.46 | 150.85 | 338 | 0 | 0 | 73 | 0.06 | 27.41 | 1.04 | 51.90 |
| | Gbf05 | borehole | Spektakel Mine | 309.10 | 22.65 | 372.20 | 2416.98 | 6405 | 0 | 0 | 1000 | 0.01 | 325.74 | 16.71 | 31.30 |
| | Gbf06 | Borehole | Spektakel Mine | 613.50 | 33.54 | 1597.00 | 1929.00 | 3572 | 44 | 0 | 16441 | < 0.01 | 2444. | 6.81 | 0.00 |
| | Gbf07 | borehole | Dikgat (Oom Joek se plaas) | 629.30 | 82.83 | 389.40 | 2857.00 | 8841 | 0 | 0 | 658 | 0.01 | 168.80 | 22.71 | 170.00 |
| | Gbf08 | borehole | de Beers Borehole | 132.40 | 15.46 | 77.75 | 426.13 | 1047 | 0 | 84 | 227 | 0.17 | 82.84 | 3.24 | 69.30 |
| | BF01 | Spring | Kommegas | 11.74 | 6.11 | 23.22 | 94.11 | 4 | 0 | 5 | 4 | 0.09 | 9.30 | 0.78 | 17.30 |
| Orange | OG01 | River | Alexander Bay | 283.90 | 247.40 | 830.20 | 6903.00 | 3830 | 0 | 0 | 360 | 0.01 | 578.8 | 53.08 | 84.20 |
| | OG02 | River | Spogplaas Guesthouse | 47.65 | 5.42 | 22.79 | 98.19 | 51 | 0 | 0 | 33 | 0.01 | 31.95 | 0.62 | 101.40 |
| | OG03 | River | Brandkoras camping ground and farm | 50.41 | 5.41 | 21.69 | 90.21 | 123 | 0 | 4 | 92 | 0.13 | 33.07 | 0.77 | 87.30 |
| | OG04 | River | Potjiespram Mine (Namibia) | 27.31 | 3.85 | 15.25 | 51.07 | 44 | 0 | 0 | 55 | < 0.01 | 19.76 | 0.31 | 74.70 |
| | OG05 | River | Fish & Orange River confluence | 40.66 | 8.54 | 8.19 | 147.60 | 114 | 0 | 0 | 168 | 0.01 | 59.01 | 0.44 | 79.20 |
| | OG06 | River | Amanzi Trails | 26.69 | 2.99 | 13.72 | 30.97 | 60 | 0 | 0 | 22 | 0.01 | 10.29 | 0.18 | 91.95 |
| Tsauchab | B45 | Borehole | Tsauchab River Camp (Pitgat) | 49.16 | 2.24 | 83.63 | 116.60 | 96 | 0 | 0 | 89 | 0.01 | 32.76 | 0.69 | 647.00 |
| | TS02 | Borehole | Tsauchab River Camp (Dissie Water) | 46.99 | 2.06 | 66.87 | 138.87 | 105 | 3 | 0 | 146 | 0.01 | 52.34 | 0.63 | 535.00 |
| | S83 | Spring | Neurus | 94.46 | 1.77 | 11.78 | 68.70 | 36 | 10 | | 86 | < 0.01 | 30.56 | 0.24 | 379.00 |
| | S84 | Spring | Neurus | 94.69 | 1.94 | 11.81 | 68.54 | 37 | 10 | 0 | 82 | < 0.01 | 30.53 | 0.24 | 383.00 |
| | TS03 | Borehole | Zebra River | 100.20 | 1.82 | 9.67 | 59.49 | 32 | 10 | 0 | 94 | < 0.01 | 33.59 | 0.21 | 364.00 |
| | STS01 | Spring | Hauchabfontein | 54.71 | 3.99 | 45.72 | 131.60 | 98 | 0 | 0 | 189 | < 0.01 | 66.41 | 0.50 | 384.00 |
| | TS04 | Borehole | Betesda | 127.20 | 6.48 | 44.62 | 272.92 | 226 | 36 | 16 | 411 | < 0.01 | 131.57 | 0.83 | 491.00 |
| | B41 | Borehole | Little Sossus Lodge | 101.90 | 4.51 | 40.52 | 142.74 | 133 | 25 | | 177 | < 0.01 | 64.30 | 0.59 | 473.00 |
| | B71 | Borehole | Sesreim Campsite | 72.60 | 3.28 | 40.77 | 125.70 | 75 | 11 | 2 | 130 | 0.06 | 48.78 | 0.40 | 4624.00 |
| | TS07 | Borehole | Kulala Desert Lodge | 16.14 | 4.68 | 17.59 | 358.49 | 176 | 18 | 0 | 265 | 0.01 | 94.94 | 0.83 | 468.00 |
| | B32 | Borehole | Little Kulala Lodge | 23.42 | 11.07 | 23.86 | 247.55 | 190 | 25 | 0 | 198 | < 0.01 | 69.27 | 0.91 | 310.00 |
| Tsondab | B05 | Borehole | Ababis | 49.45 | 5.75 | 81.67 | 98.21 | 79 | 4 | 0 | 113 | 0.02 | 40.51 | 0.53 | 570.00 |
| | TD01 | Borehole | Ababis (Mittel Posten) | 224.20 | 6.03 | 56.10 | 233.96 | 296 | 20 | 0 | 742 | < 0.01 | 221.39 | 1.26 | 258.00 |
| | TD02 | Borehole | Ababis (Schwarzer Berg) | 151.40 | 12.94 | 123.00 | 237.92 | 388 | 40 | 0 | 529 | 0.05 | 163.06 | 2.12 | 480.00 |
| | TD03 | Borehole | Ababis (Constantia Posten) | 84.75 | 9.87 | 132.70 | 300.09 | 444 | 3 | 0 | 510 | < 0.01 | 156.67 | 2.27 | 498.00 |
| | TD04 | Borehole | Ababis (Panorama) | 142.60 | 7.17 | 37.10 | 300.57 | 229 | 3 | 0 | 836 | < 0.01 | 240.28 | 0.81 | 123.00 |
| | B37 | Borehole | Panorama | 79.89 | 3.25 | 23.42 | 60.87 | 57 | 20 | 21 | 53 | 0.01 | 19.32 | 0.44 | 345.00 |
| | TD05 | Borehole | Zais | 61.21 | 4.43 | 94.37 | 113.00 | 78 | 8 | 0 | 119 | 0.02 | 43.77 | 0.58 | 699.00 |
| | B09 | Borehole | Namib Naukluft Lodge | 72.71 | 5.85 | 46.38 | 29.15 | 33 | 13 | 0 | 38 | 0.04 | 14.68 | 0.24 | 427.00 |
| | B59 | Borehole | Namib Desert Lodge | 41.66 | 2.62 | 58.11 | 27.40 | 37 | 31 | 0 | 40 | 0.01 | 14.38 | 0.24 | 357.00 |
| | Sol-08 | Borehole | Solitaire | 174.40 | 7.39 | 35.61 | 170.50 | 171 | 38 | 0 | 484 | < 0.01 | 149.17 | 0.88 | 210.00 |
| Kuiseb | KR01 | Borehole | Homeb | 129.10 | 15.86 | 28.87 | 175.00 | 273 | 0 | 0 | 117 | 0.06 | 41.63 | 0.66 | 457.00 |
| | KR02 | Borehole | Gobabeb | 203.00 | 34.99 | 62.93 | 756.51 | 1186 | 10 | 0 | 481 | 0.07 | 159.44 | 2.39 | 0.00 |
| | KR03 | Borehole | Rooibank | 264.10 | 30.18 | 134.30 | 241.42 | 399 | 0 | 0 | 780 | 0.04 | 242.59 | 0.57 | 505.00 |
| | KR04 | Borehole | Rooibank | 78.95 | 15.73 | 42.80 | 123.58 | 116 | 2 | 0 | 284 | 0.08 | 89.73 | 0.21 | 250.00 |

**Table 2:** Summary table of the hydrochemical parameters analysed and referred to in this thesis (trace elements):

| | | | | Trace element concentrations | | | | | | | | | | | | | | | | | | | |
|---|---|---|---|---|---|---|---|---|---|---|---|---|---|---|---|---|---|---|---|---|---|---|---|
| | Sample Name | Sample Type | Location | Li | Be | B | Al | Ti | V | Cr | Mn | Fe | Co | Ni | Cu | Zn | As | Se | Sr | Mo | Cd | Ba | Pb | U |
| | | | | µg/L | | | | | | | | | | | | | | | | | | | | |
| Berg | BR01 | River | Swartjiesbaai | 124.65 | 0.00 | 3976.67 | 3.50 | 0.14 | 1.12 | 0.34 | 39.51 | 8.05 | 0.09 | 0.50 | 0.59 | 1.97 | 2.27 | 0.96 | 7036.00 | 9.41 | 0.20 | 63.47 | 0.04 | 3.00 |
| | Gbr01 | Borehole | Langrietvlei | 4.88 | 0.07 | 173.39 | 1.72 | 0.12 | 0.06 | 0.24 | 162.24 | 4537.49 | 0.64 | 0.61 | < 0.15 | 7.43 | 4.78 | < 0.6 | 746.47 | 0.19 | 0.05 | 52.69 | 0.02 | 0.00 |
| | Gbr02 | Well | Kersefontein | 16.20 | 0.22 | 393.40 | 5.73 | 0.19 | 0.16 | 0.30 | 330.85 | 70.12 | 0.47 | 15.09 | 0.36 | 77.39 | 0.24 | 1.33 | 1408.00 | 0.42 | 0.42 | 97.76 | 0.52 | 0.11 |
| | BR02 | River | Kersefontein | 1.28 | 0.06 | 51.50 | 126.74 | 2.18 | 0.45 | 0.28 | 43.63 | 65.88 | 0.15 | 0.88 | 0.36 | 2.68 | 0.64 | < 0.6 | 181.09 | 0.12 | 0.00 | 22.21 | 0.06 | 0.04 |
| | Gbr03 | Borehole | Outside Hopefield | 4.57 | 0.00 | 87.83 | 3.44 | 0.05 | 0.09 | 0.29 | 1.62 | 8.64 | 0.03 | 0.77 | < 0.15 | 25.43 | 0.06 | < 0.6 | 265.26 | 0.02 | 0.13 | 30.28 | 24.39 | 0.01 |
| | BR03 | River | Outside Piketberg | 0.74 | 0.00 | 15.77 | 25.27 | 0.37 | 0.55 | 0.31 | 23.45 | 152.13 | 0.06 | 0.37 | 0.38 | 1.75 | 0.95 | < 0.6 | 49.06 | 0.11 | 0.00 | 10.10 | 0.40 | 0.05 |
| Verforenvlei | Gvv01 | Borehole | Skrikvanrondon | 3.19 | 0.00 | 112.84 | 1.09 | 0.22 | 0.50 | 0.35 | 0.35 | 2.46 | 0.30 | 5.41 | 1.24 | 30.73 | 0.11 | 0.43 | 257.33 | 0.54 | 0.04 | 75.62 | 0.26 | 0.12 |
| | Gvv02 | Borerhole | Valskuil | 24.51 | 0.00 | 66.42 | 8.39 | < 0.5 | 0.05 | 0.09 | 244.49 | 346.67 | 0.87 | 4.84 | 0.53 | 47.64 | 2.24 | 0.07 | 571.97 | 0.13 | 0.02 | 205.02 | 0.02 | |
| | Gvv03 | Borehole | Namaqausfontein | 22.86 | 0.17 | 51.79 | 2.24 | < 0.5 | 0.05 | < 0.08 | 138.78 | 320.19 | 0.58 | 6.04 | 0.24 | 25.90 | 1.61 | < 0.05 | 560.21 | 0.16 | 0.01 | 40.37 | < 0.02 | |
| | VV01 | Stream | Moutonshoek | 1.00 | 0.00 | 8.72 | 28.87 | 0.11 | 0.24 | 0.32 | 20.09 | 53.45 | 0.15 | 0.81 | < 0.15 | 5.02 | 1.09 | < 0.6 | 2.93 | 0.36 | 0.01 | 1.32 | 0.01 | 0.02 |
| | VV02 | River | Outside Reydelingshuys | 2.18 | 0.14 | 146.52 | 1.77 | 0.20 | 0.09 | 0.45 | 603.87 | 106.64 | 0.58 | 0.84 | < 0.15 | 19.73 | 0.31 | < 0.6 | 242.35 | 0.40 | 0.01 | 42.20 | 0.03 | 0.03 |
| | GVV04 | Borehole | Fonteinjie | 4.02 | 0.86 | 47.98 | 1619.01 | 0.02 | 0.05 | 0.37 | 226.78 | 33.97 | 8.86 | 2.79 | 2.59 | 46.68 | 0.05 | < 0.6 | 86.39 | 0.04 | 0.09 | 56.41 | 0.12 | 0.99 |
| Olifants | OR01 | River | Surface | 0.32 | 0.00 | 17.44 | 7.11 | 0.15 | 0.09 | 0.30 | 2.25 | 65.03 | 0.02 | 0.22 | < 0.15 | 5.94 | 0.19 | < 0.6 | 24.92 | 0.21 | < 0.005 | 12.98 | 0.02 | 0.01 |
| | Gor01 | Borehole | Uitkyk | 41.20 | 0.22 | 250.49 | 0.89 | 0.12 | 0.06 | 0.27 | 477.46 | 992.86 | 0.46 | 0.98 | < 0.15 | 19.36 | 0.88 | < 0.6 | 399.49 | 0.24 | 0.01 | 135.61 | 0.00 | 0.07 |
| | Gor02 | Borehole | Jomar Boerdery | 18.52 | 0.15 | 771.13 | 1.67 | 0.10 | 0.14 | 1.35 | 10.09 | 2.67 | 0.01 | 0.23 | 0.54 | 16.02 | 0.12 | 5.10 | 621.85 | 0.93 | 0.01 | 0.67 | 0.51 | 3.59 |
| | Gor03 | Borehole | Jomar Boerdery | 9.72 | 0.00 | 295.39 | 1.79 | 0.12 | 0.06 | 0.30 | 118.92 | 10.43 | 0.03 | 0.20 | < 0.15 | 6.30 | 0.19 | 0.54 | 211.02 | 0.92 | 0.01 | 0.82 | 0.04 | 1.43 |
| | OR02 | River | Jomar Boerdery | 11.07 | 0.00 | 796.99 | 9.43 | 0.17 | 0.57 | 0.35 | 457.37 | 10.62 | 0.34 | 0.63 | 0.18 | 4.33 | 1.10 | < 0.6 | 486.24 | 1.31 | < 0.005 | 88.99 | 0.01 | 1.94 |
| | OR03 | River | Outside Lutzville | 23.50 | 0.08 | 1553.59 | 11.05 | 0.18 | 4.91 | 0.41 | 764.57 | 9.00 | 1.17 | 1.38 | 0.75 | 2.27 | 1.52 | 1.00 | 1173.00 | 2.21 | 0.00 | 153.80 | 0.04 | 4.92 |
| | Gor04 | Borehole | Koekenaap | 13.15 | 0.08 | 2409.13 | 1.16 | 0.06 | 19.67 | 4.34 | 0.14 | 1.87 | 0.07 | 0.76 | < 0.15 | 13.47 | 4.02 | 2.51 | 215.16 | 19.18 | 0.01 | 37.43 | 0.03 | 7.82 |
| | OR04 | River | Elrhyn | 24.02 | 0.00 | 1676.41 | 9.89 | 0.21 | 7.92 | 0.40 | 2.19 | 7.87 | 0.49 | 2.10 | 7.69 | 9.58 | 1.92 | 0.92 | 1341.00 | 2.88 | 0.01 | 179.54 | 0.11 | 5.34 |
| Groen | Ggr01 | borehole | Unknown | 68.59 | 0.08 | 1840.78 | 1.11 | 0.14 | 0.36 | 0.35 | 18.62 | 695.05 | 0.12 | 0.81 | < 0.15 | 824.15 | 0.07 | 5.36 | 2056.00 | 3.56 | 0.20 | 5.72 | 0.01 | 17.25 |
| | Ggr02 | borehole | Dikdoorn | 14.61 | 0.00 | 573.53 | 2.14 | 0.08 | 0.44 | 0.49 | 359.85 | 20.02 | 0.82 | 1.99 | 9.34 | 17.59 | 0.21 | < 0.6 | 2894.00 | 0.93 | 0.04 | 153.37 | 0.02 | 1.98 |
| | Ggr03 | Borehole | Perdekraal | 435.85 | 0.16 | 1266.69 | 1.01 | 0.15 | 0.04 | 0.31 | 156.08 | 1004.64 | 0.10 | 0.24 | 0.06 | 288.32 | 0.26 | < 0.6 | 4038.00 | 6.79 | 0.01 | 34.05 | 0.15 | 4.42 |
| | Ggr04 | | Nooitvergeten | 192.47 | 0.25 | 1721.67 | 0.67 | 0.06 | 0.07 | 0.38 | 50.30 | 2.35 | 0.01 | 0.14 | < 0.15 | 91.14 | 0.05 | 1.47 | 5244.00 | 2.73 | 0.17 | 20.93 | 0.09 | 36.29 |
| | Ggr05 | Borehole | Groenriviersvallei | 40.12 | 0.08 | 907.83 | 0.99 | 0.14 | 5.04 | 0.38 | 409.48 | 3.48 | 0.62 | 2.05 | 2.29 | 5.85 | 0.47 | < 0.6 | 4152.00 | 5.50 | 0.04 | 86.81 | <0.000 | 10.39 |
| Buffels | Gbf01 | borehole | Kommagas | 16.73 | 0.08 | 624.10 | 12.00 | 0.25 | 0.80 | 18.79 | 6.11 | 103.70 | 0.14 | 17.55 | 0.89 | 26.94 | 0.02 | 0.53 | 550.72 | 2.60 | 0.02 | 30.02 | 0.14 | 0.22 |
| | Gbf02 | borehole | Kommagas | 2.46 | 0.00 | 89.99 | 0.61 | 0.15 | 1.80 | 0.37 | 0.18 | 2.76 | 0.01 | 0.45 | < 0.15 | 33.17 | 0.03 | < 0.6 | 120.54 | 0.27 | 0.02 | 42.05 | 0.17 | 0.03 |
| | Gbf03 | borehole | Kommagas | 5.28 | 0.08 | 114.63 | 0.35 | 0.02 | 0.30 | 0.43 | 0.31 | 4.61 | 0.01 | 0.66 | 0.61 | 21.18 | 0.04 | 0.48 | 240.88 | 0.59 | 0.02 | 70.99 | 0.13 | 0.07 |
| | Gbf04 | Borehole | Buffels River | 5.32 | 0.08 | 163.18 | 0.43 | 0.01 | 1.04 | 0.31 | 15.78 | 1.72 | 0.09 | 0.57 | 1.20 | 14.06 | 0.10 | < 0.6 | 299.84 | 2.52 | 0.02 | 64.94 | 0.00 | 0.07 |
| | Gbf05 | borehole | Spektakel Mine | 65.93 | 0.00 | 797.29 | 1.68 | 0.11 | 0.05 | 0.44 | 418.03 | 3.03 | 0.22 | 3.28 | 0.31 | < 0.5 | 0.65 | < 0.6 | 3891.36 | 6.01 | 0.00 | 16.29 | 0.01 | 4.05 |
| | Gbf06 | Borehole | Spektakel Mine | 1395.78 | 153.56 | 2351.05 | 57232.82 | 0.18 | 0.16 | 0.68 | 75959.22 | 465100.00 | 2306.98 | 5665.44 | 65417.12 | 5164.15 | 6.55 | 73.74 | 6003.00 | 0.36 | 45.73 | 40.20 | 235.72 | 603.75 |
| | Gbf07 | borehole | Dikgat (Oom Joek se plaas) | 73.39 | 0.16 | 1698.21 | 9.88 | 0.03 | 0.04 | 0.33 | 2547.48 | 361.08 | 0.22 | 1.08 | 4.08 | 1.88 | 0.09 | < 0.6 | 5832.00 | 1.79 | 0.02 | 98.48 | 0.05 | 0.34 |
| | Gbf08 | borehole | de Beers Borehole | 14.68 | 0.00 | 397.28 | 2.35 | 0.19 | 4.51 | 0.27 | 224.47 | 85.50 | 2.30 | 1.68 | 5.35 | 38.35 | 0.36 | 0.63 | 1155.00 | 2.91 | 0.04 | 64.07 | 0.07 | 12.98 |
| | BF01 | Spring | Kommegas | 6.03 | 0.23 | 104.38 | 2.99 | 0.18 | 2.31 | 0.75 | 4.16 | 12.48 | 0.23 | 1.89 | 3.34 | 41.57 | 0.04 | 0.16 | 123.47 | 0.20 | 0.01 | 47.13 | 0.07 | 0.06 |
| Orange | OG01 | River | Alexander Bay | 101.01 | 0.00 | 2851.35 | 4.17 | 0.04 | 2.91 | 0.36 | 176.89 | 8.51 | 0.39 | 0.67 | 2.44 | 1.98 | 1.50 | < 0.6 | 5274.53 | 6.50 | 0.05 | 77.64 | 0.03 | 3.17 |
| | OG02 | River | Spogplaas Guesthouse | 17.38 | 0.07 | 155.66 | 4.14 | 0.13 | 5.25 | 0.18 | 4.39 | 2.62 | 0.08 | 0.67 | 0.73 | 3.67 | 1.26 | < 0.6 | 422.13 | 2.92 | < 0.005 | 111.71 | 0.01 | 0.51 |
| | OG03 | River | Brandkoras camping ground and farm | 15.41 | 0.07 | 166.85 | 13.62 | 0.29 | 5.01 | 0.28 | 6.11 | 13.28 | 0.12 | 1.04 | 4.03 | 14.03 | 1.14 | < 0.6 | 421.52 | 1.77 | 0.06 | 105.25 | 0.26 | 3.07 |
| | OG04 | River | Potjiespram Mine (Namibia) | 14.40 | 0.00 | 107.16 | 19.32 | 0.21 | 6.17 | 0.32 | 2.36 | 15.11 | 0.10 | 0.83 | 2.06 | 10.84 | 1.52 | 0.31 | 253.49 | 1.52 | 0.01 | 77.26 | 0.05 | 3.28 |
| | OG05 | River | Fish & Orange River confluence | 131.30 | 0.00 | 216.39 | 17.94 | 0.10 | 5.73 | 0.59 | 2.26 | 13.68 | 0.15 | 0.73 | 2.81 | 15.63 | 2.45 | 0.39 | 515.80 | 3.85 | 0.02 | 114.29 | 0.06 | 2.72 |
| | OG06 | River | Amanzi Trails | 4.70 | 0.00 | 71.62 | 8.71 | 0.17 | 4.17 | 0.43 | 1.91 | 12.90 | 0.07 | 0.64 | 2.17 | 13.86 | 0.85 | < 0.6 | 180.96 | 1.17 | 0.01 | 53.85 | 0.05 | 2.84 |
| Tsauchab | B45 | Borehole | Tsauchab River Camp (Pitgat) | 84.60 | 0.18 | 175.53 | 1.70 | 0.11 | 3.67 | 0.38 | 1.68 | 6.24 | 0.03 | 0.26 | 1.01 | 28.18 | 0.72 | 0.40 | 567.08 | 0.87 | 0.01 | 16.71 | 0.09 | 3.72 |
| | TS02 | Borehole | Tsauchab River Camp (Dissie Water) | 183.49 | 0.00 | 254.68 | 2.62 | 0.09 | 2.52 | 0.48 | 1.53 | 7.05 | 0.03 | 0.46 | 1.11 | 13.21 | 1.04 | 0.44 | 1911.00 | 0.62 | < 0.005 | 15.38 | 0.14 | 5.04 |
| | S83 | Spring | Neurus | 212.49 | 0.25 | 170.51 | 1.20 | 0.17 | 1.25 | 0.40 | 1.44 | 5.10 | 0.02 | 0.14 | 1.05 | 17.92 | 0.78 | < 0.6 | 3573.00 | 0.76 | < 0.005 | 39.22 | 0.03 | 2.08 |
| | S84 | Spring | Neurus | 211.34 | 0.08 | 179.64 | 1.44 | 0.07 | 1.33 | 0.50 | 1.30 | 4.04 | 0.03 | 0.12 | 0.52 | 32.66 | 0.78 | < 0.6 | 3586.00 | 0.92 | 0.01 | 40.07 | 0.13 | 2.14 |
| | TS03 | Borehole | Zebra River | 169.54 | 0.00 | 157.79 | 1.79 | 0.10 | 1.37 | 0.53 | 0.86 | 5.32 | 0.02 | 0.16 | 1.02 | 13.19 | 0.89 | < 0.6 | 3110.00 | 0.94 | 0.01 | 32.84 | 0.15 | 1.65 |
| | STS01 | Spring | Hauchabfontein | 263.50 | 0.00 | 251.85 | 0.90 | 0.18 | 1.98 | 0.53 | 7.96 | 7.38 | 0.06 | 0.18 | 0.90 | 1.51 | 0.55 | < 0.6 | 3573.00 | 0.89 | < 0.005 | 22.63 | 0.02 | 4.06 |
| | TS04 | Borehole | Betesda | 316.25 | 0.56 | 591.69 | 0.86 | 0.13 | 26.30 | 0.65 | 0.15 | 2.24 | 0.02 | 0.17 | 0.20 | 14.21 | 1.47 | 2.66 | 4064.00 | 6.27 | < 0.005 | 23.48 | 0.06 | 20.96 |
| | B41 | Borehole | Little Sossus Lodge | 119.30 | 0.09 | 343.89 | 2.24 | 0.15 | 22.43 | 0.60 | 1.48 | 9.19 | 0.02 | 0.22 | 0.78 | 505.71 | 0.80 | 0.81 | 2188.00 | 4.97 | 0.01 | 40.30 | 0.08 | 19.19 |
| | B71 | Borehole | Sesreim Campsite | 162.93 | 0.09 | 267.27 | 10.82 | 0.21 | 7.37 | 0.82 | 2.23 | 5.45 | 0.04 | 0.27 | 1.55 | 35.14 | 0.34 | < 0.6 | 2598.00 | 1.15 | 0.01 | 26.36 | 0.20 | 4.96 |
| | TS07 | Borehole | Kulala Desert Lodge | 80.32 | 0.00 | 1056.92 | 1.23 | 0.21 | 120.28 | 37.16 | 0.93 | 10.30 | 0.02 | 0.18 | 0.66 | 71.53 | 3.94 | 2.21 | 777.37 | 59.68 | 0.01 | 1.70 | 0.11 | 55.62 |
| | B32 | Borehole | Little Kulala Lodge | 138.99 | 0.09 | 489.36 | 14.95 | 0.21 | 53.08 | 5.38 | 1.15 | 11.93 | 0.03 | 0.30 | 1.17 | 7.39 | 1.35 | 2.24 | 2124.97 | 5.72 | 0.01 | 28.22 | 0.07 | 31.68 |
| Tsondab | B05 | Borehole | Ababis | 178.76 | 0.09 | 240.91 | 2.03 | 0.06 | 4.91 | 0.55 | 2.71 | 13.68 | 0.03 | 0.25 | 0.87 | 82.63 | 0.85 | 0.60 | 411.77 | 1.29 | < 0.005 | 28.23 | 0.01 | 2.27 |
| | TD01 | Borehole | Ababis (Mittel Posten) | 153.68 | 0.00 | 489.45 | 1.37 | < 0.1 | 8.76 | 0.47 | 5.69 | 242.23 | 0.05 | 0.35 | 0.26 | 352.51 | 0.29 | 2.13 | 6023.00 | 3.38 | < 0.005 | 15.53 | 0.00 | 10.99 |
| | TD02 | Borehole | Ababis (Schwarzer Berg) | 153.05 | 0.10 | 440.78 | 2.98 | 0.10 | 52.12 | 0.64 | 22.84 | 12.14 | 0.15 | 0.42 | 0.93 | 294.15 | 0.93 | 3.44 | 3359.00 | 1.37 | 0.01 | 70.29 | 0.14 | 11.95 |
| | TD03 | Borehole | Ababis (Constantia Posten) | 161.11 | 0.20 | 387.80 | 1.19 | 0.20 | 4.75 | 0.53 | 24.31 | 28.91 | 0.14 | 0.86 | 0.49 | 261.85 | 0.10 | 2.55 | 1514.00 | 1.83 | 0.01 | 22.53 | 0.10 | 12.68 |
| | TD04 | Borehole | Ababis (Panorama) | 86.98 | 0.19 | 610.58 | 2.11 | 0.21 | 1.12 | 0.53 | 14.29 | 100.56 | 0.10 | 0.43 | 0.36 | 178.63 | 0.13 | < 0.6 | 11010.00 | 6.17 | 0.02 | 27.16 | 0.07 | 7.65 |
| | B37 | Borehole | Panorama | 6.33 | 0.45 | 105.03 | 1.47 | < 0.1 | 5.40 | 0.51 | 0.45 | 5.10 | 0.01 | 0.32 | 0.08 | 83.41 | 1.11 | 0.30 | 407.39 | 1.00 | 0.01 | 90.36 | 0.37 | 19.65 |
| | TD05 | Borehole | Zais | 187.78 | 0.00 | 304.45 | 2.10 | 0.18 | 4.10 | 0.51 | 1.84 | 38.00 | 0.06 | 0.45 | 0.93 | 185.12 | 0.68 | 1.98 | 438.57 | 0.68 | 0.02 | 39.66 | 0.16 | 2.45 |
| | B09 | Borehole | Namib Naukluft Lodge | 26.08 | 0.00 | 93.48 | 2.55 | 0.05 | 7.70 | 1.04 | 0.52 | 3.74 | 0.02 | 0.98 | 0.60 | 55.31 | 1.27 | 0.27 | 282.24 | 0.52 | 0.03 | 47.45 | 0.27 | 1.94 |
| | B59 | Borehole | Namib Desert Lodge | 13.90 | 0.00 | 64.19 | < 0.1 | 0.10 | 17.01 | 36.03 | < 0.05 | 1.12 | < 0.01 | 0.07 | < 0.15 | 0.97 | 0.13 | 0.87 | 329.03 | 1.25 | < 0.005 | 1.68 | < 0.008 | 1.03 |
| | Sol-08 | Borehole | Solitaire | 95.24 | 0.00 | 163.30 | 0.44 | < 0.1 | 3.28 | 0.61 | 29.66 | 6.42 | 0.05 | 0.35 | 0.08 | 79.59 | 0.21 | 0.47 | 4257.00 | 1.65 | 0.02 | 24.49 | 0.21 | 4.18 |
| Kuiseb | KR01 | Borehole | Homeb | 6.84 | 0.09 | 124.01 | 1.29 | 0.03 | 23.53 | 0.43 | 327.77 | 8.53 | 0.16 | 0.47 | 1.01 | 13.66 | 1.17 | < 0.6 | 626.57 | 2.16 | 0.01 | 277.17 | 0.05 | 7.41 |
| | KR02 | Borehole | Gobabeb | 11.89 | 0.00 | 428.21 | 2.07 | 0.00 | 7.99 | 0.38 | 706.55 | 25.04 | 0.27 | 0.71 | 0.38 | 26.90 | 1.30 | 1.86 | 1212.00 | 13.99 | 0.03 | 117.17 | 0.08 | 13.05 |
| | KR03 | Borehole | Rooibank | 7.97 | 0.18 | 274.10 | 3.66 | 0.07 | 22.99 | 0.47 | 456.35 | 23.18 | 0.32 | 1.56 | 1.10 | 32.08 | 1.04 | < 0.6 | 1562.00 | 6.98 | 0.04 | 42.79 | 0.09 | 29.27 |
| | KR04 | Borehole | Rooibank | 6.15 | 0.17 | 196.57 | 5.95 | 0.32 | 10.88 | 0.44 | 305.68 | 20.10 | 0.12 | 0.40 | 0.29 | 27.65 | 2.09 | < 0.6 | 396.45 | 5.57 | 0.01 | 3.62 | 0.23 | 9.92 |

**Notes**: These parameters were analysed at (1) The Central Analytical facility, Earth Sciences Department, Stellenbosch University (cations & trace elements) (2) The Stable Isotope Laboratory, Department of Geosciences, University of Lausanne, Switzerland (anions).

# 8. APPENDIX 2: Isotopes

**Table 3:** Summary table of the isotopic parameters analysed for this project:

| | | | | Isotopes (‰) | | | | | |
|---|---|---|---|---|---|---|---|---|---|
| | Sample Name | Sample Type | Location | $\delta^{13}$C-DIC | $\delta^{18}$O | δD | $^{87}Sr/^{86}Sr$ | $\delta^{26}$Mg | $\delta^{44/40}$Ca |
| | | | | VPDB | VSMOW | | | | |
| Berg | BR01 | River | Swartjiesbaai | -4.26 | 1.68 | 7.1 | 0.713570 | -0.89 | 0.13 |
| | Gbr01 | Borehole | Langrietvlei | -11.48 | -3.3 | -14.9 | | | |
| | Gbr02 | Well | Kersefontein | -9.92 | -3.08 | -14.9 | | -0.83 | -0.28 |
| | BR02 | River | Kersefontein | -8.1 | 2.17 | 8.8 | | | |
| | Gbr03 | Borehole | Outside Hopefield | -12.42 | -2.35 | -11.6 | | | |
| | BR03 | River | Outside Piketberg | -9.79 | -1.09 | -3.8 | 0.713102 | -0.67 | |
| | | | | | | | | | |
| Verlorenvlei | Gvv01 | Borehole | Skrikvanrondon | -6.05 | -3.43 | -18.5 | 0.713733 | -0.80 | |
| | Gvv02 | Borerhole | Valskuil | -10.46 | -2.83 | -14.5 | 0.714754 | -0.72 | -1.06 |
| | Gvv03 | Borehole | Namaqausfontein | -11.47 | -2.78 | -11.8 | | | |
| | VV01 | Stream | Moutonshoek | -15.2 | -3.34 | -13.4 | | -0.79 | |
| | VV02 | River | Outside Reydelingshuys | -17.72 | -1.46 | -8.6 | 0.713033 | -0.92 | -0.63 |
| | GVV04 | Borehole | Fonteinjie | -10.76 | -2.99 | -13.6 | 0.712436 | -0.86 | |
| | | | | | | | | | |
| Olifants | OR01 | River | Surface | -10.06 | -1.48 | -8.4 | | | |
| | Gor01 | Borehole | Uitkyk | -11.65 | -3.16 | -13.8 | | -0.79 | |
| | Gor02 | Borehole | Jomar Boerdery | -8.35 | -2.78 | -13 | | | |
| | Gor03 | Borehole | Jomar Boerdery | -8.6 | -1.48 | -9.3 | 0.713741 | -1.30 | -0.63 |
| | OR02 | River | Jomar Boerdery | -10.33 | -1.77 | -10.7 | | | |
| | OR03 | River | Outside Lutzville | -10.29 | -2.16 | -10.9 | | | -0.73 |
| | Gor04 | Borehole | Koekenaap | -12.95 | -1.54 | -10.1 | | | |
| | OR04 | River | Elrhyn | -10.66 | | | | -0.88 | |
| | | | | | | | | | |
| Groen | Ggr01 | borehole | Unknown | | -3.63 | -17.9 | 0.721214 | -0.93 | -0.88 |
| | Ggr02 | borehole | Dikdoorn | -10.62 | -2.74 | -15.5 | 0.733137 | -0.93 | |
| | Ggr03 | Borehole | Perdekraal | -9.96 | -2.82 | -17.1 | | | |
| | Ggr04 | | Nooitvergeten | -9.91 | -3.93 | -20.4 | 0.728503 | -0.93 | |
| | Ggr05 | Borehole | Groenriviersvallei | -11.98 | | | | | |
| | | | | | | | | | |
| Buffels | Gbf01 | borehole | Kommagas | -7.77 | -3.56 | -15 | | | |
| | Gbf02 | borehole | Kommagas | -10.85 | -3.66 | -16 | 0.748041 | -0.59 | |
| | Gbf03 | borehole | Kommagas | -9.81 | -3.46 | -14.8 | | | |
| | Gbf04 | Borehole | Buffels River | -11.78 | -3.6 | -18.8 | 0.741264 | -0.72 | -0.53 |
| | Gbf05 | borehole | Spektakel Mine | -9.55 | -3.2 | -16.8 | | -0.83 | 0.01 |
| | Gbf06 | Borehole | Spektakel Mine | | -0.34 | -4.3 | | | |
| | Gbf07 | borehole | Dikgat (Oom Joek se plaas) | -4.71 | -0.74 | -5.7 | | | |
| | Gbf08 | borehole | de Beers Borehole | -11.67 | -2.71 | -13.1 | 0.730125 | -1.01 | |
| | BF01 | Spring | Kommegas | -9.59 | -2.69 | -13.3 | 0.743474 | -0.53 | -0.73 |
| | | | | | | | | | |
| Orange | OG01 | River | Alexander Bay | -5.5 | 0.55 | 0.3 | 0.720587 | -0.95 | |
| | OG02 | River | Spogplaas Guesthouse | -5.76 | 2.15 | 6.2 | | | |
| | OG03 | River | Brandkoras camping ground and farm | -6.3 | 2.67 | 8.2 | 0.719394 | -0.73 | |
| | OG04 | River | Potjiespram Mine (Namibia) | -5.91 | 1.94 | 5.8 | 0.720756 | -0.58 | -0.55 |
| | OG05 | River | Fish & Orange River confluence | -4.88 | 3.51 | 3 | 0.721107 | -0.90 | -0.34 |
| | OG06 | River | Amanzi Trails | -3.81 | 2.21 | 6.9 | 0.721000 | -0.53 | |

**Table 4:** Summary table of the isotopic parameters analysed and referred to in this thesis (continued):

| | | | | | | | | | |
|---|---|---|---|---|---|---|---|---|---|
| Tsauchab | B45 | Borehole | Tsauchab River Camp (Pitgat) | -10.81 | -4.84 | -33.3 | 0.714643 | -1.27 | 0.79 |
| | TS02 | Borehole | Tsauchab River Camp (Dissie Water) | -8.84 | -6.1 | -43.1 | | | |
| | S83 | Spring | Neurus | -9.76 | -6.5 | -43.3 | | | |
| | S84 | Spring | Neurus | -9.12 | -6.43 | -42.8 | 0.711229 | -1.15 | -0.89 |
| | TS03 | Borehole | Zebra River | -8.51 | -6.54 | -43.9 | | | |
| | STS01 | Spring | Hauchabfontein | -8.58 | -3.65 | -29.8 | 0.711071 | -1.22 | -0.38 |
| | TS04 | Borehole | Betesda | -8.86 | -6.59 | -46.2 | | | |
| | B41 | Borehole | Little Sossus Lodge | -8.35 | -7.03 | -48.4 | 0.713706 | -1.28 | -0.78 |
| | B71 | Borehole | Sesreim Campsite | -8.99 | -6.55 | -45.9 | 0.712311 | -1.33 | |
| | TS07 | Borehole | Kulala Desert Lodge | -4.69 | -5.52 | -40.1 | 0.712311 | -0.94 | |
| | B32 | Borehole | Little Kulala Lodge | -6.23 | -6.48 | -45.3 | 0.717207 | -0.75 | |
| | | | | | | | | | |
| Tsondab | B05 | Borehole | Ababis | -9.53 | -6.43 | -42.5 | | | |
| | TD01 | Borehole | Ababis (Mittel Posten) | -6.57 | -6.69 | -46.8 | | | |
| | TD02 | Borehole | Ababis (Schwarzer Berg) | -9.56 | -5.83 | -39.6 | | | |
| | TD03 | Borehole | Ababis (Constantia Posten) | -6.04 | -6.55 | -47.8 | | | |
| | TD04 | Borehole | Ababis (Panorama) | -9.15 | -6.54 | -46 | | | |
| | B37 | Borehole | Panorama | -10.94 | -5.25 | -32.6 | 0.725572 | -1.40 | |
| | TD05 | Borehole | Zais | -10.04 | -5.61 | -39.1 | | | |
| | B09 | Borehole | Namib Naukluft Lodge | 1.75 | -5.63 | -34.8 | 0.717516 | -1.64 | |
| | B59 | Borehole | Namib Desert Lodge | -8.95 | -6.64 | -47.4 | | | |
| | Sol-08 | Borehole | Solitaire | -8.86 | -6.29 | -44.4 | | | |
| | | | | | | | | | |
| Kuiseb | KR01 | Borehole | Homeb | -13.27 | -4.98 | -31.5 | | -1.10 | |
| | KR02 | Borehole | Gobabeb | -12.4 | -5.78 | -40.2 | | -0.82 | -0.80 |
| | KR03 | Borehole | Rooibank | -11.91 | -6.17 | -43.2 | | | |
| | KR04 | Borehole | Rooibank | -10.79 | -6.66 | -44.9 | | -0.74 | |

**Notes**: The isotopes were analysed at (1) The Stable Isotopes Laboratory, Department of Geological Sciences, University of Cape Town ($^{87}Sr/^{86}Sr$) (2) The Stable Isotope Laboratory, Department of Geosciences, University of Lausanne, Switzerland ($\delta^{13}$C-DIC) (3) The Higgins Lab, Department of Geosciences, Princeton University ($\delta^{26}$Mg, $\delta^{44/40}$Ca).